UNIVERSITY OF CALIFORNIA, SAN DIEGO

The Fine-Structure Constant and Wavelength Calibration

A dissertation submitted in partial satisfaction of the
requirements for the degree
Doctor of Philosophy

in

Physics

by

Jonathan Whitmore

Committee in charge:

Professor Kim Griest, Chair
Professor Bruce Driver
Professor Hans Paar
Professor Barney Rickett
Professor Arthur Wolfe

2011

ProQuest LLC.
789 East Eisenhower Parkway
P.O. Box 1346
Ann Arbor, MI 48106 - 1346

The dissertation of Jonathan Whitmore is approved, and it is acceptable in quality and form for publication on microfilm and electronically:

_____

_____

_____

_____

_____
Chair

University of California, San Diego

2011

EPIGRAPH

The important thing in science
is not so much to obtain new facts
as to discover new ways of thinking about them.
—William Lawrence Bragg

TABLE OF CONTENTS

Signature Page iii

Epigraph iv

Table of Contents v

List of Figures vii

List of Tables viii

Acknowledgements ix

Vita and Publications x

Abstract of the Dissertation xi

Chapter 1 Introduction 1
1.1 Physical Constants 2
1.2 Theoretical Motivations and Implications 7
1.3 Current Constraints on the Fine-Structure Constant . . . 9
1.3.1 Atomic Clocks 9
1.3.2 Oklo Reactor 10
1.3.3 Meteorite Dating 13
1.3.4 Cosmic Microwave Background 14
1.3.5 Big Bang Nucleosynthesis 17
1.4 Atomic Physics as a Fine-Structure Constancy Probe . . 17
1.4.1 Quasar Absorption Spectra 19
1.4.2 Alkali Doublet Method 19
1.4.3 Many-Multiplet Method 25
1.5 Review of Claimed Detections 27
1.5.1 Keck-HIRES 29
1.5.2 VLT-UVES 30
1.5.3 Current Status 33

Chapter 2 Keck-HIRES 43
2.1 HIRES 46
2.2 Data and Extraction 51
2.3 Standard Wavelength Calibration 53
2.4 Iodine Cell 53
2.5 Supercalibration Method 56
2.6 Understanding the Calibration Shifts 67

2.7 Using the Calibration 72
2.8 VPFIT analysis 72
2.9 Discussion 79

Chapter 3 VLT-UVES 86
3.1 UVES 87
3.2 VLT Observations 88
3.3 Analysis 91
3.4 Degree Polynomial Calibration Effects 94
3.5 Effect on Fine-Structure Constant Measurements 95
3.6 Conclusions 105

LIST OF FIGURES

Figure 1.1: Example Absorption Spectrum 6
Figure 1.2: Simulated α Shift 8
Figure 1.3: Atomic Clock Schematic 11
Figure 1.4: CMB theoretical $\frac{\Delta\alpha}{\alpha}$ dependence 16
Figure 1.5: CMB $\frac{\Delta\alpha}{\alpha}$ Constraint 18
Figure 1.6: Photoabsorption 20
Figure 1.7: Energy Correction to Hydrogen 23
Figure 1.8: Alkali Doublet Emission Constraint 25
Figure 1.9: Transition Sensitivity 28
Figure 1.10: Keck Telescope 29
Figure 1.11: Murphy 2004's Statistical Result 31
Figure 1.12: VLT Telescope 32
Figure 1.13: Transition Sensitivities via q value 34
Figure 1.14: Critical Statistical Error Analysis 35
Figure 1.15: $\frac{\Delta\alpha}{\alpha}$ Dipole Claim 36

Figure 2.1: Simulated Data 47
Figure 2.2: HIRES schematic 48
Figure 2.3: HIRES Lightpath 50
Figure 2.4: Arc Calibration File Example 54
Figure 2.5: Iodine Cell Resolution Difference 57
Figure 2.6: QSO absorption with Iodine Cell Absorption 58
Figure 2.7: Continuum Test 61
Figure 2.8: Best Fit Convolution 62
Figure 2.9: Calibration Shift Results 64
Figure 2.10: Single Order Correction 66
Figure 2.11: Applied Iodine Cell Correction 68
Figure 2.12: Applied Iodine Cell Interpolation 69
Figure 2.13: Temperature Dependence 71
Figure 2.14: Voigt Profile 74
Figure 2.15: VPFIT Alpha Measurements 80

Figure 3.1: UVES Schematic 89
Figure 3.2: VLT-UVES Calibration Shifts 92
Figure 3.3: Histogram of Wavelength Calibration Shifts 93
Figure 3.4: Higher Ordered Polynomial Fit Analysis 96
Figure 3.5: Polynomial Calibration Shifts 97
Figure 3.6: Monte Carlo Results 103

LIST OF TABLES

Table 1.1: A Listing of Fundamental Physical Constants[a] 4

Table 2.1: Line Information 45
Table 2.2: Journal of PHL957 Observations 52
Table 2.3: Results from VPFIT 78
Table 2.4: Results from VPFIT 78

Table 3.1: VLT-UVES Journal of Observations 90
Table 3.2: Means[a] and Standard Deviations[a] of Calibration Shifts 94
Table 3.3: Monte Carlo results[a] for mean and standard deviation of $\frac{\Delta\alpha}{\alpha}$ . . 99
Table 3.4: Standard deviation[a] of $\frac{\Delta\alpha}{\alpha}$ from wavelength calibration errors as a function of the number of transitions. 101
Table 3.5: Monte Carlo results[a] for mean and standard deviation of $\frac{\Delta\alpha}{\alpha}$ . . 104
Table 3.6: Coefficients for Model 105

ACKNOWLEDGEMENTS

I would like to thank Professor Kim Griest for being the chair of my committee. I greatly appreciate his guidance and support and marvel that his patience has rivaled that of Ghandi at times. I would also like to thank my family for their love and support. My parents, Greg and Mary, and my sister Jacquelyn have given me encouragement throughout my entire life. I always know that I can count on my family to be there for me, and that stability gives me strength every day.

I would like to thank my office-mate for the past four years, Marc Rafelski, for interesting conversations, helpful advice, and his unflagging optimism. Thanks also go out to Jeff Noel for being a great roommate for the past 5 years. The late night discussions on science, politics, religion, and riddles will always be remembered fondly. I would also like to thank Stephanie Moyerman for her support – it helped me a great deal. To my fellow participants in the CASS tea time, thank you for being good debate partners and providing interesting perspectives on every conceivable conversation topic.

Finally, I thank my thesis committee: Professors Bruce Driver, Hans Paar, Barney Rickett, and Arthur Wolfe for reading my thesis, giving valuable feedback and for being on my committee.

VITA

2011	Ph. D. in Physics, University of California, San Diego
2007	M. S. in Physics, University of California, San Diego
2005	B. S. in Physics (with honors); Philosophy; and Mathematics, *magna cum laude*, Vanderbilt University

PUBLICATIONS

Whitmore, J. *An Empirical Wavelength Correction for Keck-HIRES*, in prep.

Whitmore, J., Murphy, M., Griest, K. *Wavelength Calibration of the VLT-UVES Spectrograph*, Astrophysical Journal, 723, 89 (2010) link

Griest, K., **Whitmore, J.**, Wolfe, A., Prochaska, J., Howk, C., Marcy, G. *Wavelength Accuracy of the Keck HIRES Spectrograph and Measuring Changes in the Fine Structure Constant*, The Astrophysical Journal, 708, 158 (2010) link

NON-REFEREED PUBLICATIONS

Whitmore, J. *Wavelength Calibration Errors in Keck-HIRES/VLT-UVES and Variation in the Fine-Structure Constant*, Thesis Presentation No. 412.01D, AAS 2011 meeting link

Whitmore, J. *Variation in the Fine-Structure Constant*, CAL10 Meeting of The American Physical Society, 55, 12 (2010) link

Whitmore, J., Griest, K., Wolfe, A. M., Prochaska, J. X., Howk, C., Marcy, G. *Wavelength Accuracy of the Keck HIRES Spectrograph and Measuring Changes in the Fine Structure Constant*, American Astronomical Society, AAS Meeting 213, No. 609.05 (2009)

ABSTRACT OF THE DISSERTATION

The Fine-Structure Constant and Wavelength Calibration

by

Jonathan Whitmore

Doctor of Philosophy in Physics

University of California, San Diego, 2011

Professor Kim Griest, Chair

The fine-structure constant is a fundamental constant of the universe – and widely thought to have an unchanging value. However, the past decade has witnessed a controversy unfold over the claimed detection that the fine-structure constant had a different value in the distant past. These astrophysical measurements were made with spectrographs at the world's largest optical telescopes. The spectrographs make precise measurements of the wavelength spacing of absorption lines in the metals in the gas between the quasar background source and our telescopes on Earth. The wavelength spacing gives a snapshot of the atomic physics at the time of

the interaction. Whether the fine-structure constant has changed is determined by comparing the atomic physics in the distant past with the atomic physics of today. We present our contribution to the discussion by analyzing three nights data taken with the HIRES instrument (High Resolution Echelle Spectrograph) on the Keck telescope. We provide an independent measurement on the fine-structure constant from the Damped Lyman alpha system at a redshift of $z = 2.309$ (10.8 billion years ago) quasar PHL957. We developed a new method for calibrating the wavelength scale of a quasar exposure to a much higher precision than previously achieved. In our subsequent analysis, we discovered unexpected wavelength calibration errors that has not been taken into account in the previously reported measurements. After characterizing the wavelength miscalibrations on the Keck-HIRES instrument, we obtained several nights of data from the main competing instrument, the VLT (Very Large Telescope) with UVES (Ultraviolet and Visual Echelle Spectrograph). We applied our new wavelength calibration method and uncovered similar in nature systematic errors as found on Keck-HIRES. Finally, we make a detailed Monte Carlo exploration of the effects that these miscalibrations have on making precision fine-structure constant measurements.

Chapter 1

Introduction

The introduction is setup as follows. We begin with a discussion of physical constants in § 1.1. Next, we review some recent theoretical work that suggests the constants are not constant in § 1.2. We continue with constraints on the fine-structure constant through various experiments in § 1.3. A review of atomic physics and quasar absorption system detection methods are explained in § 1.4. The claimed detections of a varying fine-structure constant are reviewed in § 1.5.

The outline of the rest of this thesis is as follows. We describe our attempts at making a new measurement to either rule out or detect a change in $\frac{\Delta\alpha}{\alpha}$. Chapter 2 deals with the data and analysis from the HIRES spectrograph on the Keck telescope. It details some of the unforeseen conclusions that we had to draw: notably the wavelength scale miscalibrations. After finding unexpected wavelength calibration issues in the first of the two main telescopes being used to measure the fine-structure constant today, we turn our attention to the second instrument: the UVES spectrograph on the VLT telescope. We characterize its wavelength calibration issues and make a detailed investigation into the effect these miscalibrations might

have on $\frac{\Delta\alpha}{\alpha}$. We derive a formula for estimating the statistical effect of the number of absorption lines and systems that are being used. Finally, we investigate both the statistical effect for Keck and utilize recent star data. This new star data suggests a method to correct miscalibrations from 600 m s^{-1} to 1000 m s^{-1}; and a reanalysis of $\frac{\Delta\alpha}{\alpha}$ on the newly corrected spectra are in progress.

1.1 Physical Constants

Universal physical constants describe physical quantities that are thought to have the same value everywhere in space and everywhere in time. A particularly useful way to categorize the physical constants is to separate them based on whether they have physical dimensions: i.e., dimensionless and dimensionful physical constants. The choice of units sets the numerical value for a given dimensionful physical quantity. For example, the speed of light, $c \equiv 299792458$ m s^{-1}, has units of length divided by time. The speed of light was defined to have that numerical value, and so the numerical value has no intrinsically important meaning. In contrast, one can combine different dimensional constants into ratios where the units completely cancel, leaving a dimensionless ratio of the physical constants. This dimensionless ratio, however, is often a relationship whose number has physical meaning. A few examples of these relationships include the ratio of the proton and electron masses, m_p/m_e, and the fine-structure constant, α. The fine-structure constant is defined as the square of the charge of the electron, e, divided by Plank's constant, $\hbar$, times the speed of light, c, and has the measured value (Mohr et al., 2006):

$$\alpha \equiv \frac{e^2}{\hbar c} \approx \frac{1}{137.035999679(94)}. \tag{1.1}$$

The fine-structure constant sets the strength of the electromagnetic interactions and is a ratio whose numerical value is the same in every system of physical units. Thus, the numerical value itself appears to have a fundamental connection with underlying physics. Put another way, if one reworks a physics calculation with a change in units, one has changed the *numbers*. If one reworks a physics calculation with a change in α, one has changed the *physics*. A selection of fundamental constants and their current best values is given in Table 1.1.

Table 1.1. A Listing of Fundamental Physical Constants[a]

Quantity	Value	Uncertainty	Units
Avogadro constant	6.022 141 79 e23	0.000 000 30 e23	mol^{-1}
Bohr radius	0.529 177 208 59 e-10	0.000 000 000 36 e-10	m
Boltzmann constant	1.380 6504 e-23	0.000 0024 e-23	$\mathrm{J\ K}^{-1}$
electric constant (ϵ_0)	8.854 187 817 e-12	(defined)	$\mathrm{F\ m}^{-1}$
electron g factor	-2.002 319 304 3622	0.000 000 000 0015	
electron gyromag. ratio	1.760 859 770 e11	0.000 000 044 e11	$\mathrm{s}^{-1}\ \mathrm{T}^{-1}$
elementary charge	1.602 176 487 e-19	0.000 000 040 e-19	C
fine-structure constant (α)	7.297 352 5376 e-3	0.000 000 0050 e-3	
α^{-1}	137.035 999 679	0.000 000 094	
G (Newton's constant)	6.674 28 e-11	0.000 67 e-11	$\mathrm{m}^3\ \mathrm{kg}^{-1}\ \mathrm{s}^{-2}$
Planck constant (h)	6.626 068 96 e-34	0.000 000 33 e-34	J s
$\hbar$	1.054 571 628 e-34	0.000 000 053 e-34	J s
Planck length	1.616 252 e-35	0.000 081 e-35	m
Planck mass	2.176 44 e-8	0.000 11 e-8	kg
Planck time	5.391 24 e-44	0.000 27 e-44	s
proton-electron mass ratio (μ)	1836.152 672 47	0.000 000 80	
proton g factor	5.585 694 713	0.000 000 046	
Rydberg constant	10 973 731.568 527	0.000 073	m^{-1}
speed of light (c)	299 792 458	(defined)	$\mathrm{m\ s}^{-1}$
Stefan-Boltzmann constant	5.670 400 e-8	0.000 040 e-8	$\mathrm{W\ m}^{-2}\ \mathrm{K}^{-4}$
weak mixing angle	0.222 55	0.000 56	

[a]From: `http://physics.nist.gov/constants`

Are these constants the same everywhere and for all time? The question about the "constancy" of constants might seem frivolous, but it has been a topic of inquiry since Dirac first suggested the possibility with his Large Number Hypothesis (Dirac, 1937, 1938). If the fine-structure constant is changing, a common temptation is to ask which of the constituent constants, $\hbar$, c, or e, is responsible for the change. In fact, the values of those dimensionful constants can be thought of as derived quantities from the more fundamental constant, α. Thus, as long as the fine-structure constant maintains the same numerical value, any theory or measurement of a change in any one of the constituent constants can be reinterpreted as a corresponding change in the other constants. However, a change in the measured value of α cannot be reinterpreted–the ratio of the constants has changed in every systems of units. The term that is used for the fractional change in the fine-structure constant is $\frac{\Delta\alpha}{\alpha}$, and is defined as:

$$\frac{\Delta\alpha}{\alpha} = \frac{\alpha_z - \alpha_0}{\alpha_0}, \tag{1.2}$$

where α_z is the value of the fine-structure constant at a redshift value of z, and α_0 is the present day value.

In the years since Dirac's hypothesis, many different methods have been utilized to measure the constancy for many fundamental constants. The methods range from atomic clock measurements that constrain $\frac{\Delta\alpha}{\alpha}$ to 1 part in 10^{17} over a few years on Earth, to measuring the primordial abundance left over from Big Bang nucleosynthesis to constrain $\frac{\Delta\alpha}{\alpha}$ to 1 part in 10^2 over the span of 13.7 billion years in time and billions of lightyears in space.

In the past ten years, astronomical measurements of the fine-structure constant have given the first empirical suggestions that α might have had a different value in the past. These measurements have been made by analyzing the atomic

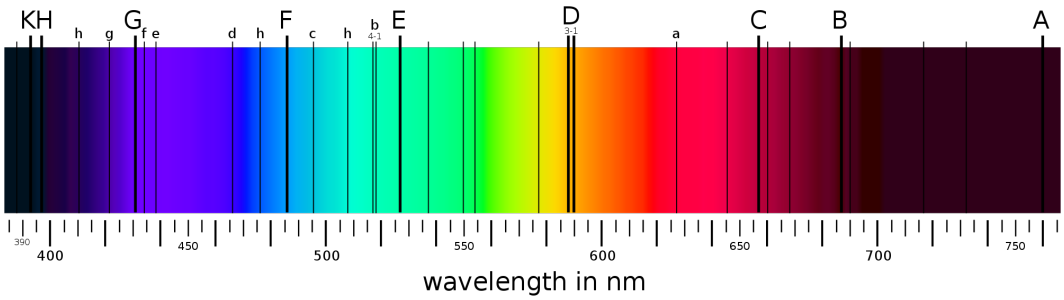

Figure 1.1 An example of the Fraunhofer absorption lines of the spectrum from our sun. Source: `http://en.wikipedia.org/wiki/File:Fraunhofer_lines.svg`.

physics in the gas clouds between quasars and telescopes on Earth. The physical process starts with light emitted by a quasar that is eventually detected by a telescope on Earth. The light passes through all of the clouds of gas and galaxies between the quasar and the telescope that lie on that trajectory. Atomic and molecular gas will scatter precise wavelengths of light via the processes of photoabsorption and reemission. The precise wavelengths that are absorbed correspond to the energy level spacings available to the electrons in the respective elements. When the light arrives on Earth and is dispersed through a spectrograph, we observe a number of dark bands at those wavelengths in the otherwise smooth continuum of the quasar spectrum. The wavelengths of these dark bands come from the energy level spacings of the atomic gas that produce them, and are unique to each element. A representation of absorption lines is shown in Figure 1.1. Detailed measurements of these quasar spectra give astrophysicists a snapshot of the atomic physics of that specific time and place in the universe. By comparing the atomic physics in cosmologically remote locations to atomic physics measured today in laboratories on Earth, it becomes possible to detect whether fundamental physics has changed.

Light gets redshifted (shifted toward the longer wavelengths) as it travels over cosmological distances due to the expansion of the universe. In order for a change in α to be detected, the change must shift the absorption line spectrum in a way that is different from a redshift, or it would be impossible to disentangle the two effects. Theoretical advances have been made in calculating the complicated effects that a different fine-structure constant would have on atomic physics. They reveal that the energy level spacing in different atoms shift in many different ways from a change in the fine-structure constant. Since the energy level spacing is measured as an absorption spectrum, changing α yields a unique spectral fingerprint, e.g., Figure 1.2.

1.2 Theoretical Motivations and Implications

There are many theoretical approaches that incorporate varying constants. We only briefly review a selection of these. For an especially accessible review of the theoretical foundations of varying constants we refer the reader to § 2 of Lorén-Aguilar et al. (2003), and for a comprehensive review we refer to § 5 of Uzan (2011). We closely follow the discussion in Lorén-Aguilar et al. (2003) throughout this section.

One class of theoretical investigations are the theories that make use of extra dimensions. The methods that are used to compactify the extra dimensions into our 4-D (at the large scale) universe give rise to predicted physical interactions. The physical parameters are set by both the overall size of the extra dimensions and a new set of constants. For example, in an attempt to unify electromagnetism with general relativity, Kaluza-Klein theory was formulated. The approach that Kaluza

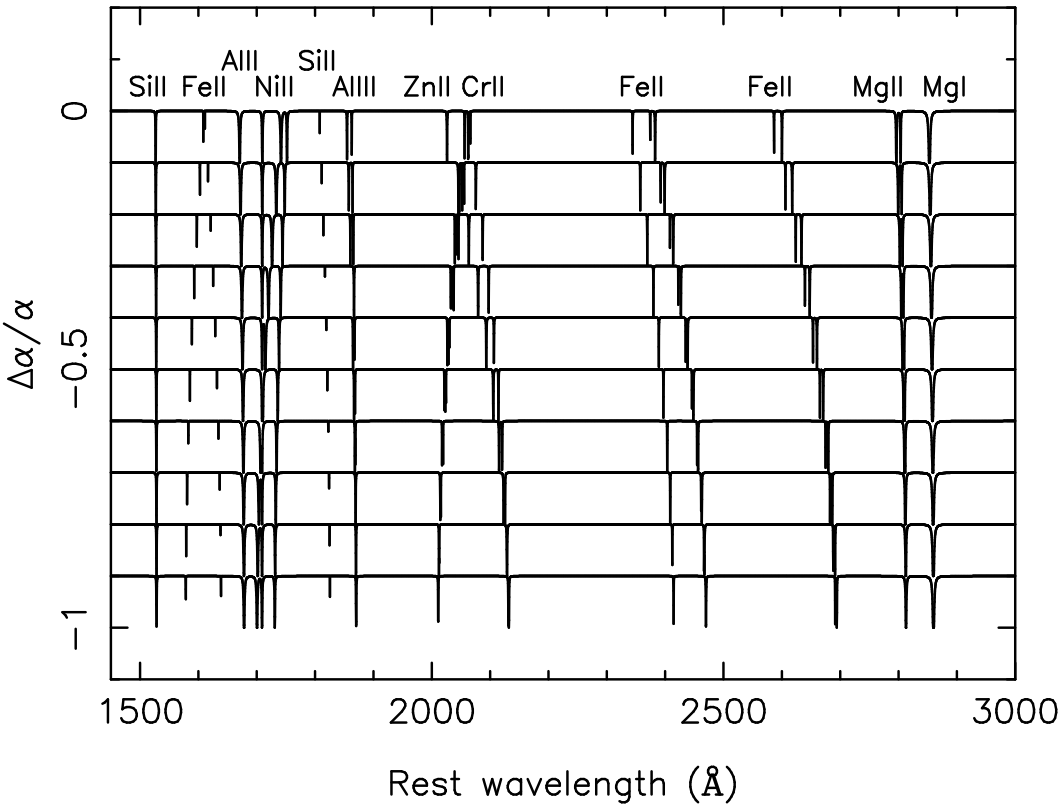

Figure 1.2 A simulated spectrum of the relative effects that a change in α would have on the positions of different atomic transitions. The top line shows the absorption features in a spectrum as it would be measured with the current value of the fine-structure constant. Several different atomic transitions are labeled directly above their respective features. The same spectra is repeated for different values of the fine-structure constant. The further down on the y-axis corresponds to a larger deviation in the fine-structure constant and a progressively larger effect on the relative spacing of the absorption features of the spectrum. Notice that several lines are relatively insensitive to the change (Si II feature on the left), while others are very sensitive the change (Fe II features that split further apart directly to the right of the Si II feature). Source: (Webb et al., 2003).

(1921) and Klein (1926) took was to formulate the theories in five dimensional space, with the fourth spatial dimension rolled into a circular dimension. The physical size of the circular dimension sets the coupling constant between the gravitational and electromagnetic fields. A changing of the scale size of the compactified dimension leads directly to a changing coupling constant between the unified fields. Further, the expansion of the universe changes the scale size of the larger three spatial dimensions, and so there is reason to suggest that the scale size for all spatial dimensions could change. Within this framework, the mechanism for a change in the coupling constants is a natural consequence.

1.3 Current Constraints on the Fine-Structure Constant

In this section, we give a brief overview of the various detection methods people have used to constrain a variation in the fine-structure constant. These methods vary widely in both their relative sensitivity and their extent in both space and time from extremely precise and very local atomic clock measurements to extremely large spatial and time but less precise Big Bang nucleosynthesis. We separately review the claimed detections in § 1.5.

1.3.1 Atomic Clocks

Atomic clocks take advantage of the quantum mechanics of atomic transitions to provide extremely precise frequency measurements. A precisely tunable laser induces a prepared group of atoms to undergo an atomic transition. The prepared group of atoms is monitored while the laser frequency sweeps through a range of

values. Quantum mechanics calculations predict the frequency of incident light that will most favorably induce an atomic transition. We match the calculated frequency of light with the laser frequency that yields the highest percentage of atoms that transition. A change in the fine-structure constant has different effects on different atomic transitions for different elements. Comparing atomic clocks utilizing different atomic species and transitions allows for a precise probe of possible drifts in several fundamental constants. We review the literature for a summary of the current results.

One of the basic approaches measures the relative ratio of frequencies between atomic clocks made from different atoms. After a length of time, the ratio of frequencies is taken again and compared with the earlier measurement to ascertain a change in the rates. For example, Peik et al. (2008) compared an optical transition frequency of 688 THz in $^{171}Yb^{+}$ with a cesium atomic clock over a span of six years. They found that combining their measurements with $^{199}Hg^{+}$ and ^{87}Rb they attained a constraint on $\mathrm{d}\ln\alpha/\mathrm{d}t = (-0.26 \pm 0.39) \times 10^{-15}$ yr^{-1}. Rosenband et al. (2008) has the tightest constraint on a variation in the fine-structure constant's present day rate of change. They used the optical transitions of two single-ion atomic clocks ($^{27}Al^{+}$ and $^{199}Hg^{+}$) to constrain the current rate of change of $\dot{\alpha}/\alpha = (-1.6 \pm 2.3) \times 10^{-17}$ yr^{-1}. A schematic of their experiment is shown in Figure 1.3. This result is a very tight constraint, but only probes the extremely local space-time.

1.3.2 Oklo Reactor

An example of a naturally occurring nuclear reactor is found in Oklo, Gabon, in Africa. The reactor occurred from a fortuitous combination of uranium and water

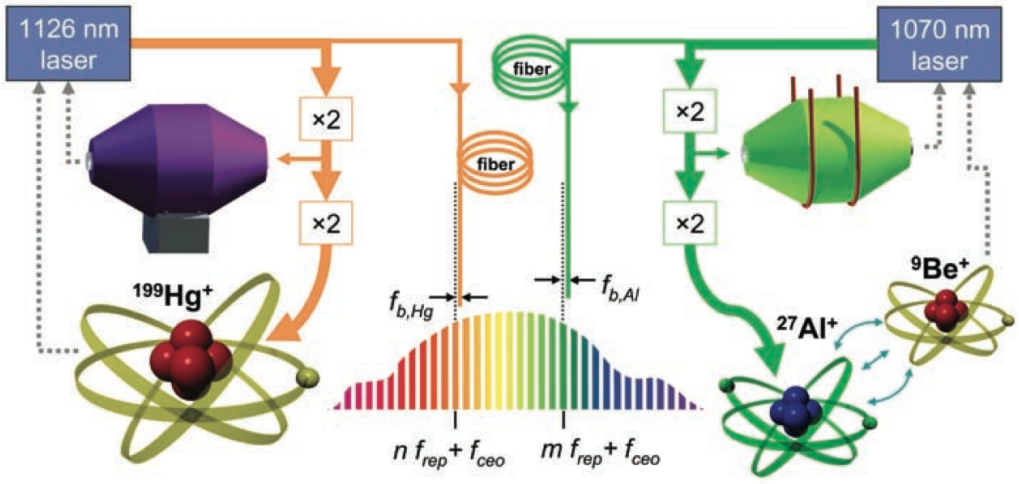

Figure 1.3 Figure 1 of Rosenband et al. (2008) showing the $^{27}Al^{+}$ and $^{199}Hg^{+}$ Source: (Rosenband et al., 2008).

about 1.8 billion years ago, and resulted in the natural nuclear reactor running for several million years before shutting down(Naudet, 1974). Shlyakhter (1976) argued that the Oklo reactor could be used as a test of the variation of fundamental constants, and the basic principle takes advantage of a number of physically relevant measurements. He argued that the value of the fine-structure constant at the time the reactor was active can be derived from the consideration of several lines of reasoning. First, the relative abundance of the isotopes of samarium (Sm) depends on an energy resonance that strongly depends on the value of the fine-structure constant. The specific dependence of the energy resonance level has to be calculated based on nuclear physics models of the nucleus and high energy physics. Next, the abundance of various other elements can be used to indicate the total neutron flux of the natural reactor. Several physical assumptions have to be made to derive a model that yields a constraint on $\frac{\Delta\alpha}{\alpha}$, such as the geometry of the reactor, the

amount of water that is present, and the shape of the neutron spectrum, among several others. His analysis led to a constraint of $|\dot{\alpha}/\alpha| < \times 10^{-17}\ \mathrm{yr}^{-1}$, assuming a linear rate of change with time.

More recent analysis on the Oklo reactor has been carried out by a number of authors in recent years. For example, Petrov et al. (2006) finds a constraint of $-5.6 \times 10^{-8} < \frac{\Delta\alpha}{\alpha} < 6.6 \times 10^{-8}$, and Gould et al. (2006) find the value of $-1.1 \leq \times 10^{-8} \leq \frac{\Delta\alpha}{\alpha} \leq 2.4 \times 10^{-8}$. Both results are consistent with no change in $\frac{\Delta\alpha}{\alpha}$. However, Flambaum (2008) contends that the α dependence is small compared with the effects due to other fundamental constant changes, i.e. the mass of the strange quark divided by the quantum chromodynamics scale:

$$\left| 0.01\frac{\delta\alpha}{\alpha} - 0.1\frac{\delta X_q}{X_q} - \frac{\delta X_s}{X_s} \right| < 10^{-9} \tag{1.3}$$

where $X_q = m_q/\Lambda_{QCD}$, $X_s = m_s/\Lambda_{QCD}$, Λ_{QCD} is the quantum chromodynamics scale (defined as the position of the Landau pole in the logarithm for the strong coupling constant), $m_q = (m_u + m_d)/2$ and m_s is the strange quark mass. And he strongly concludes that, "The contribution of the α variation in this equation is very small and should be neglected since the accuracy of the calculation of the main term is low. Thus, the Oklo data cannot give any limit on the variation of α" (Flambaum, 2008). In other words, when considering the possibility of changing fundamental constants, the α constraint only holds under the assumption that it is the only fundamental constant that can change. The Oklo measurements depend much more strongly on variation in several fundamental constants other than α and have large errors in the current calculations. We comment that these are difficult measurements to make, and the Oklo reactor remains a unique probe into a further exploration of fundamental physics.

1.3.3 Meteorite Dating

Meteorites present a unique opportunity to test a nonzero $\frac{\Delta\alpha}{\alpha}$ over the approximately 4.6 Gyr age of the solar system. There are two main approaches that are used to constrain the fundamental constants using meteorites: alpha decay and beta decay. All limits in this section are calculated under the assumption that only the fine-structure constant is allowed to vary, i.e., the other fundamental constants are held fixed.

Wilkinson (1958) introduced the idea of using alpha decay to constrain the variation of constants via the abundance of radioactive isotopes in meteorite samples. Today's tightest constraints on $\frac{\Delta\alpha}{\alpha}$ from meteorite methods comes from Olive et al. (2002), who used alpha decay of samarium into neodymium to give: $\left|\frac{\Delta\alpha}{\alpha}\right| \leq \times 10^{-5}$. The decay reaction is:

$$^{147}_{62}\mathrm{Sm} \rightarrow ^{4}_{2}\mathrm{He}^{+} + ^{143}_{60}\mathrm{Nd} \tag{1.4}$$

The first researchers to measure constraints using beta decay in meteorites were Peebles & Dicke (1962). They looked at the beta decay of rhenium into osmium, specifically:

$$^{187}_{75}\mathrm{Re} \rightarrow \ ^{187}_{75}\mathrm{Os} + \bar{\nu_e} + e^{-}.$$

They constrained the variation to be less than 3 parts in 10^{13} year^{-1} assuming a linear rate of change over the age of the solar system. The current (1σ) limits are given by Olive et al. (2004) using this same decay process are: $\frac{\Delta\alpha}{\alpha} = -8 \pm 8 \times 10^{-7}$.

The situation for the meteorite measurements suffer from similar difficulties as the Oklo reactor: they depend heavily on the physical models including complicated quantum chromodynamics calculations and on a number of fundamental constants. Also, Fujii & Iwamoto (2005); Uzan (2011) point out that the average

decay rates are what is actually measured, which makes interpreting the results more difficult to quantify.

1.3.4 Cosmic Microwave Background

A high-z method of measuring the values of fundamental constants comes from the Cosmic Microwave Background (CMB). After the Big Bang, the universe expanded and cooled adiabatically. Eventually, the plasma of protons and electrons could combine into hydrogen atoms without being immediately ionized again in an event called recombination. Shortly after recombination, the photons decoupled from the plasma as the mean free path for photons became larger than the Hubble length. This resulted in the universe becoming transparent roughly 300,000 years after the Big Bang, at a redshift of $z \approx 1100$. The photons that last scattered with the plasma have been free-streaming through the universe ever since, and permeate all of space. From present day earth, we observe the 3000 K blackbody spectrum from the surface of last scattering redshifted to temperature of 2.7 K.

There are a couple of processes that a changing fine-structure constant alters at the time of recombination and decoupling. A thorough review is given by Uzan (2011), and so we limit ourselves to a brief overview. In the time before photon decoupling, photons would frequently interact with the free electrons of the surrounding plasma via Thomson scattering. The proportion of radiation that is absorbed as it goes through a medium is defined as the optical depth. The differential optical depth of photons in the early universe due to Thomson scattering is given by:

$$\dot{\tau} = x_e n c \sigma_T \tag{1.5}$$

where x_e is the proportion of free electrons n_e to n (their total number density), c

is the speed of light, and σ_T is the Thomson cross section. The Thomson scattering cross section gives the strength of the interaction between a photon and a free electron, and is defined as:

$$\sigma_T = \frac{8\pi}{3}\frac{\hbar^2}{m_e^2 c^2}\alpha^2. \tag{1.6}$$

The dependence on α^2 is explicit. There are many consequences for the CMB with a non-zero $\frac{\Delta\alpha}{\alpha}$, but we focus on the largest effects. A larger value for α would result in stronger electromagnetic interactions. The binding energy of hydrogen scales as $m_e\alpha^2$, and thus, hydrogen would form more easily and more strongly, and consequently, it would take a higher energy photon to ionize. These two effects mean that neutral hydrogen forms when the universe is younger and hotter. The universe became transparent when the photon mean-free path length grew larger than the Hubble length. A nonzero $\frac{\Delta\alpha}{\alpha}$ would imply that the universe would become transparent earlier and the surface of last scattering would occur at a higher redshift (younger universe). An earlier decoupling means the sound horizon is smaller, and this shifts the C_l spectrum of the CMB to higher multipoles. Since the smaller scales are frozen into the CMB, there is a larger signal in the higher multipoles. A visualization of the theoretical measured difference is given in Figure 1.4.

The current limits on the fundamental constants are given by Landau & Scóccola (2010), who gets a value of: $\alpha_z/\alpha_0 = 0.986 \pm 0.007$ (where they use the value of α at the CMB divided by the current value – a value of 1 is consistent with no change). They combined the WMAP-7yr data release with the measured value of the Hubble constant, H_0 from (Riess et al., 2009). They also combined the WMAP-7yr data release with the power spectrum measured by the Sloan Digital Sky Survey Luminous Red Galaxies (Reid et al., 2010). Landau & Scóccola (2010) stressed that their constraints are limited by the significant degeneracies between α,

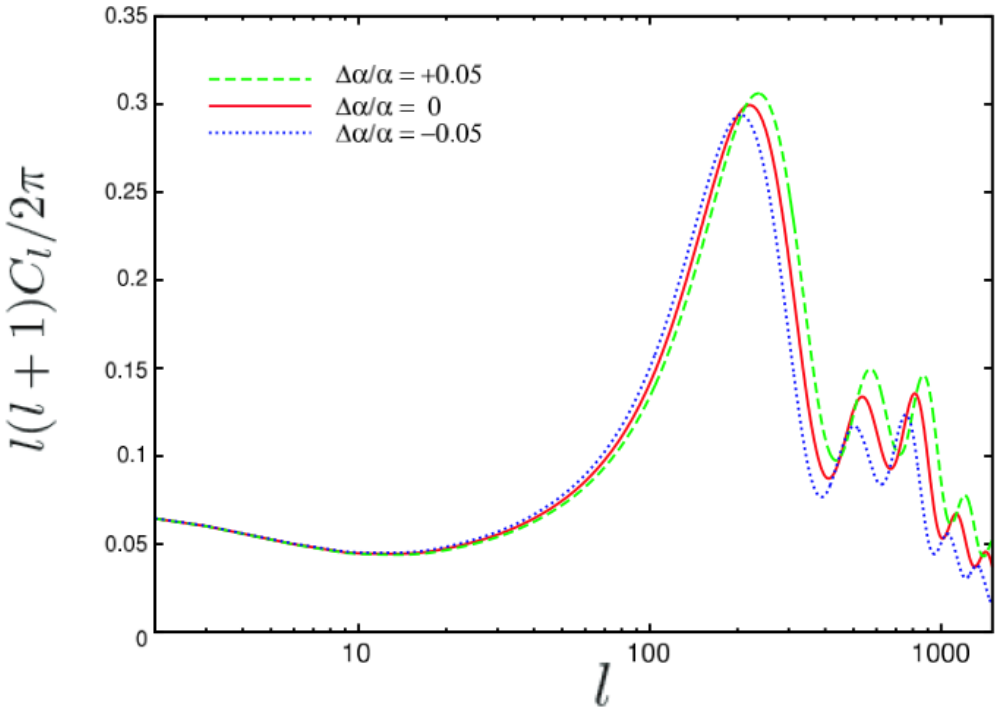

Figure 1.4 Figure 5 of Ichikawa et al. (2006) showing the effect of a non-constant $\frac{\Delta\alpha}{\alpha}$ on the the CMB fluctuations. Source: (Ichikawa et al., 2006).

H_0 and m_e. A figure of the confidence levels of measuring H_0 and α_z/α_0 is shown in Figure 1.5.

1.3.5 Big Bang Nucleosynthesis

The longest time interval that has been used to constrain fundamental constants comes from Big Bang Nucleosynthesis (BBN). Occurring in the first few minutes after the Big Bang, BBN allows a probe of fundamental physics at a redshift of $z \approx 10^8$. However, there are many effects that have to be modeled together in order to get a value. Taking into account the slight discrepancies between primordial abundances of deuterium, ^{4}He, and ^{7}Li and the predictions of standard BBN, Ichikawa & Kawasaki (2004) find the simultaneous existence of both a non-zero $\frac{\Delta\alpha}{\alpha}$ and a nonstandard expansion rate yields a consistent result. The dependencies on multiple fundamental constants and on the underlying physical models make it difficult to constrain their potential variation very precisely, and the current limits on a changing fine-structure constant remain around 10^{-2} level.

1.4 Atomic Physics as a Fine-Structure Constancy Probe

The tests of the fundamental constants that we will focus on rely heavily on atomic physics, so we begin with background principles and notation. When referring to the ionization state of atoms, the standard method is to begin with Roman numeral I for the neutral atom, and to count up with each increasingly ionized state. Neutral hydrogen is: H I; singly ionized hydrogen is: H II, and so on.

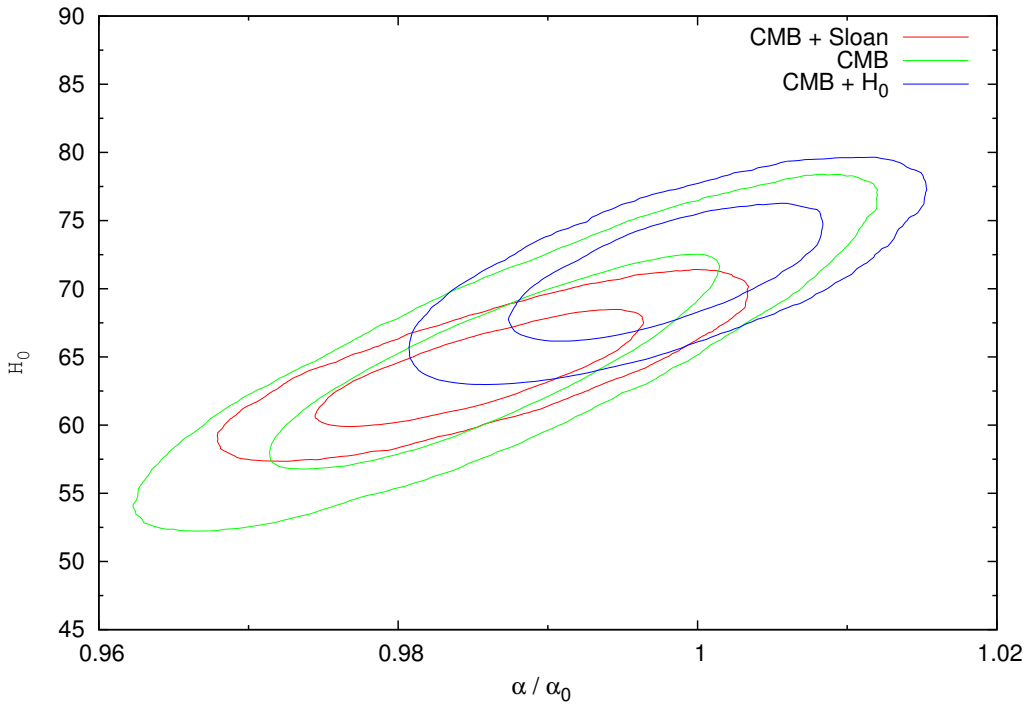

Figure 1.5 Figure 1 of Landau & Scóccola (2010), showing the constraint on α_z/α versus H_0 when only α is allowed to vary. The two levels of curves are the 68% and 95% confidence level contours for each color shown. The red curves show the result of the CMB data and the Sloan data used together (Reid et al., 2010). The green curves give the intervals for the CMB measurement on its own. Finally, the green curves show the result from the CMB data and the H_0 taken from (Riess et al., 2009) Source: (Landau & Scóccola, 2010).

1.4.1 Quasar Absorption Spectra

Quasar absorption spectra give us a unique method of measuring fundamental physics in regions that are remote in both space and time. The methods that have been employed for measuring $\frac{\Delta\alpha}{\alpha}$ are simpler than many of the methods in § 1.3. The shifts that have to be calculated avoid the complicated physics that encumbers measurements that rely on nuclear physics. The effects come from atomic physics, and while complicated, avoid the quantum chromodynamics of nuclear physics and remain in the domain of quantum electrodynamics. Since the majority of our work involves the use of quasar absorption lines as a probe of fundamental extragalactic physics, the physical phenomenon should be explained with some detail.

A quasar is a very luminosity active galactic nucleus that emits electromagnetic radiation at comparable intensities over a large wavelength range. This feature simplifies detecting and characterizing absorption lines due to interactions with intervening gas clouds. As seen from the earth, the background quasar light excites electrons of the metal atoms in clouds of gas in the line-of-sight to the quasar from the earth. This excited atom then reradiates the photon in a random direction leaving a deficit of photons at the wavelength of that transition relative to the surrounding wavelengths. Resonance scattering by atomic metals in the intervening gas thus imposes dark bands onto the continuum of the quasar.

1.4.2 Alkali Doublet Method

We begin our discussion of the Alkali Doublet method by considering the most simple atomic system, atomic hydrogen, and refine the model incrementally to attain a more physically accurate understanding. Atomic hydrogen consists

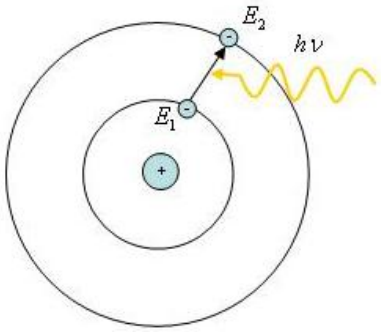

Figure 1.6 A cartoon of an electron getting kicked into an excited state via photoabsorption. Source: `http://www.thespectroscopynet.eu/Index.php?Physical_Background:Atomic_Emission:Transition_Moments`.

of a single electron orbiting a single proton. The energy levels of atoms depend sensitively on the value of the fine-structure constant. To first order, the energy of the electron orbital states in a hydrogen-like atom is:

$$E_n = -\frac{m\alpha^2}{2}\frac{Z^2}{n^2}. \tag{1.7}$$

The m is the mass of the electron, Z is the charge of the bare nucleus and n is the principle quantum number. As you can see from Eq. 1.7, a change in the fine-structure constant would be equivalent to multiplying the energy levels by an overall constant. A multiplicative shift of energy levels is degenerate with the cosmological redshift of the system, thus, one cannot determine a change in α considering effects from this equation alone. However, higher order corrections to the energy level spacings are sensitive to changes in the fine-structure constant in different ways relative to each other. The quasar absorption techniques to measure $\frac{\Delta\alpha}{\alpha}$ take advantage of that fact, and so we consider the next order energy level

corrections. We begin with the following modification to the Hamiltonian:

$$H = H_0 + H_{\text{kinetic}} + H_{\text{SO}} + H_{\text{Darwin}}. \tag{1.8}$$

Following the derivation given in Bransden & Joachain (2003), the first order correction to the kinetic energy term gives:

$$H_{\text{kinetic}} = -\frac{p^4}{8m^3c^2}, \tag{1.9}$$

which leads to energy correction of:

$$\Delta E_{\text{kinetic}} = -E_N \frac{(Z\alpha)^2}{n^2}\left[\frac{3}{4} - \frac{n}{l+1/2}\right]. \tag{1.10}$$

The n is the principle quantum number and l is the orbital angular momentum. The second term of the correction comes from considering the spin-orbit interaction of the outer most electron. The spin-orbit correction term in the Hamiltonian is:

$$H_{\text{SO}} = \frac{Z\alpha\hbar}{2m^2c}\frac{1}{r^3}\mathbf{L}\cdot\mathbf{S}, \tag{1.11}$$

with the energy correction:

$$\Delta E_{\text{SO}} = -E_N \frac{(Z\alpha)^2}{2nl(l+1/2)(l+1)} \times \begin{cases} l & j = l + 1/2 \\ -l-1 & j = l - 1/2. \end{cases} \tag{1.12}$$

The j term is the total angular momentum. Finally, the Darwin term:

$$H_{\text{Darwin}} = \frac{\pi\hbar^3}{2m_e^2c}\left(Z\alpha\right)\delta^3(\vec{r}) \tag{1.13}$$

leads to the following energy correction:

$$\Delta E_{\text{Darwin}} = -E_N \frac{(Z\alpha)^2}{n}, \quad l = 0. \tag{1.14}$$

The total energy of the electron with all of the above corrections added together is:

$$E_{nj} = E_n \left[1 + \frac{(Z\alpha)^2}{n^2} \left(\frac{n}{j+1/2} - \frac{3}{4} \right) \right] \tag{1.15}$$

The fact that j can take on different values means that the overall energy level corrections are shifted in different ways. The effect of each of these shifts is shown in Figure 1.7. We now have the basis on which to build an understanding of the complicated calculations that give rise to the atomic methods used in fine-structure measurements.

If the fine-structure constant has a different value, the relative spacing of the atomic metal line transitions would differ in theoretically calculable ways. One of the strengths of the quasar absorption line methods is the dependence on only α and not some combination of other dimensionless constants. When considering a possible change in the fine-structure constant, a natural line of investigation is the effect on the fine-structure splitting energy levels that give the constant its name. Some of the earliest limits on the possibility of a change in fundamental constants came from astronomical tests of the fine-structure energy level spacings. The alkali doublet (AD) method compares the shift in the spacing of the fine-structure energy levels of alkali atoms, and over the past few decades upper limits on variation in α were found by many different researchers.

The AD method measures a change in the fine-structure constant by the relation given by Levshakov (2004); Bahcall & Schmidt (1967) as:

$$\frac{\alpha_z}{\alpha} = \left(\frac{\Delta\lambda_z}{\langle\lambda\rangle_z} \Big/ \frac{\Delta\lambda_0}{\langle\lambda_0\rangle} \right)^{1/2}, \tag{1.16}$$

where the subscripts z and 0 are the values at redshift of z and current laboratory values, respectively, $\Delta\lambda$ is the fine-structure separation, and $\langle\lambda\rangle$ is the weighted

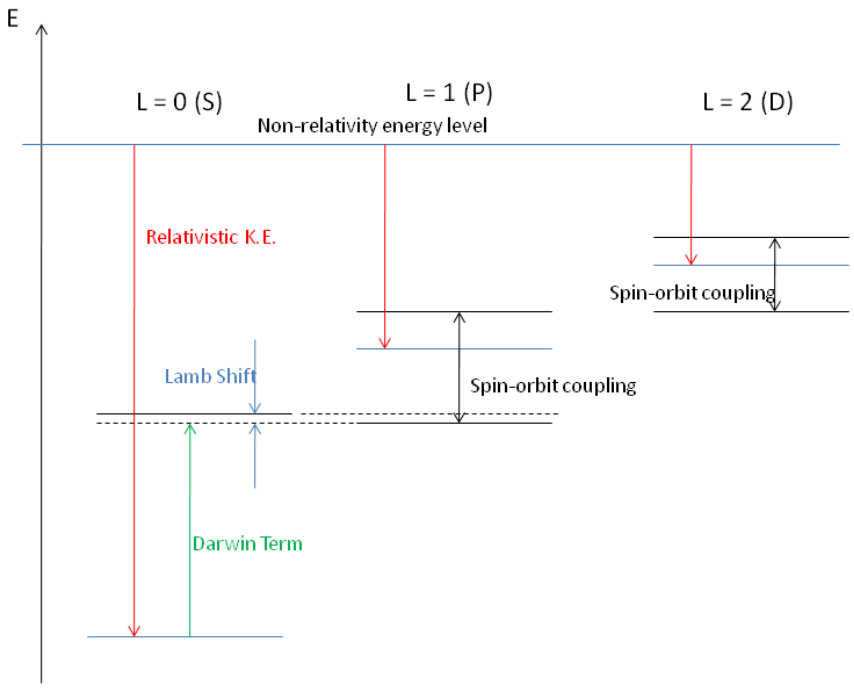

Figure 1.7 The relativistic, spin-orbit, and Darwin energy corrections to the first three orbitals of the Hydrogen atom. Source: `http://en.wikipedia.org/wiki/Fine_structure`.

mean λ for a given doublet.

The AD method was first used by Savedoff (1956) to compare the emission lines of N II and Ne III in the nearby Cygnus A galaxy. He reports a value of $\alpha_z/\alpha = 1.0036 \pm 0.0032$. Bahcall & Salpeter (1965) were the first to use the AD method on distant quasars by measuring the intrinsic emission lines from the quasars 3C 47 and 3C 147. They used the O III and Ne III transitions that occurred at the quasar itself and report a value of $d \ln \alpha^2/dt \leq 10^{-11}$ yr^{-1}. The next innovation came with Bahcall et al. (1967) using AD method on intrinsic quasar absorption (rather than emission) lines: Si II and Si IV in the quasar 3C 191 at a redshift of $z = 1.95$. He reports his constraint as $\alpha_z/\alpha = 0.98 \pm 0.05$. Using the AD method on the absorption features of a damped Lyman-α (DLA) system, Wolfe et al. (1976) innovated the use of absorption features imprinted in the intervening gas along the line-of-sight between a quasar and telescope. He quotes his limit as $|\ln \alpha/dt| \leq 4 \times 10^{-12}$ yr^{-1}.

Over the years, many more limits have been published using the AD method, and we give a summary of the latest constraints. Using the Keck-HIRES spectrograph on 21 Si IV doublet absorption features, Murphy et al. (2001b) found an upper limit of $\frac{\Delta\alpha}{\alpha} < 3.9 \times 10^{-5}$. A tighter constraint was found by Chand et al. (2005) using ESO-UVES to measure 15 Si IV doublets: $\frac{\Delta\alpha}{\alpha} = (-0.15 \pm 0.43) \times 10^{-5}$ for $1.59 \leq z \leq 2.92$. And Bahcall et al. (2004) revived the AD method on emission lines by using O III from SDSS quasars to report $\frac{\Delta\alpha}{\alpha} = (12 \pm 7) \times 10^{-5}$, see Figure 1.8.

The AD method has a number of drawbacks. The first is that the method fails to take advantage of the fact that the largest relative shift is between the ground state and the doublet, not between the doublet transitions. Second, it fails to take advantage of the remaining absorption features that would be affected by

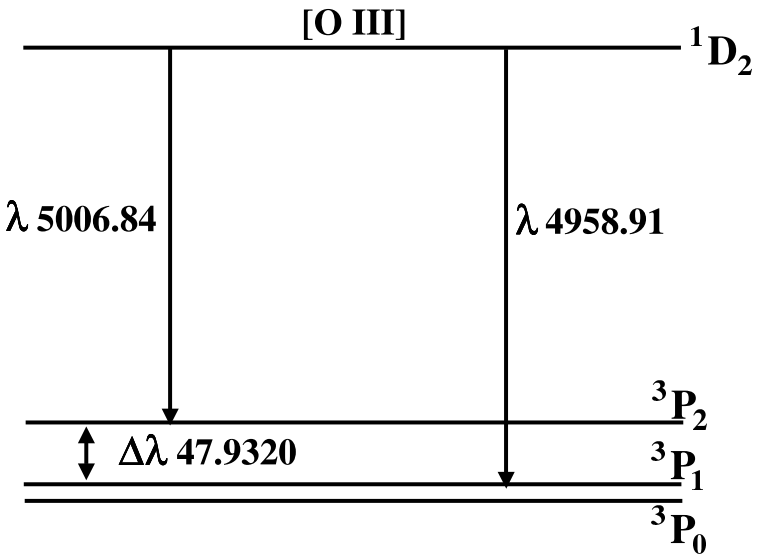

Figure 1.8 Energy level diagram for two fine-structure emission lines from excited level $^1D_2$ doubly ionized oxygen (O III). Source: Bahcall et al. (2004).

a change in $\frac{\Delta\alpha}{\alpha}$. These drawbacks are addressed by a generalization of the AD method, the Many-Multiplet method.

1.4.3 Many-Multiplet Method

The Many-Multiplet method was introduced in 1999 and allows for an order of magnitude increase in precision in the measuring the fine-structure constant for the same quality data. The method was first used by Webb et al. (1999) on a sample of 30 absorption systems. Whereas the AD method takes advantage of the relative spacing of the fine-structure doublet in a single species, the MM method utilizes the relative spacing shift of many transitions within several elements.

The Many Multiplet (MM) method takes advantage of the differential effects on the relative spacing of an atom's energy levels due to higher order contributions that arise from relativistic and many-body effects. Dzuba et al. (1999b,a) and

Webb et al. (1999) introduced the MM method, and Dzuba et al. (1999b) expressed the relativistic energy correction as the following:

$$\Delta_n = \frac{E_n \left(Z\alpha\right)^2}{\nu} \left[\frac{1}{j+1/2} - C(j,l)\right], \tag{1.17}$$

with Δ_n the relativistic energy correction, Z the charge of the nucleus, l and j are the orbital and total electron angular momenta, ν as the effective quantum number defined as $E_n = -\frac{me^4}{2\hbar^2}\frac{Z_a^2}{\nu^2}$, with $Z_a = 2$ for singly ionized atoms (1 for neutral atoms), and the $C(j,l)$ term to describe many-body effects.

The many-body correction and the relativistic correction have opposite signs for straightforward reasons. The relativistic correction increases the interaction between the electrons and the nucleus as α increases, causing the inner electron cloud to contract closer in. The contraction of the inner electron clouds increases the effective shielding of the nucleus to the outer electrons which weakens their attraction to the nucleus. The outer electrons with a high j-value have wavefunctions which peak further away from the nucleus, and the increased shielding thus decreases their binding energy.

Dzuba et al. (1999a) writes the energy correction for one multiplet as:

$$\begin{aligned} E = E_0 + Q_1 \left[\left(\frac{\alpha_z}{\alpha}\right)^2 - 1\right] + Q_2 \left[\left(\frac{\alpha_z}{\alpha}\right)^4 - 1\right] \\ + K_1 (\mathbf{L}\cdot\mathbf{S}) \left(\frac{\alpha_z}{\alpha}\right)^2 + K_2 \left(\mathbf{L}\cdot\mathbf{S}\right)^2 \left(\frac{\alpha_z}{\alpha}\right)^4, \end{aligned} \tag{1.18}$$

where α_z is the value of the fine-structure constant at some redshift, α is the present day value, and E_0, Q_1, and Q_2 describe the configuration center, and K_1 and K_2 describe the level splitting within one configuration.

Once they have calculated the respective dependencies, they rewrite the equation as:

$$\omega = \omega_0 + q_1 x + q_2 y \tag{1.19}$$

with $\omega_0 = E_0 + K_1(\mathbf{L}\cdot\mathbf{S}) + K_2(\mathbf{L}\cdot\mathbf{S})^2$, $x = (\alpha_z/\alpha) - 1$, $y = (\alpha_z/\alpha)^2 - 1$, $q_1 = Q_1 + K_1(\mathbf{L}\cdot\mathbf{S})$, and $q_2 = Q_2 + K_2(\mathbf{L}\cdot\mathbf{S})^2$. The relativistic corrections scale as Z^2, and so are larger in heavier atoms. Their analysis predicts that different transitions will react to a change in the fine-structure constant in different ways. The q-coefficient for each transition gives the direction and sensitivity of that transition to a change in the fine-structure constant. One way to visualize this dependence is in Figure 1.9.

1.5 Review of Claimed Detections

Quasar absorption lines measured by high resolution spectrographs on the world's largest optical telescopes give one of the most promising probes into measuring whether the value of the fine-structure constant has changed over cosmological times. Analysis of the quasar absorption spectra enable accurate measurements of atomic physics at cosmological times and distances from the local universe. We review the measurements and controversy around the reported detection of a non-zero $\frac{\Delta\alpha}{\alpha}$ using the MM method on quasar absorption spectra. The two main telescopes that have been used in the search for a changing fine-structure constant have been the Keck telescope in Hawaii, and the VLT telescope in Chile. Over the past decade, the published results have ranged from detecting a significant change in the fine-structure constant to measurements that claim to rule out the previous detection. The claim to have measured a change in α is extraordinary and requires extraordinary evidence. We can break the earlier results into two main categories: groups using the Keck-HIRES spectrograph, and groups using the VLT-UVES spectrograph. We conclude with the most recent analyses using both

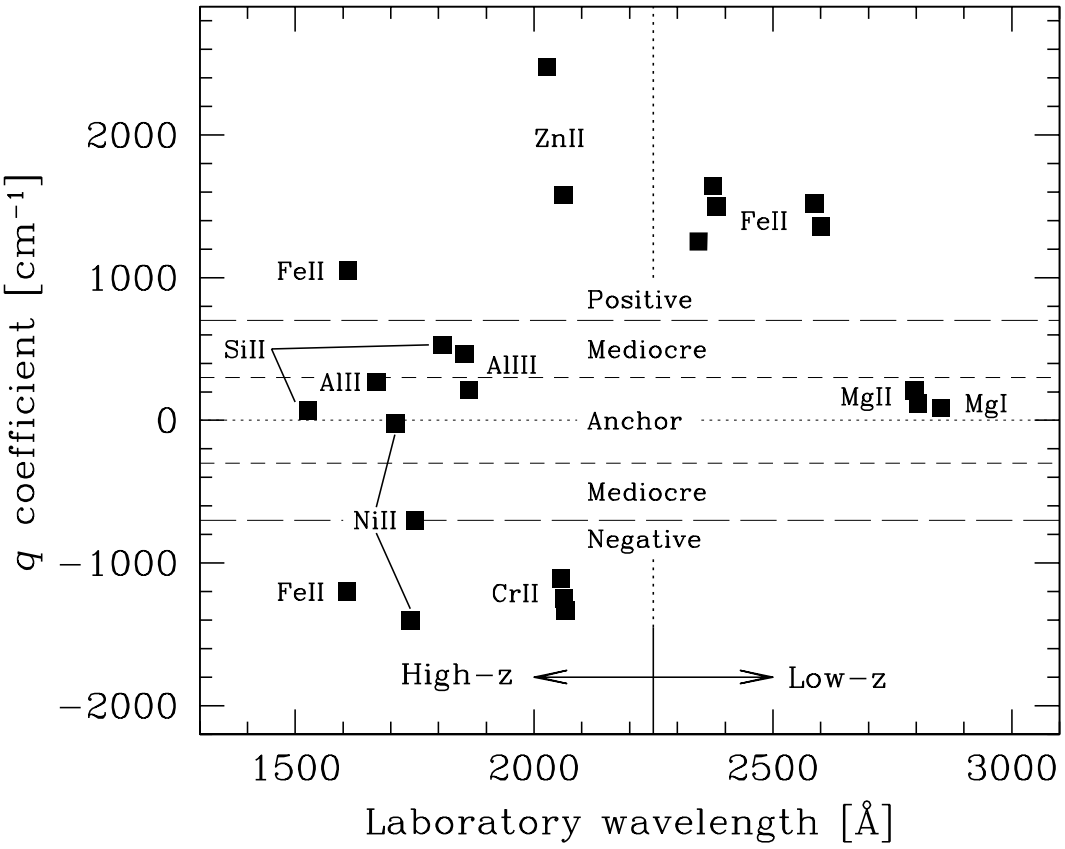

Figure 1.9 The range of sensitivities (q) of specific transitions to a change in the fine-structure constant is shown for a number of transitions regularly observed. Notice that the magnesium (Mg) transitions are relatively unchanged (close to the zero line), while the iron (Fe) transitions appear far above and below the zero line. Source: Murphy et al. (2004).

Figure 1.10 The two 10 meter Keck telescopes atop Mauna Kea, Hawaii. Source: `http://www.nasa.gov/centers/jpl/images/content/92208main_pia04493-browse.jpg`.

telescopes.

1.5.1 Keck-HIRES

The Keck Observatory has two 10 meter telescopes located at the Mauna Kea, Hawaii, see Figure 1.10. The primary mirror is 10 meters in diameter and composed of hexagonal segments. The instrument used for quasar absorption spectra is the high resolution echelle spectrometer (HIRES). An exposure with HIRES is captured on a CCD after HIRES disperses the incoming light. We will return to the instrument in detail in § 2.1.

Beginning with a statistical analysis of 30 absorption systems and using the Many-Multiplet method for the first time, Webb et al. (1999) reported a result

$$\frac{\Delta\alpha}{\alpha} = (-11 \pm 4) \times 10^{-6}. \tag{1.20}$$

In the years immediately following, Murphy et al. (2001a); Webb et al. (2001) analyzed 49 systems covering a redshift range of $0.5 < z < 3.5$ and reported their

result:

$$(-7.2 \pm 1.8) \times 10^{-6} \tag{1.21}$$

The size of the statistical sample and the redshift ranges covered grew to 128 systems with Murphy et al. (2003) claiming:

$$(-5.43 \pm 1.16) \times 10^{-6} \tag{1.22}$$

over a redshift range of $0.2 < z < 3.7$. Finally, Murphy et al. (2004) reported their most robust measurement by analyzing 143 quasar absorption systems, concluding a $\frac{\Delta\alpha}{\alpha} = (-0.57 \pm 0.11) \times 10^{-5}$ over a redshift range of $0.2 < z < 4.2$, see Figure 1.11. Criticism of this measurement by Molaro et al. (2008b) claims that Murphy et al. (2003) does not fall off as the expected $\sigma/\sqrt{N}$, suggesting their reported weighted average should be:

$$\frac{\Delta\alpha}{\alpha} = (-3.9 \pm 1.5) \times 10^{-6}, \tag{1.23}$$

due to unaccounted for systematic errors.

1.5.2 VLT-UVES

The European Southern Observatory has four 8.2 meter telescopes located at Cerro Paranal, Chile, see Figure 1.12. The instrument used to measure quasar absorption spectra is the UVES (Ultraviolet and Visual Echelle Spectrograph) on the VLT (Very Large Telescope). We return to the instrument in detail in § 3.1.

There has been controversy over the published detections, especially when considering data taken by the VLT-UVES. An analysis of a statistical sample of quasar absorption systems taken with VLT-UVES by Chand et al. (2004); Srianand et al. (2004) found a limit on $\frac{\Delta\alpha}{\alpha}$ that was inconsistent with measurements

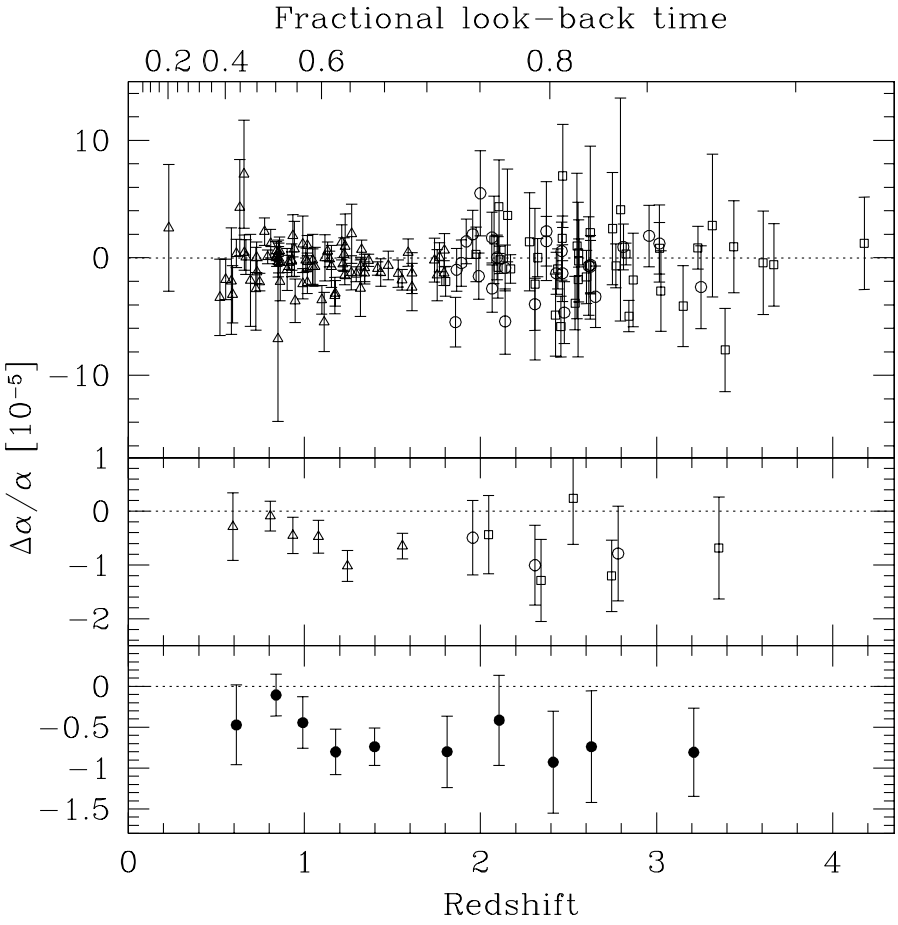

Figure 1.11 Murphy et al. (2004)'s most robust estimate. They present the results with several sub-samples highlighted: low-z sample (triangles), low-contrast (squares), and high-contrast (squares). The weighted binned results are the lower panel. $\frac{\Delta\alpha}{\alpha} = (-5.7 \pm 1.1) \times 10^{-6}$ with redshift $z \approx (.2 - 4.2)$. Source: Murphy et al. (2004).

Figure 1.12 The four 8.2 meter telescopes that comprise the VLT, Cerro Paranal, Chile. Source: `http://www.eso.org/public/archives/images/screen/esopia00079sites.jpg`.

being made with Keck. They find that for 23 systems covering a redshift range $0.4 < z < 2.3$,

$$\frac{\Delta\alpha}{\alpha} = (-0.6 \pm 0.6) \times 10^{-6}, \tag{1.24}$$

which is consistent with no change in $\frac{\Delta\alpha}{\alpha}$. Also, Levshakov et al. (2006) found a similar result using a method they called SIDAM (single-ion differential α measurement),

$$\frac{\Delta\alpha}{\alpha} = (0.4 \pm 1.5\text{stat}) \times 10^{-6} \;\; 1\sigma, \tag{1.25}$$

for analysis done on a single absorber (HE0515–4414) at redshift of $z = 1.15$.

The above VLT-UVES analysis was criticized by Murphy et al. (2008b) for statistically unsound analysis, claiming that the published results are statistically impossible based on the statistical quality of the data itself. Murphy et al. (2004)'s contention is demonstrated in Figure 1.14, where their measurements are compared to Chand et al. (2004) and Levshakov et al. (2006). The figure demonstrates that several of the claimed measurements fall into a statistically "forbidden region."

They calculate the forbidden region by analyzing the Fisher information of the data and the fit models used in the respective analysis. Detections that lie within the forbidden region claim statistical errors less than the data and model statistically allow. Further, Murphy et al. (2008b) argue that the very rough χ^2 curves published by Chand et al. (2004) indicate that the fitting procedure was failing, see Figure 1.13. Reanalysis was done on Chand et al. (2004)'s results by Murphy et al. (2008a), and they find that using the same data and profile fits, a better fit is:

$$\frac{\Delta\alpha}{\alpha} = (-0.64 \pm 0.36) \times 10^{-5}, \tag{1.26}$$

although they caution that a better fit to the data is required before the result should be believed. Finally, Srianand et al. (2009) responded to the criticism by refitting the Chand et al. (2004) using VPFIT (the program used by Murphy et al. (2008a)) and they get a limit of

$$\frac{\Delta\alpha}{\alpha} = (0.1 \pm 1.5) \times 10^{-6} \tag{1.27}$$

after excluding 2 of the 23 systems that showed a variation in $\frac{\Delta\alpha}{\alpha}$ of more than 4σ. In response, Molaro et al. (2008b) reanalyzed Levshakov et al. (2006) and increased the bounds to $\frac{\Delta\alpha}{\alpha} = (0.12 \pm 1.79) \times 10^{-6}$ at redshift $z = 1.15$ towards HE0515-4414 and $\frac{\Delta\alpha}{\alpha} = 5.66 \pm 2.67 \times 10^{-6}$ at redshift $z = 1.84$ towards Q1101-264.

1.5.3 Current Status

In an attempt to use both Keck and VLT telescopes, Webb et al. (2010) claim a detection of a spatial dipole in the value of the fine-structure constant. The claim is that in one direction in the past, the fine-structure constant had a larger value, while in the other direction, the value was smaller. In fact, they claim that

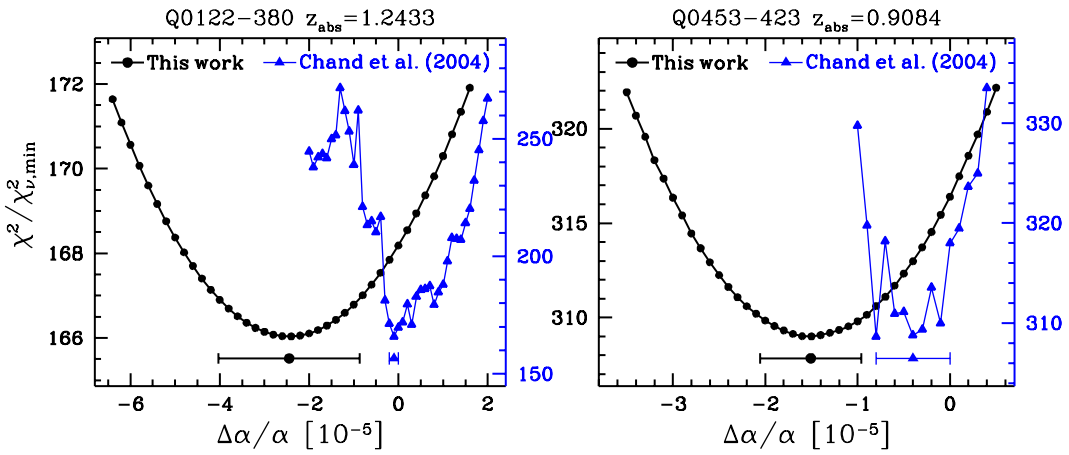

Figure 1.13 χ^2 for Chand et al. (2004) compared with Murphy et al. (2008a) (which is labeled as "this work" in the figure). Source: (Murphy et al., 2008a).

using each telescope independently yields a self-consistent dipole measurement in the same direction as shown in Figure 1.15. This means that using either telescope independently, a dipole measurement is found. Further, each independent dipole points in the same direction.

A source of known systematic error in the MM method is the potential to mischaracterize the isotope abundance of elements like magnesium. Ashenfelter et al. (2004) argued that the MM method would identify an isotope abundance that was substantially different from the assumed terrestrial values of ^{24}Mg:^{25}Mg:^{26}Mg $= 79 : 10 : 11$, as a variation in the fine-structure constant. Finally, a recent paper by Agafonova et al. (2011) claims that one of the quasar absorption systems toward quasar HE0515-4414 has a different isotope abundance than terrestrial. This fact leads them to argue that the $\frac{\Delta\alpha}{\alpha}$ measured in this system first by Chand et al. (2004) and later by Murphy et al. (2008a) is "obviously a consequence of the unaccounted Mg isotope shift," (Agafonova et al., 2011). There remains controversy about the

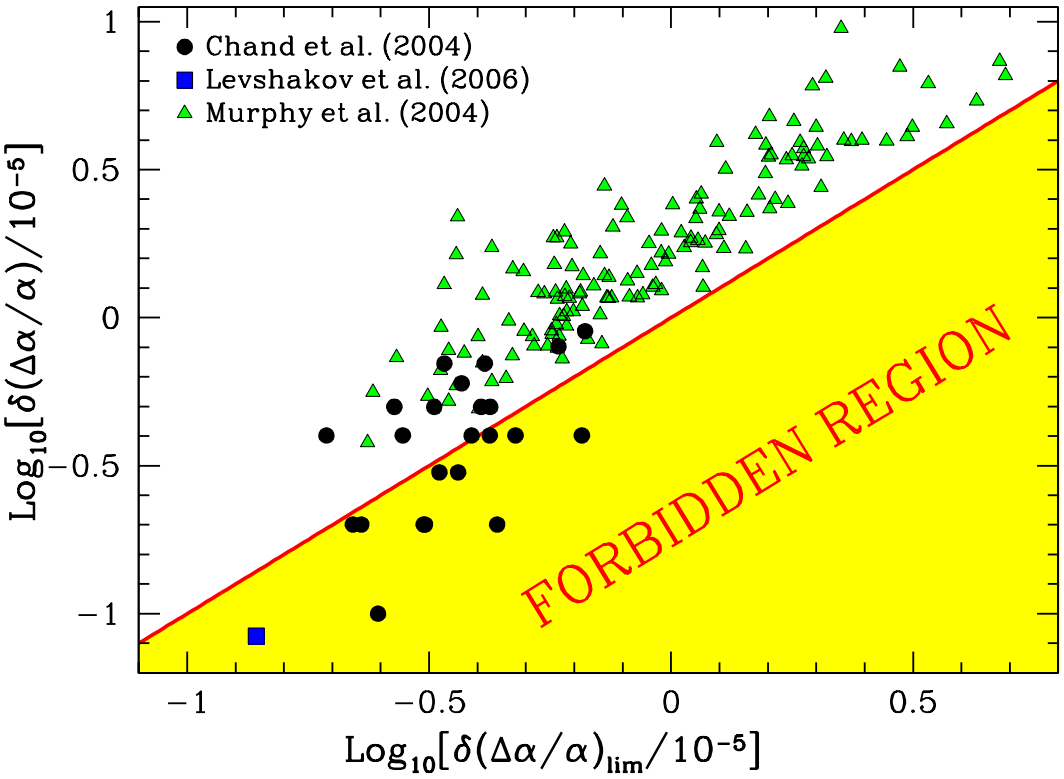

Figure 1.14 Comparison of claimed errors against limiting statistical error. Source: (Murphy et al., 2008a).

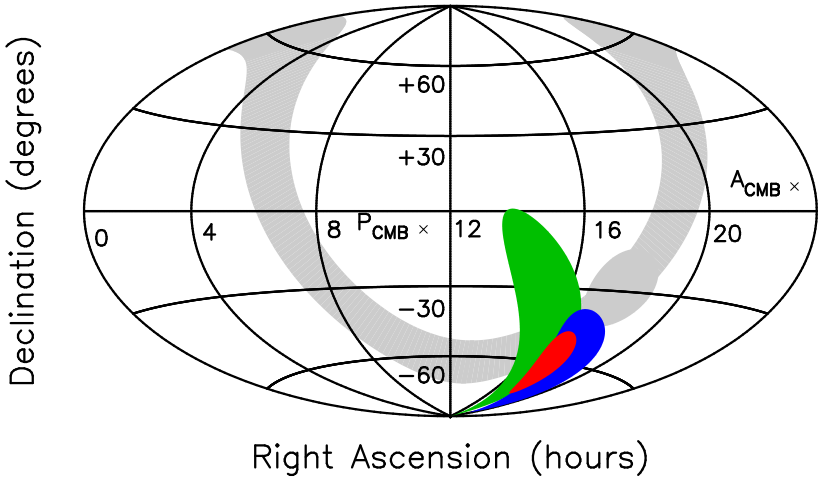

Figure 1.15 The 1σ best fit contours for the dipole measurements of Keck (green) and VLT (blue) telescopes, and their combined data (red). Source: Webb et al. (2010).

status of $\frac{\Delta\alpha}{\alpha}$ as measured in quasar absorption spectra.

Bibliography

Agafonova, I. I., Molaro, P., Levshakov, S. A., & Hou, J. L. 2011, Astronomy and Astrophysics, 529, 28

Ashenfelter, T. P., Mathews, G. J., & Olive, K. A. 2004, The Astrophysical Journal, 615, 82

Bahcall, J. N. & Salpeter, E. E. 1965, Astrophysical Journal, 142, 1677

Bahcall, J. N., Sargent, W. L. W., & Schmidt, M. 1967, Astrophysical Journal, 149, L11

Bahcall, J. N. & Schmidt, M. 1967, Physical Review Letters, 19, 1294

Bahcall, J. N., Steinhardt, C. L., & Schlegel, D. 2004, The Astrophysical Journal, 600, 520, published in: Astrophys.J.600:520,2004 Added analysis of larger quasar sample from SDSS Data Release One. Accepted for publication ApJ

Beaver, E. A., Burbidge, E. M., McIlwain, C. E., Epps, H. W., & Strittmatter, P. A. 1972, The Astrophysical Journal, 178, 95

Bransden, B. H. & Joachain, C. J. 2003, Physics of Atoms and Molecules, 2nd edn. (Benjamin Cummings), book on Atomic Physics from UCSD library.

Butler, R. P., Marcy, G. W., Williams, E., McCarthy, C., Dosanjh, P., & Vogt, S. S. 1996, Publications of the Astronomical Society of the Pacific, 108, 500

Carswell, R. F., Webb, J. K., Cooke, A. J., & Irwin, M. J. 2008, VPFIT 9.5, `http://www.ast.cam.ac.uk/~rfc/vpfit.html`

Chand, H., Petitjean, P., Srianand, R., & Aracil, B. 2005, Astronomy and Astrophysics, 430, 47

Chand, H., Srianand, R., Petitjean, P., & Aracil, B. 2004, Astronomy and Astrophysics, 417, 853

Dirac, P. A. M. 1937, Nature, 139, 323

Dirac, P. A. M. 1938, in Proceedings of the Royal Society of London. Series A, 199–208

Dzuba, V. A., Flambaum, V. V., & Webb, J. K. 1999a, Physical Review A (Atomic, 59, 230

—. 1999b, Physical Review Letters, 82, 888

Edlén, B. 1966, Metrologia, 2, 71

Flambaum, V. V. 2008, The European Physical Journal Special Topics, 163, 159

Fujii, Y. & Iwamoto, A. 2005, Modern Physics Letters A, 20, 2417

García-Berro, E., Isern, J., & Kubyshin, Y. A. 2007, The Astronomy and Astrophysics Review, 14, 113

Gould, C. R., Sharapov, E. I., & Lamoreaux, S. K. 2006, Physical Review C, 74, 24607

Griest, K., Whitmore, J. B., Wolfe, A. M., Prochaska, J. X., Howk, J. C., & Marcy, G. W. 2010, The Astrophysical Journal, 708, 158

Ichikawa, K., Kanzaki, T., & Kawasaki, M. 2006, Physical Review D, 74, 23515

Ichikawa, K. & Kawasaki, M. 2004, Physical Review D, 69, 123506

Kaluza, T. 1921, Sitz Preuss Akad Wiss Phys Math

Kaufer, A., D'Odorico, S., Kaper, L., Ledoux, C., & James, G. 2007, Very Large Telescope Paranal Science Operations UV-Visual Echelle Spectrograph User manual, issue 82 edn.

Klein, O. 1926, Zeitschrift für Physik, 37, 895

Landau, S. J. & Scóccola, G. 2010, Astronomy and Astrophysics, 517, 62

Levshakov, S. A. 2004, Lecture Notes in Physics, 648, 151

Levshakov, S. A., Centurión, M., Molaro, P., D'Odorico, S., Reimers, D., Quast, R., & Pollmann, M. 2006, Astronomy and Astrophysics, 449, 879

Lorén-Aguilar, P., García-Berro, E., Isern, J., & Kubyshin, Y. A. 2003, Classical and Quantum Gravity, 20, 3885

Mohr, P. J., Taylor, B. N., & Newell, D. B. 2006, The 2006 CODATA Recommended Values of the Fundamental Physical Constants, `http://physics.nist.gov/constants`, this database was developed by J. Baker, M. Douma, and S. Kotochigova. National Institute of Standards and Technology, Gaithersburg, MD 20899. [Online; accessed 2011-03-15]

Molaro, P., Levshakov, S. A., Monai, S., Centurión, M., Bonifacio, P., D'Odorico, S., & Monaco, L. 2008a, Astronomy and Astrophysics, 481, 559

Molaro, P., Reimers, D., Agafonova, I. I., & Levshakov, S. A. 2008b, European Physical Journal Special Topics, 163, 173

Murphy, M. T., Flambaum, V. V., Webb, J. K., & al, e. 2004, Lecture Notes in Physics, 648, 131

Murphy, M. T., Tzanavaris, P., Webb, J. K., & Lovis, C. 2007, Monthly Notices of the Royal Astronomical Society, 378, 221

Murphy, M. T., Webb, J. K., & Flambaum, V. V. 2003, Monthly Notices of the Royal Astronomical Society, 345, 609

—. 2008a, Monthly Notices of the Royal Astronomical Society, 384, 1053

—. 2008b, Precision Spectroscopy in Astrophysics, 95

Murphy, M. T., Webb, J. K., Flambaum, V. V., Dzuba, V. A., Churchill, C. W., Prochaska, J. X., Barrow, J. D., & Wolfe, A. M. 2001a, Monthly Notices of the Royal Astronomical Society, 327, 1208

Murphy, M. T., Webb, J. K., Flambaum, V. V., Prochaska, J. X., & Wolfe, A. M. 2001b, Monthly Notices of the Royal Astronomical Society, 327, 1237

Naudet, R. 1974, Bull. Inf. Sci. Tech. (Paris)., no. 193, pp. 7-45

Olive, K. A., Pospelov, M., Qian, Y.-Z., Coc, A., Cassé, M., & Vangioni-Flam, E. 2002, Physical Review D, 66, 45022

Olive, K. A., Pospelov, M., Qian, Y.-Z., Manhès, G., Vangioni-Flam, E., Coc, A., & Cassé, M. 2004, Physical Review D, 69, 27701

Osterbrock, D. E., Waters, R. T., Barlow, T. A., Slanger, T. G., & Cosby, P. C. 2000, The Publications of the Astronomical Society of the Pacific, 112, 733

Peebles, P. J. & Dicke, R. H. 1962, Physical Review, 128, 2006

Peik, E., Lipphardt, B., Schnatz, H., Tamm, C., Weyers, S., & Wynands, R. 2008, THE ELEVENTH MARCEL GROSSMANN MEETING On Recent Developments in Theoretical and Experimental General Relativity, 941

Petrov, Y. V., Nazarov, A. I., Onegin, M. S., Petrov, V. Y., & Sakhnovsky, E. G. 2006, Physical Review C, 74, 64610

Reid, B. A., Percival, W. J., Eisenstein, D. J., Verde, L., Spergel, D. N., Skibba, R. A., Bahcall, N. A., Budavari, T., Frieman, J. A., Fukugita, M., Gott, J. R., Gunn, J. E., Ivezić, Z., Knapp, G. R., Kron, R. G., Lupton, R. H., McKay, T. A., Meiksin, A., Nichol, R. C., Pope, A. C., Schlegel, D. J., Schneider, D. P., Stoughton, C., Strauss, M. A., Szalay, A. S., Tegmark, M., Vogeley, M. S., Weinberg, D. H., York, D. G., & Zehavi, I. 2010, Monthly Notices of the Royal Astronomical Society, 404, 60

Reynaud, S., Salomon, C., & Wolf, P. 2009, Space Science Reviews, 148, 233, 145 pages, 10 figures, Review for Living Reviews in Relativity

Riess, A. G., Macri, L., Casertano, S., Sosey, M., Lampeitl, H., Ferguson, H. C., Filippenko, A. V., Jha, S. W., Li, W., Chornock, R., & Sarkar, D. 2009, The Astrophysical Journal, 699, 539

Rosenband, T., Hume, D. B., Schmidt, P. O., Chou, C. W., Brusch, A., Lorini, L., Oskay, W. H., Drullinger, R. E., Fortier, T. M., Stalnaker, J. E., Diddams, S. A., Swann, W. C., Newbury, N. R., Itano, W. M., Wineland, D. J., & Bergquist, J. C. 2008, Science, 319, 1808

Savedoff, M. P. 1956, Nature, 178, 688

Shlyakhter, A. I. 1976, Nature, 264, 340

Srianand, R., Chand, H., Petitjean, P., & Aracil, B. 2004, Physical Review Letters, 92, 121302

Srianand, R., Petitjean, P., Chand, H., Noterdaeme, P., & Gupta, N. 2009, Memorie della Società Astronomica Italiana, 80, 842

Suzuki, N., Tytler, D., Kirkman, D., O'Meara, J. M., & Lubin, D. 2003, The Publications of the Astronomical Society of the Pacific, 115, 1050

Uzan, J.-P. 2011, Living Reviews in Relativity, 14, 2

Vogt, S. S. 1994, HIRES User's Manual, `http://www2.keck.hawaii.edu/inst/hires/manual2.pdf`, [Online; accessed 2011-03-22]

Webb, J., Murphy, M., Flambaum, V., & Curran, S. 2003, Astrophysics and Space Science, 283, 565

Webb, J. K., Flambaum, V. V., Churchill, C. W., Drinkwater, M. J., & Barrow, J. D. 1999, Physical Review Letters, 82, 884

Webb, J. K., King, J. A., Murphy, M. T., Flambaum, V. V., Carswell, R. F., & Bainbridge, M. B. 2010, arXiv, 1008, 3907, 5 pages, 5 figures, submitted to Physical Review Letters

Webb, J. K., Murphy, M. T., Flambaum, V. V., Dzuba, V. A., Barrow, J. D., Churchill, C. W., Prochaska, J. X., & Wolfe, A. M. 2001, Physical Review Letters, 87, 91301

Whitmore, J. B., Murphy, M. T., & Griest, K. 2010, The Astrophysical Journal, 723, 89

Wilkinson, D. H. 1958, Philosophical Magazine, 3, 582

Wolfe, A. M., Brown, R. L., & Roberts, M. S. 1976, Physical Review Letters, 37, 179, a&AA ID. AAA018.022.121

Chapter 2

Keck-HIRES

This chapter outlines our attempt to help settle the current controversy over the status of the claimed detection of a non-zero $\frac{\Delta\alpha}{\alpha}$ using quasar absorption line measurements. We detail the specifics of HIRES in § 2.1. We then describe the data and extraction process in § 2.2. The standard method for wavelength calibrating quasar absorption spectra is reviewed in § 2.3. The iodine cell apparatus that we use is described in § 2.4, and the new method we develop to utilize it is explained in § 2.5. The results of our new method are discussed in § 2.6 and ways to implement the results are investigated in § 2.7. We attempted to get a value for $\frac{\Delta\alpha}{\alpha}$ using standard software in § 2.8. We conclude with a final § 2.9.

We attempted to measure a possible change in the fine-structure constant with three nights of Keck data. Using new software and a new observational technique of observing a damped Lyman-α (DLA) system with an iodine cell in place, we measured the redshift and relative wavelength spacing of several metal lines (Ni II, Fe II, Si II, and Al II). The iodine cell method that we developed revealed unknown wavelength calibration errors in the standard ThAr method of calibrating Keck HIRES exposures. We found errors of up to 600 m s^{-1} in a single order of a single exposure, and absolute shifts between exposures of up to 2000 m s^{-1}. The surprising wavelength miscalibrations are highly relevant to fine-structure

constant research, as the claimed detections are carried out by comparing the relative wavelength spacing between absorption features that are in the tens of m s^{-1} to a couple hundred m s^{-1}.

There are both theoretical and experimental reasons that suggest the fine-structure constant might have a changing value and there are several informative reviews in the literature (García-Berro et al., 2007; Reynaud et al., 2009). Three nights of Keck data were acquired for us by Wolfe et al. on quasar PHL957 with about half of the exposures taken with the iodine cell in place. The iodine cell imprints thousands of sharp, well-calibrated molecular absorption lines which gives us an unprecedented ability to wavelength calibrate quasar absorption features. With this supercalibrated quasar absorption spectra, we hoped to measure the absorption spectra imposed by the atomic physics of the DLA to find the value of the fine-structure constant at the time of interaction. We would then compare that value with the fine-structure constant value of today.

The value of the fine-structure constant in a DLA is determined by measuring the relative wavelength spacing of many atomic transitions in different elements. A change in the fine-structure constant is measured by comparing the values of the DLA wavelength spacing with the modern day laboratory measurements. For small changes in the value of the fine-structure constant, the wavelength shifts can be estimated by the following formula:

$$\omega_\alpha = \omega_0 + 2q\frac{\Delta\alpha}{\alpha} \tag{2.1}$$

where $\omega_0 = \frac{1}{\lambda_0}$ is the modern value for a specific atomic transition, ω_α is the value of the transition in the DLA system, q is the dependence of the frequency shift on a change in the fine-structure constant, and $\frac{\Delta\alpha}{\alpha}$ has been defined in equation 1.2. The q-values have been calculated by including relativistic and many-body effects for many absorption lines that are regularly observed in quasar spectra. See Table 2.1 for a list of values.

Table 2.1. Line Information

Transition	Echelle order	q value (cm^{-1})[a]	min σ_v (m/s) (2004 data)	Iodine cell coverage?
Fe II λ1608.45	67	$-1030 \pm 300^{*}$	25.0	yes
Fe II λ1611.20	67	$1560 \pm 500^{*}$	153	yes
Al II λ1670.79	65	$270 \pm ?^{\ddagger}$	34.0	yes
Ni II λ1709.60	63	$-20 \pm 250^{**}$	83.1	yes
Ni II λ1741.55	62	$-1400 \pm 250^{**}$	48.7	yes
Ni II λ1751.92	62	$-700 \pm 250^{**}$	70.8	yes
Si II λ1808.01	60	$520 \pm 30^{**}$	36.4	yes
Al III λ1854.72	58	$458 \pm 2^{***}$	76.0	yes
Al III λ1862.79	58	$224 \pm 1^{***}$	125	yes
Si II λ1526.71	71	$50 \pm 30^{**}$	28.8	no
Zn II λ2026.14	53	$2488 \pm 25^{\dagger}$	129	no
Zn II λ2062.66	52	$1585 \pm 25^{\dagger}$	229	no
Cr II λ2056.26	52	$-1030 \pm 150^{**}$	89.9	no
Cr II λ2062.24	52	$-1168 \pm 150^{**}$	102	no
Cr II λ2066.16	52	$-1360 \pm 150^{**}$	143	no
Fe II λ2344.21	46	$1540 \pm 400^{*}$	41.7	no

[a] q-values marked * are from Dzuba, et al (2001); marked ** from Porsev, et al (2007); marked ‡ from Murphy, et al. 2001; marked † from Savukov & Dzuba (2007); marked *** from Dzuba & Flambaum (2008).

It is important to note that for the measured transitions, each has an unique shift caused by a change in α: both in the magnitude and sign. This difference occurs because of relativistic and many-body effects that change the environment around the initial and final states of the transition. If all of the transitions all had identical dependence on a change in α, the shift due to a non-zero $\frac{\Delta\alpha}{\alpha}$ would be almost impossible to accurately disentangle from the redshift of the system.

Given the conflicting measurements explained in § 1.5, we hoped to measure the shift between Fe II λ1608/1611. First of all, these two transitions are strongly shifted by a change in α and in opposite directions. Second, they are in the same ionization state in the same element – which helps negate potential problems in combining different abundances and isotope ratios. Finally, wavelength calibration issues were thought to be at a minimum because in our exposures the two transitions are are close together near the center of the same echelle order. Murphy et al. (2004)

claims a detection of $(-5.7 \pm 1.1) \times 10^{-6}$; that would correspond to an increase in the separation of the two lines by ≈ 130 m s^{-1}. We hoped to centroid the two lines to an accuracy that would allow us to detect or rule out an effect of this magnitude. To give a sense of the size of the predicted shift, we plot the effect exaggerated by a factor of 10 in Figure 2.1.

The previous results published by Murphy et al. (2003) and Chand et al. (2004) used a statistical methods to detect a change in the fine-structure constant because their data did not have high enough signal-to-noise ratio (S/N) to measure the effect directly in a single absorption system. This means that there are several potential sources of error that could compromise their measurements: selection bias, calibration errors, and averaging errors. Our method differs mainly by the added use of the iodine cell to be able to calibrate the wavelength scale to an unprecedented accuracy and a very high S/N.

2.1 HIRES

The high resolution spectrograph (HIRES) is the primary instrument used on the Keck telescope to detect quasar absorption lines for fine-structure constant work. In order to understand the following analysis, it is important to understand the HIRES schematic shown in Fig. 2.2. The most straightforward way to introduce the components is to trace the path that the light takes once it enters the HIRES enclosure through the hatch (labeled on the lefthand side of the figure). When an exposure is being taken with the iodine cell in place, the light enters through the hatch and travels through the iodine cell. The iodine cell has molecular iodine gas held at a constant 50°C by several heaters Vogt (1994). The iodine gas imprints a

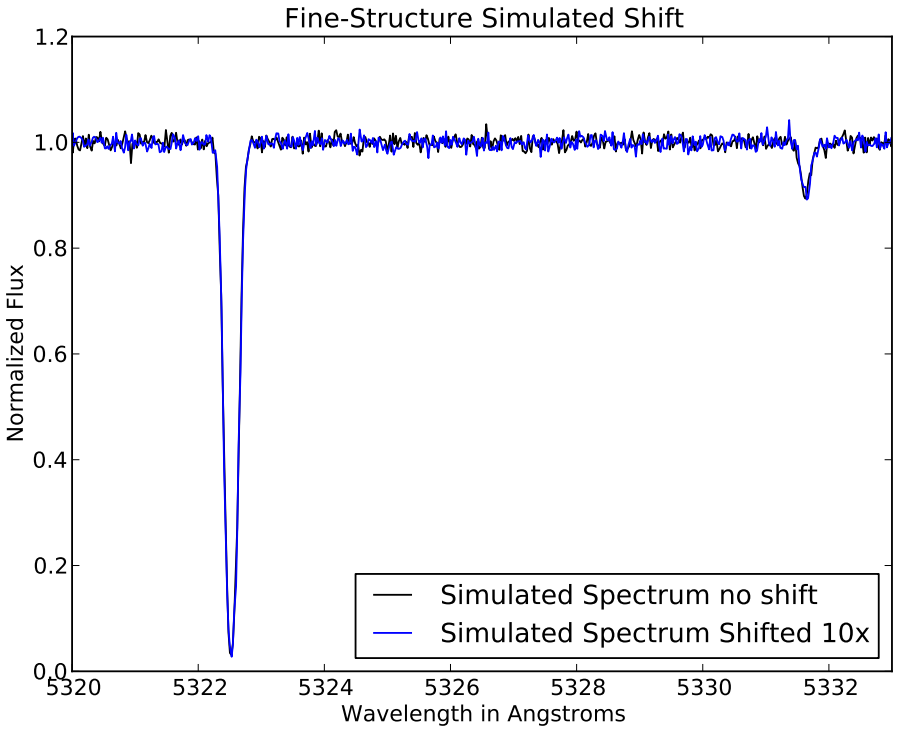

Figure 2.1 Two simulated spectra are plotted on top of each other. The black line is a simulated single component spectrum of Fe II 1608 (prominent absorption feature on left) and Fe II 1611 (small feature on the right) with a S/N of 100, column density of N(log) 14.3, and a velocity b-value of 5.0 km/s. The blue line is exactly the same as the black except that the 1611 line has been shifted by 1300 m s^{-1}. This shift is 10 times the expected amount if $\frac{\Delta\alpha}{\alpha}$ had the value measured by Murphy et al. (2004). Even with an exaggerated shift, the centroid difference is difficult to detect.

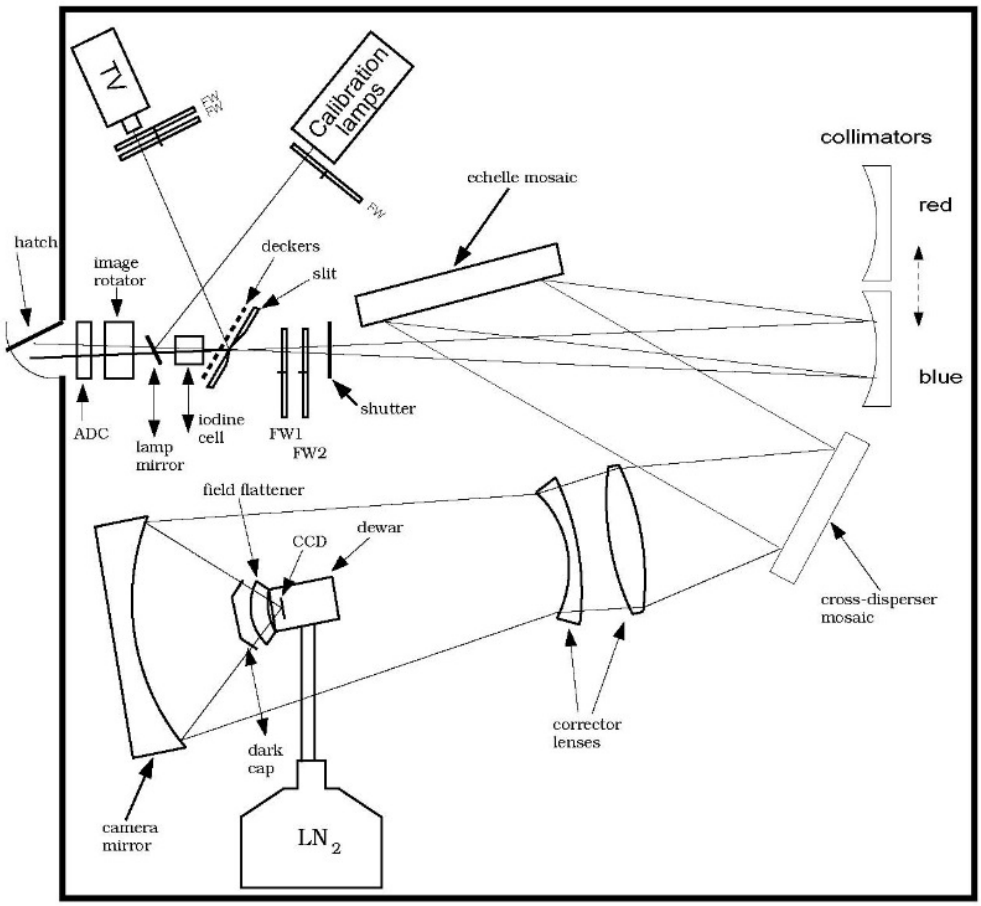

Figure 2.2 A schematic of the inside of HIRES. Source: Vogt (1994).

dense forest of very sharp and narrow absorption features on the incoming spectrum in the wavelength range of about 5000–6000Å. The light then encounters the slit which blocks the light from the sky and other astronomical objects, and selects the light from the astronomical object of interest. The light then reflects off of a collimator which narrows and aligns the incoming light into a parallel beam. There are two collimators available (red and blue), but only one is used each night. The setup that is used for the night is labeled by which collimator is being used, with the red setup called HIRESr and the blue setup HIRESb. Next the light strikes an echelle (the French word for 'row') mosaic which breaks the light into rows. The light is then spread out by reflecting off of the cross-disperser mosaic before going through a few more optics (several lenses and a camera mirror) before finally landing on the CCD. The CCD is kept at $-130°$C with liquid nitrogen. The slit size and the angles of both the echelle and cross-disperser grating are set by the observers and change depending on the astronomical object being observed. The angles are chosen such that the wavelength range of interest falls onto the CCD in favorable locations. A second schematic is included that more clearly demonstrates the light dispersion through HIRES in Figure 2.3.

When a calibration exposure is taken, the hatch is closed, and the lamp mirror (located near the iodine cell in the schematic) is rotated into place. The thorium-argon (ThAr) arc lamp is one of calibration lamps labeled at the top of the schematic. The ThAr lamp produces sharp emission lines across a large wavelength range and are reflected off of the lamp mirror (shown just before the iodine cell) and proceed through the rest of the instrument as previously described. One possible source of systematic error comes from the slightly different paths that the lamp light takes compared with the telescope light. The lamp mirror is rotated out of

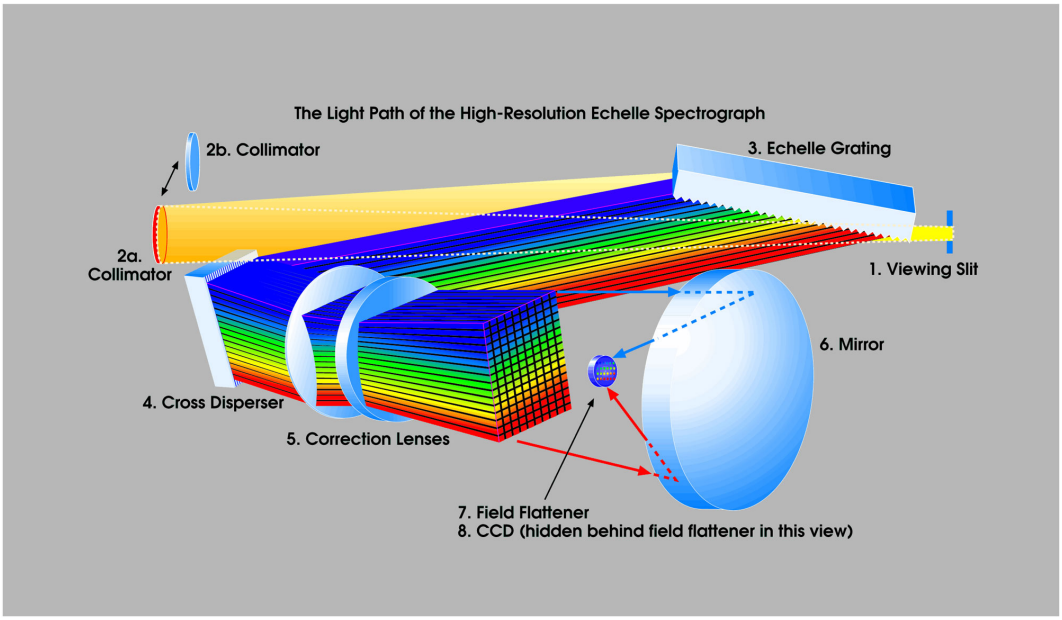

Figure 2.3 The light path through HIRES. Source: `http://www.ucolick.org/~vogt/images/hires.jpg`.

the way during astronomical observations, and rotated back in the path when the calibration exposures are being taken. The ThAr calibration exposures are taken at different times from the science exposures themselves, and this fact is an important distinction to the iodine cell methods we describe later.

2.2 Data and Extraction

We have thirteen hours of Keck exposure time on the bright (B = 16.6) quasar PHL957. The quasar is located at a redshift of $z = 2.7$ with a damped Lyα system at $z = 2.309$ (Beaver et al., 1972). Roughly half of the exposures were taken with the iodine cell in place. We include a Journal of Observation in Table 2.2. The table includes several relevant pieces of information: whether the echelle or cross disperser gratings were moved between when the ThAr calibration exposure and science exposures were taken; the temperature at the time of exposure; and whether the iodine cell was in place. We also took exposures of bright standard stars with and without the iodine cell in place. The data was taken on HIRESr with the C1 decker, the kv418 blocking filter in place, and the image rotator in vertical angle mode. When the non-iodine cell exposures are co-added, the resultant spectrum has a signal-to-noise ratio (S/N) of about 70 pixel^{-1}.

Table 2.2. Journal of PHL957 Observations

Date	ID	Iodine	Time (UT)	Exp (s)	Tempin[a] (^{0}C)	Moved?[b]	Δ Tempin (^{0}C)
3 oct 04	67/3-0	out	9:18	3600	4.26	no	0.042
3 oct 04	68/3-1	in	10:31	3600	4.21	no	0.097
3 oct 04	69/3-2	in	11:33	3600	4.07	no	0.236
3 oct 04	70/3-3	out	12:35	3600	4.00	no	.0306
4 oct 04	1096/4-0	out	9:25	3600	3.00	yes	-0.153
4 oct 04	1098/4-1	in	10:56	3600	2.97	yes	-0.125
4 oct 04	1099/4-2	in	11:57	3600	3.01	yes	-0.167
4 oct 04	1100/4-3	out	12:58	3600	2.93	yes	-0.083
5 oct 04	2094/5-0	in	8:25	3600	2.87	yes	0.125
5 oct 04	2095/5-1	out	9:27	3600	2.86	yes	0.430
5 oct 04	2096/5-2	out	10:29	3600	2.91	yes	0.375
5 oct 04	2098/5-4	out	12:32	2700	3.55	yes	-0.264

[a]Temperature inside the the HIRES enclosure.

[b]Whether or not the grating was moved between Th/Ar arc and data exposures

2.3 Standard Wavelength Calibration

We use both of the standard data reduction packages for the Keck HIRES spectrograph, XIDL HIREDUX and MAKEE, to reduce our data. Since we did not find a substantial difference between the wavelength calibration between the two packages, we only describe the process in detail for HIREDUX. HIREDUX converts the vacuum ThAr lines to air values and then fits a polynomial to the two dimensional spectrum.[1] An example of a ThAr wavelength calibration file for a single echelle order is shown in Figure 2.4. Since the measurements at Keck are made in air, the reference vacuum values have to be converted to air by fitting a wavelength scale and converting back to vacuum values using an inverse Edlen formula (Edlén, 1966). The final output is thus in vacuum wavelengths, which allows for direct comparisons between different instruments. We find that the wavelength calibrations of the independent reduction pipelines agree with each other to such a degree that we will frequently only refer to the standard method of wavelength calibration to mean the wavelength solution derived by HIREDUX.

2.4 Iodine Cell

The iodine cell at Keck has been successfully used for the Doppler method of searching for extrasolar planets. It has allowed overall wavelength calibration of $\approx 3\text{m s}^{-1}$ accuracy (Butler et al., 1996). While the planet hunters use a different procedure than we do, the motivations for using the iodine cell are essentially the same: it provides a wavelength reference frame to allow precise wavelength calibration. The standard way to wavelength calibrate the spectrograph is to take

[1] XIDL is publicly available at `http://www.ucolick.org/~xavier/IDL/index.html`

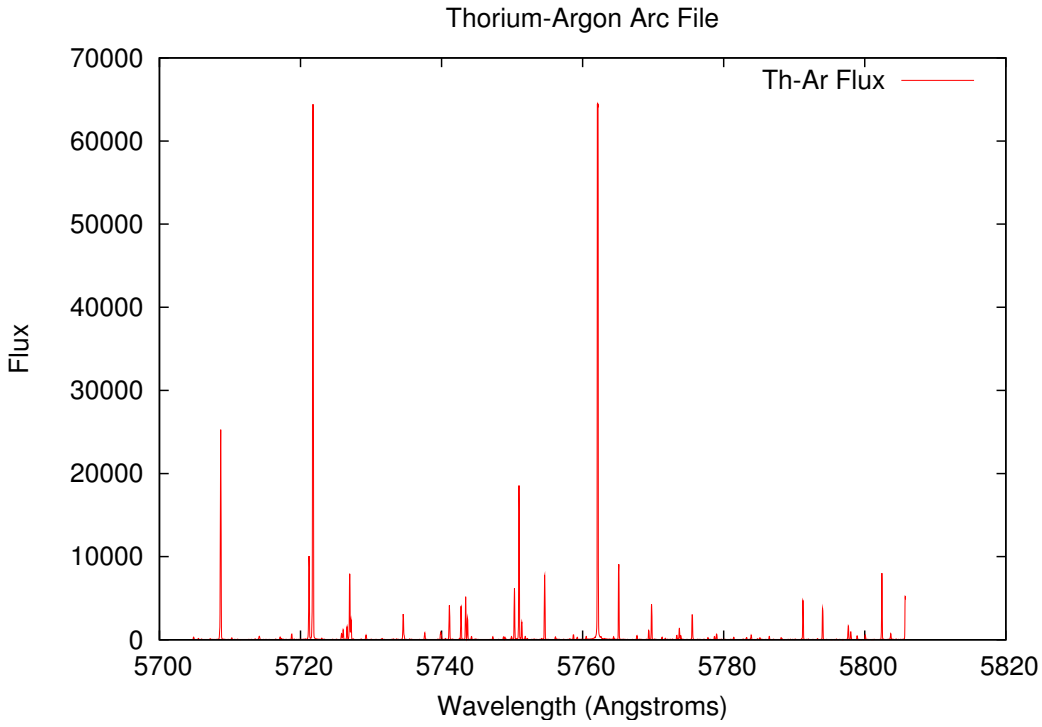

Figure 2.4 An example thorium-argon calibration file demonstrating the sharp emission lines used in the standard wavelength calibration.

an exposure of a calibration (ThAr) lamp through the same HIRES setup that the science exposure will later use. The ThAr arc lamp emits many sharp features at known wavelengths, and the location where these lines fall on the CCD is later used to extract the wavelength scale of the setup. The science exposure is taken after the calibration arc exposure, and the wavelength scale is assumed to be the same for both exposures. For most science done with Keck, this assumption is robust enough. However, for fine-structure constant work, very precise wavelength calibration is required, and it is not clear that ThAr calibration is good enough.

There are several drawbacks to the standard ThAr calibration. First, the science and calibration exposures are taken at different times. Quasar exposures typically have integration times of thousands of seconds, which means that there is ample time for conditions to change in undetected ways. For example, systematic errors that might accrue could come from changes in the atmospheric dispersion, changes in the internal air temperature, or slit guiding errors during the exposure. All of these changes would remain undetected by the standard calibration methods. In contrast, the iodine cell is in place during the science exposures themselves, and thus, the imprinted iodine lines will undergo exactly the same instrument conditions that the science exposure experienced. This means that any change in the wavelength scale due to a change in temperature or a change in the index of refraction in the air will directly affect the iodine lines themselves. Second, the light paths of the calibration arcs and the telescope light are different. Suzuki et al. (2003) explored the fact that the optical axis of Keck is not directly aligned with the the optical axis of HIRES which leads to a differential vignetting between the telescope beam and the calibration lamps. The initial trajectory that the incoming light takes is therefore slightly different than the light from the ThAr

calibration lamps, as mentioned in § 2.1. The iodine cell, in contrast, is placed directly in the telescope light path and imprints thousands of sharp absorption features onto the science exposure itself. Any environmental change, slit guiding errors, air temperature, atmospheric dispersion, angle through the instrument, and any subsequent vignetting is shared by the combined science and iodine light. By comparing the resultant exposures' iodine absorption spectrum with a fiducial iodine spectrum, a detailed analysis of any distortions can be made.

The fiducial iodine cell spectra that we use comes from the measurements made on the Keck iodine cell with the Fourier transform spectrometer (FTS) at Kitt Peak National Observatory (KPNO). The FTS has exquisite relative and absolute accuracy, and the iodine spectra taken has a S/N of 700 pixel^{-1} and a resolution of about 170,000 (Butler et al., 1996). Any wavelength errors in the FTS exposure will be minimal compared with the errors introduced by Keck HIRES, and so we take disagreement between the two to be errors from Keck. Figure 2.5 shows a comparison of the relative resolution of the same iodine cell spectra as measured by KPNO and from HIRES. We also include a figure that demonstrates the effect that adding the iodine cell has to the quasar exposure in Figure 2.6.

2.5 Supercalibration Method

We begin our iodine cell wavelength calibration method with the standard ThAr wavelength calibrated spectra as described above. This means our starting point is the final calibrated exposure that would otherwise be directly used for scientific analysis. Since the iodine cell lines undergo the exact wavelength corrections that the science exposure undergoes, we have iodine spectra that recorded any

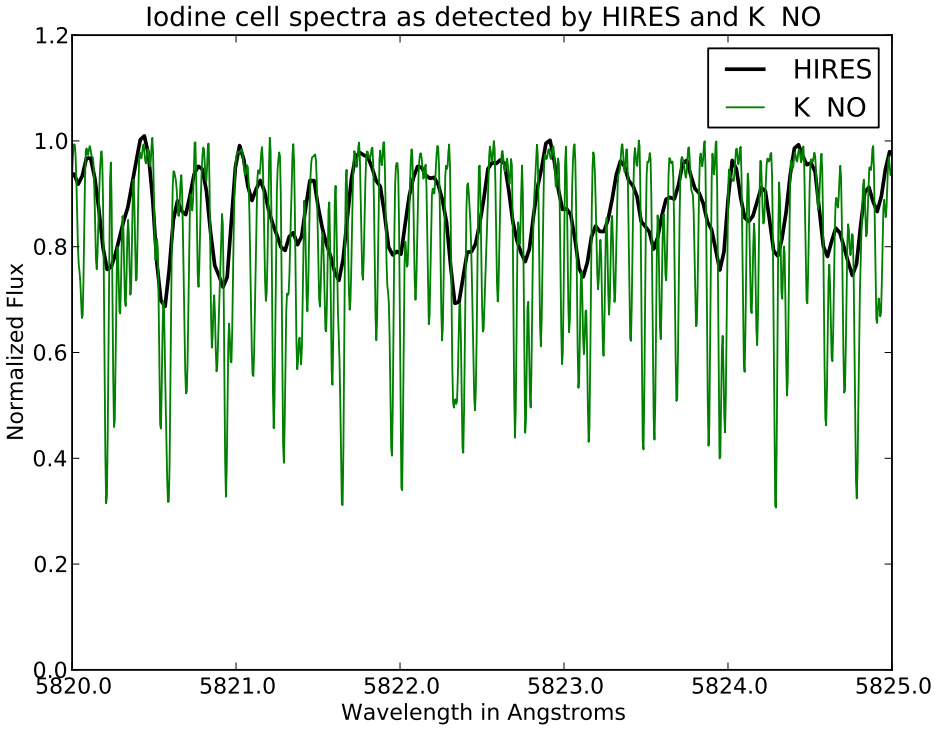

Figure 2.5 The same iodine cell absorption spectra as observed by the Fourier Transform Spectrometer and HIRES. The sharp features are fully resolved by the FTS, while the lower resolution of HIRES effectively gets a blurred image of the same underlying spectra.

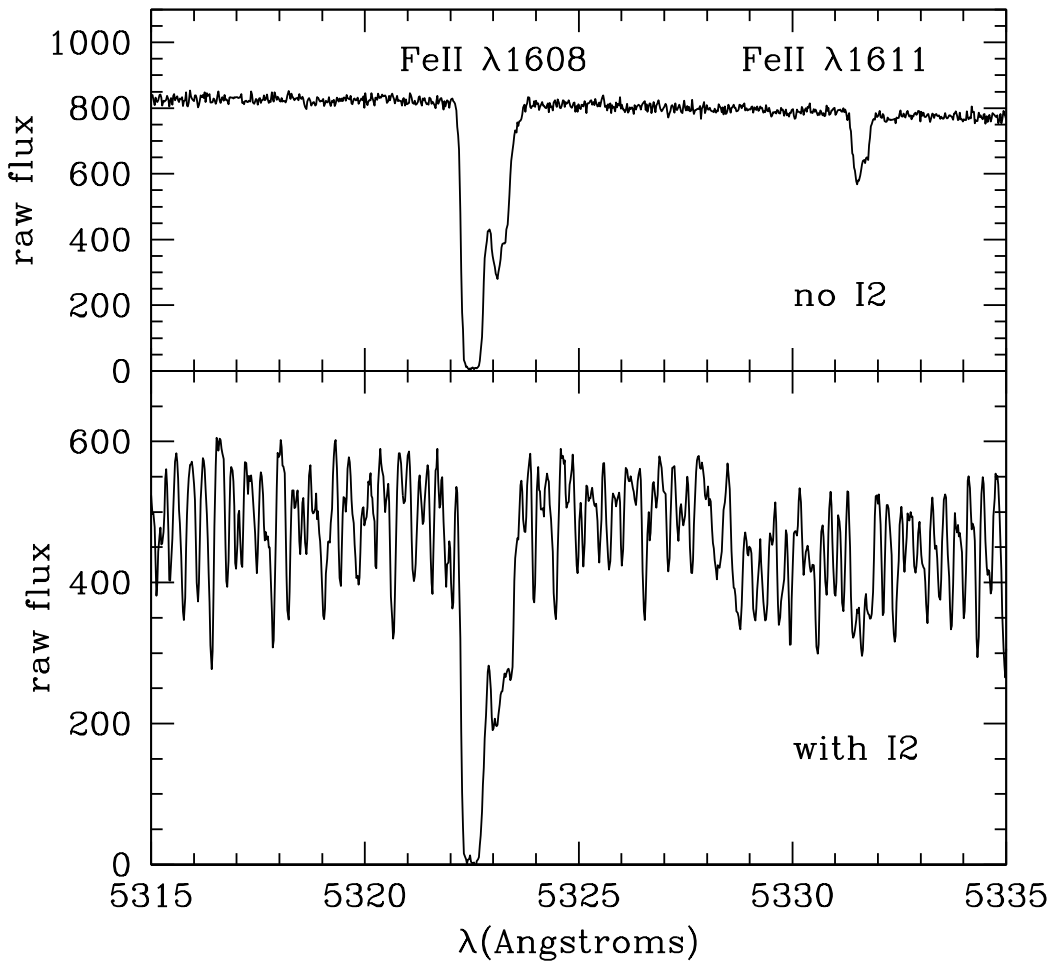

Figure 2.6 Quasar absorption features Fe II 1608 and 1611 as seen through Keck HIRES with (lower) and without (upper) the iodine cell in place. Source: (Griest et al., 2010).

wavelength transformations that were introduced by the HIRES instrument or by the wavelength calibration software. By comparing regions of the quasar exposure that contain iodine cell absorption to the fiducial iodine spectra from KPNO, we should be able to detect, in principle, any wavelength calibration distortions that the iodine spectra undergoes. The iodine absorption features are unresolved at the resolution of HIRES (see Figure 2.5), so we detail the method we use to compare the two spectra. The relative motion of the earth to the astrophysical object gets corrected by applying a single velocity Doppler shift to the entire spectrum. When comparing the iodine spectra from HIRES and FTS to each other, it is important that we compare them in the rest frame, and therefore, we do not apply the Doppler shift correction to the telescope data. However, when we compare quasar absorption features from different HIRES exposures, we do need to correct for the motion of the earth, and we used the barycenter code that Marcy (private communication) uses for planet-finding. His code is accurate to better than 1 m s^{-1}, and thus falls well below our other errors.

We cut the KPNO iodine cell spectra into 5Å pieces, and compare one piece at a time to the Keck exposures. Each piece is allowed three transformations in order to line up with observed Keck spectra: a resolution blurring, a wavelength shift, and a multiplicative normalization factor. Since the two spectra are taken with instruments of very different resolutions, the higher resolution KPNO spectra have to be smoothed, essentially blurred, to the lower resolution of HIRES. This blurring is done by convolving the slice with a Gaussian kernel; the width of the Gaussian is one of the free parameters of our fit. The second transformation is a single wavelength shift value applied to the entire 5Å piece. The final transformation is an overall normalization multiplication. A chi-square minimization is used for

the simultaneous best fit and formal errors on each parameter. We excluded regions of the quasar spectrum that included strong quasar absorption lines and linearly interpolate the shifts at line center by connecting regions on either side of the feature.

An important part of line fitting is estimating the flux from the unabsorbed part of the spectrum, i.e., the continuum. We calculate the continuum for the KPNO spectrum by averaging the three largest flux values in each 1Å bin. To continuum fit the Keck data, we use a standard continuum fitting program. However, since the iodine cell artificially suppresses the continuum flux by imposing a dense forest of absorption features, it becomes difficult to fit a physically relevant continuum. We investigate the sensitivity of our wavelength calibration to several possible continuum fitting errors. In Figure 2.7, we compare the method that we end up using in the following analysis with several systematically distorted continua. We find our method to be extremely robust to even egregious continuum errors, and conclude that any wavelength distortions that we measure cannot be attributable to continuum fitting errors. We compare the best fit convolution and shift of the KPNO iodine with the Keck exposure in Figure 2.8.

The errors in our iodine cell method scale inversely with bin size, with large bin size giving smaller uncertainties in the fit parameters. We choose a 5Å bin as a compromise between over-smoothing and fit error. We can introduce the correction as the amount that the ThAr wavelength solution needs to shift to line up with the fiducial iodine cell spectra,

$$\lambda_{\rm I}(\lambda) = \lambda_{\rm ThAr}(\lambda) + v_{\rm cal}(\lambda). \tag{2.2}$$

where $\lambda_{\rm ThAr}$ is the wavelength scale given by the ThAr calibration, $\lambda_{\rm I}$ is the wavelength scale of the KPNO spectra, and $v_{\rm cal}$ can be interpreted as the transfer

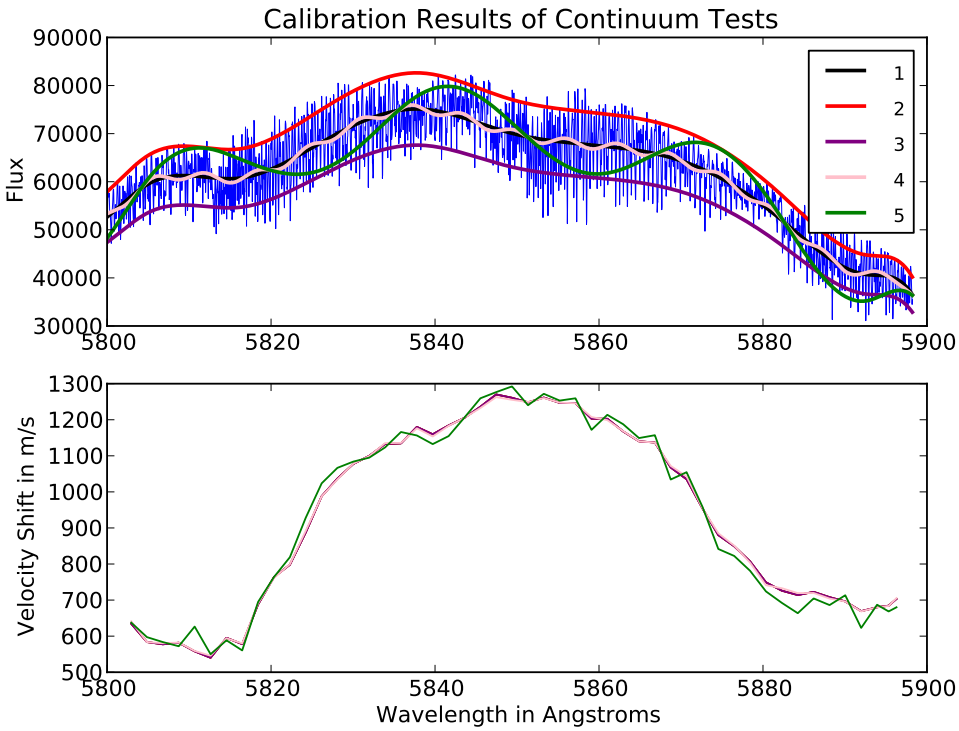

Figure 2.7 The results from a comparison of five different continua on the same Keck exposure (calibration standard star iodine cell exposure). The black line, labeled 1, is the results from our continuum program. Line 2 is a 10% overestimate from our initial continuum, and Line 3 is a 10% underestimate. Line 4 is the initial continuum plus 850 times the cosine of wavelength value. Line 5 is the initial continuum plus 6000 times the cosine of the wavelength value divided by five. The lower panel is the resulting calibration as calculated given each of the above continuums. All of the calibration results lie essentially on top of each other.

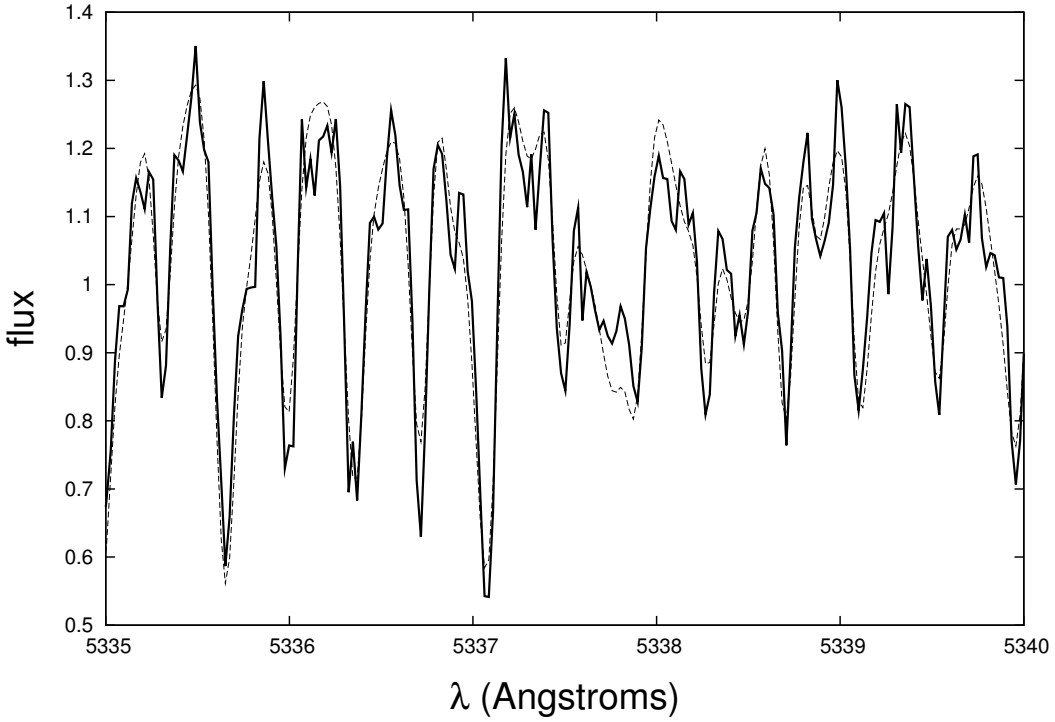

Figure 2.8 A representative example overlay of one 5Å piece of our best fit convolution of the KPNO iodine spectra (thin line) to the HIRES exposure (thick line). Source: Griest et al. (2010).

function that is required to correct the standard ThAr wavelength solution to the fiducial wavelength scale as a function of wavelength. We include Figure 2.9 that shows these calibration shifts as a function of wavelength.

There are two kinds of error that can be seen in Figure 2.9. There is an overall constant shift of about 750 m s^{-1}, and there is a repeated pattern across each order that exhibits changes of $\sim$ 600 m s^{-1}. Since a pixel corresponds to $\sim$ 1300 m s^{-1}, these intra-order shifts correspond to about half of a pixel in size. When considering the size of these miscalibrations in comparison to the size of the shifts predicted by a possible change in the fine-structure constant, which are as large as a several hundred m s^{-1}, it may appear that the miscalibrations completely overwhelm a $\frac{\Delta\alpha}{\alpha}$ measurement. However, for each atomic transition measured in a quasar absorption spectrum, the velocity shift that would occur if the fine-structure constant were different is given by:

$$v_j = v_0 + \left(\frac{\Delta\alpha}{\alpha}\right) x_j; \quad x_j = -2cq_j\lambda_{0,j} \tag{2.3}$$

where j is the transition, v_0 is a constant offset, x_j is a constant that depends on the wavelength and q-coefficient for the transition under consideration. The q-coefficient characterizes the sensitivity of the particular transition to a change in the fine-structure constant. The velocity shift for relevant quasar absorption transitions is from a few to several hundred m s^{-1} for $\frac{\Delta\alpha}{\alpha} \sim 5 \times 10^{-6}$. While the shifts between transitions expected by a changing fine-structure constant are of the same order as the miscalibrations, the measurements are made between multiple transitions in the same exposure and a constant offset should not play a role in a spurious $\frac{\Delta\alpha}{\alpha}$ detection. The measurement of $\frac{\Delta\alpha}{\alpha}$ relies on relative wavelength shifts

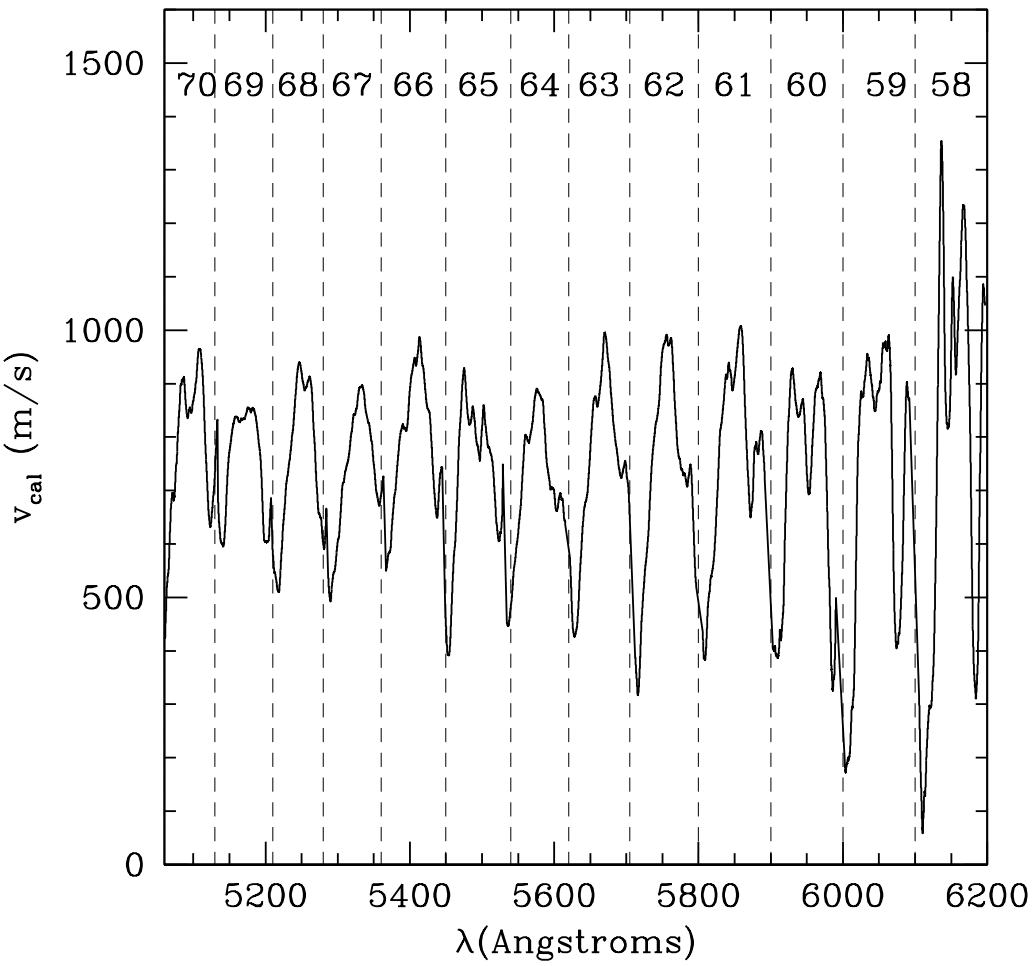

Figure 2.9 The calibration shifts for exposure 3-1 across the wavelength region that overlaps our iodine cell coverage. The echelle orders are numbered along the top and separated by vertical dashed lines. Source: Griest et al. (2010).

between two quasar absorption features i and j. The effect on $\frac{\Delta\alpha}{\alpha}$ is:

$$\frac{\Delta\alpha}{\alpha} \propto \frac{v_{ij}}{c}, \tag{2.4}$$

where v_{ij} is the velocity shift between transitions i and j as defined in equation 2.3. In other words, the constant offset from zero of about 750 m s^{-1} should not yield a spurious $\frac{\Delta\alpha}{\alpha}$ detection. However, since all of the measuring leverage comes from the relative spacing of atomic transitions, the intra-order miscalibrations would directly interfere with a $\frac{\Delta\alpha}{\alpha}$ measurement. We make note that even with these systematic errors, the statistical averaging done by Murphy, Chand, and others may still provide a robust measurement of a change in the fine-structure constant as long as these systematic errors are sufficiently random.

The intra-order shifts might be able to be corrected if they were stable with respect to time, or varied in a way that could be easily modeled. We investigate the stability of the calibration errors across our six iodine exposures. The six iodine exposures were calibrated individually, and the transfer functions for a single order are plotted in Figure 2.10.

Notice that the overall shift changes drastically between exposures. The naming convention we adopt is Date-Exposure number. The constant overall shift varies by almost 2 km s^{-1} between the extreme exposures, which was unexpected, but the more pernicious overall shape or intra-order miscalibrations have a markedly different shape. These results suggest that these miscalibrations are not stable with time, or are at the least they are sufficiently complicated to avoid simple modeling. The size of the constant shift varies in the same direction over the night, and while the iodine cell exposures were taken immediately one after the other on 3 and 4 of October, there was a longer delay between the two iodine exposures taken on 5 October.

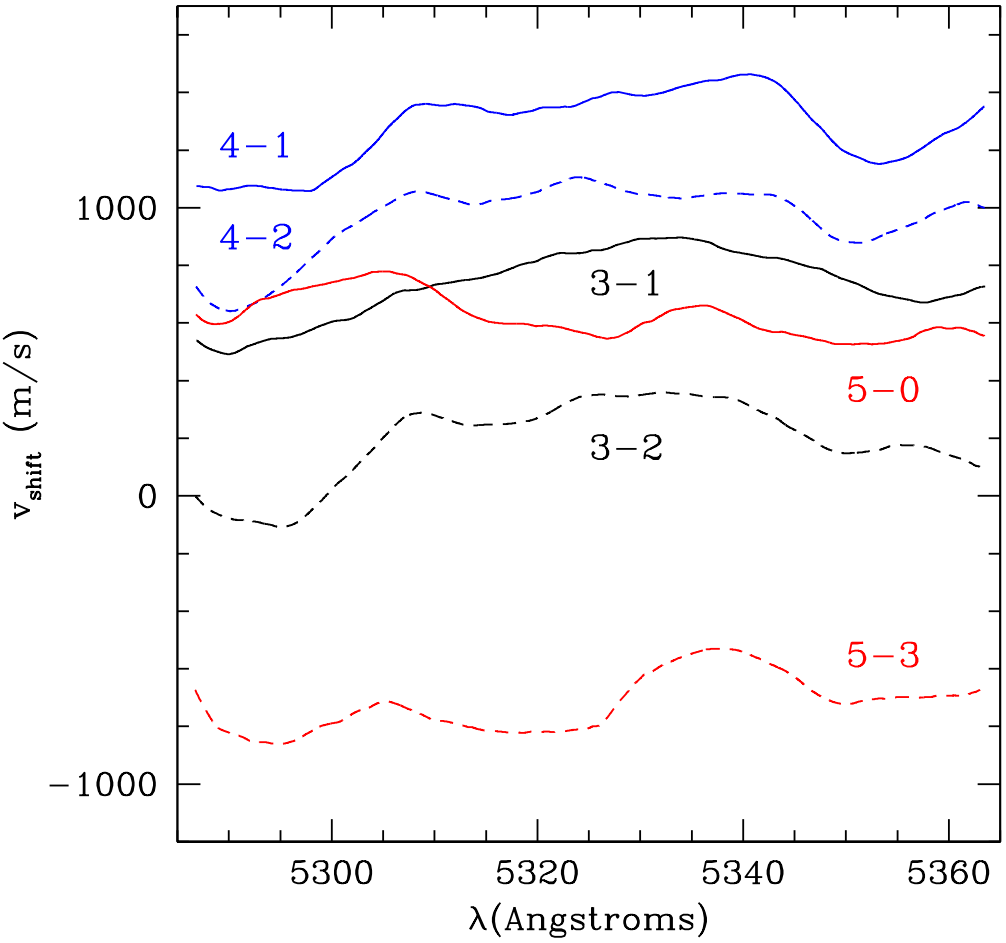

Figure 2.10 The velocity transfer shifts for the same order for each of the six iodine cell exposures taken of the quasar PHL957. The naming convention we adopt is Date-Exposure number, and the numbers correspond to the values in Table 2.2. Each night had two exposures, and for ease of discernment, the earlier exposure for each night is plotted with a solid line, with the following exposure plotted with a dashed line. Source: Griest et al. (2010).

One of the independent checks on our wavelength scale correction was to compare the quasar absorption features before and after we applied our corrections. The miscalibration function only compares the iodine absorption lines from the Keck exposure to the iodine absorption lines measured by the Fourier Transform Spectrometer. If we use the measured miscalibration as a transfer function to correct the ThAr calibration, we can create, in principle, a supercalibrated spectrum. As a test of this idea, we apply our iodine cell correction to the quasar lines and compare a sharp feature with and without our correction. We use the lefthand edge of the Fe II λ1608 absorption feature (see Figure 2.6) and line up the exposures after adding in the correct barycentric correction with and without our additional iodine correction. It is seen in Figure 2.11, the iodine correction improves the alignment substantially. This test also serves as an independent check that our iodine cell method is robust. We also attempted to improve the ThAr calibration of the non-iodine exposures by interpolating from the nearest iodine exposure's transfer function. After seeing how unstable the miscalibrations were with time, we did not expect a substantial improvement, and we include the results for completeness in Figure 2.12. While it might seem that our results are surprising, we note that shifts of similar magnitude and shifts with time were found via different methods: sky-lines by Osterbrock et al. (2000), and Lyman-α forest lines by Suzuki et al. (2003).

2.6 Understanding the Calibration Shifts

We attempted to discover the underlying causes for the two types of miscalibration shifts that we detected. The first clue seemed to be that there was

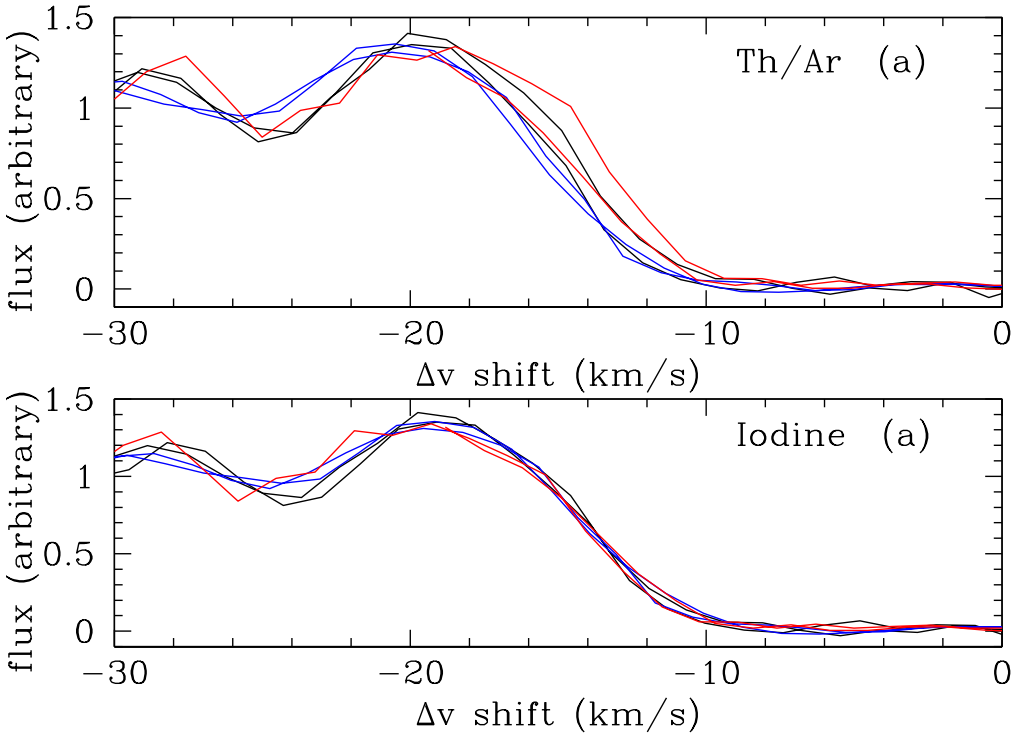

Figure 2.11 The iodine cell exposure correction. An extreme closeup of the lefthand edge of the saturated Fe II λ1608 quasar absorption feature as seen in the six iodine exposures. The black lines are the exposures from 3 October, the blue lines are from 4 October, and the red lines are from 5 October. The top plot is the standard ThAr calibration method, and the bottom is the result of our supercalibration process. Source: Griest et al. (2010).

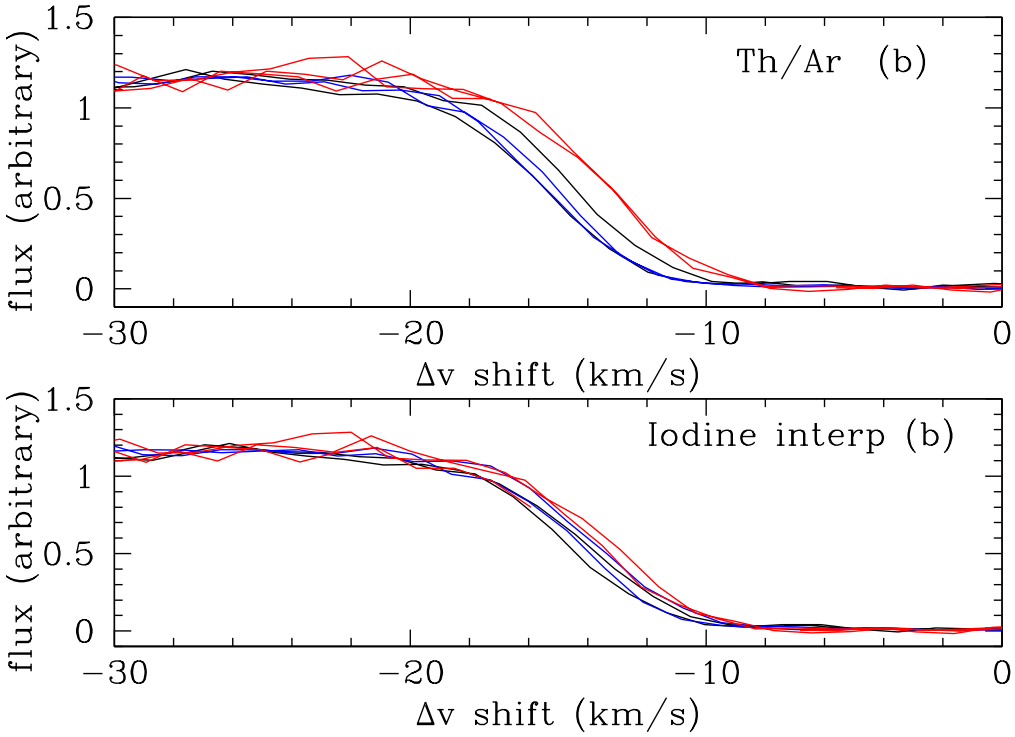

Figure 2.12 The interpolated iodine cell exposure correction. An extreme closeup of the lefthand edge of the saturated Fe II λ1608 quasar absorption feature as seen in the non-iodine exposures. The black lines are the exposures from 3 October, the blue lines are from 4 October, and the red lines are from 5 October. The top plot is the standard ThAr calibration method, and the bottom is the interpolated result of our supercalibration process. This interpolation only incrementally improves the overall calibration. Source: Griest et al. (2010).

a drift downward in wavelength calibration of about 500 m s^{-1} per hour. While that trend correlates with time, the trend is better fit by relating the change in internal air temperature of HIRES between when the calibration exposure and science exposure were taken. Fitting a single average shift per exposure and plotting against the temperature difference between the exposure and the calibration file shows a significant correlation. We plot this relationship in Figure 2.13. A similar overall shift could result from a misalignment of the object in the slit or by the gratings being moved between the arc and science exposures (Molaro et al., 2008a).

The temperature difference appears to explain the constant offset shifts for every exposure except 5-3. The intra-order distortion of the miscalibration does not appear to have a simple explanation. One of the primary suspects is the fact that the optical axis of the telescope and the optical axis of HIRES are not exactly aligned. If the telescope were to trace out a large arc in the sky, the optical axis would trace out a cone inside of HIRES with an angle of about $14'.8$ (Suzuki et al., 2003). Suzuki et al. (2003) suggested that a variable vignetting occurred between the echelle and cross-disperser, and that the changing incident light angle causes a non-uniform illumination of the cross-disperser. The repeated pattern of wavelength miscalibration suggests a similar physical cause to what Suzuki et al. (2003) found regarding a similar repeated pattern across all orders in the flux ratios between exposures. Since we see a similar repeated pattern, we speculate that something similar is occurring with the wavelength miscalibration, but cannot make a firm conclusion from our data. Thus, more work is needed in order to understand the source of these systematic errors in wavelength calibration.

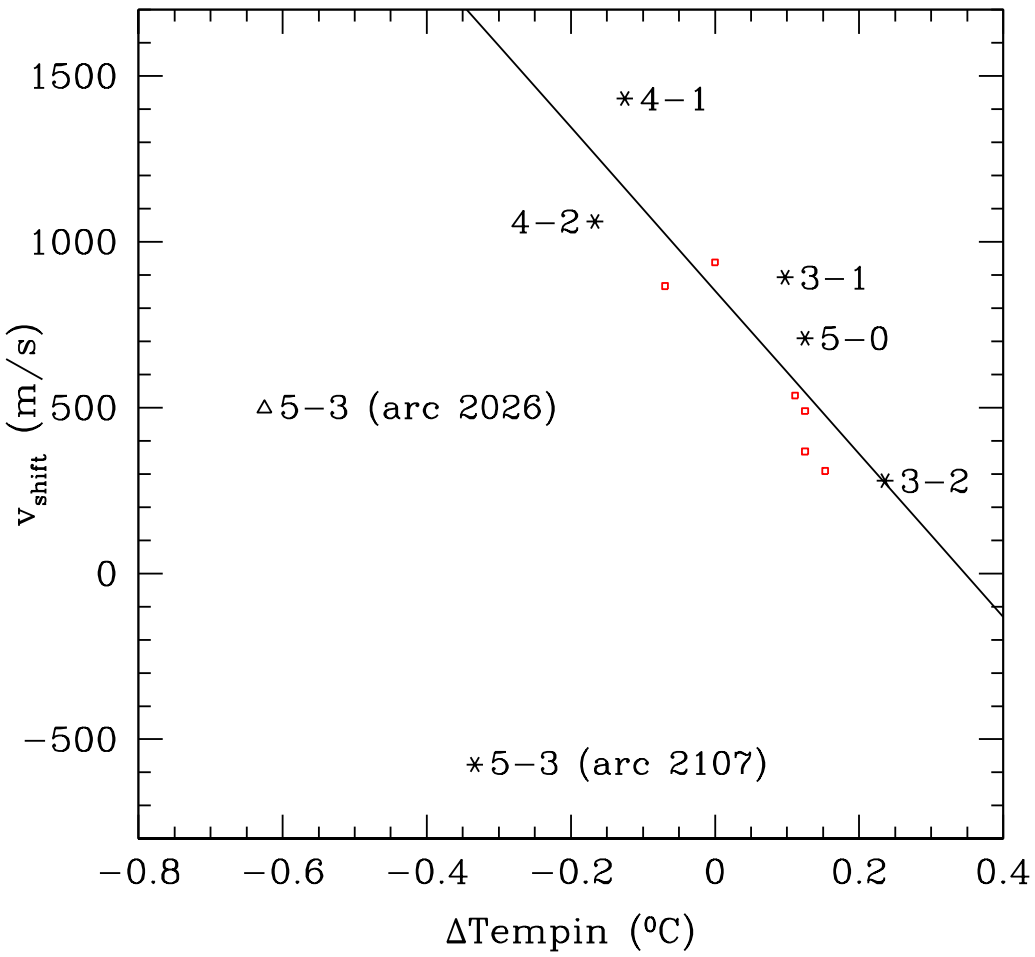

Figure 2.13 A plot of the average shift for each exposure (labeled: Day-Exposure) versus the difference in temperature between the calibration exposure and the science exposure. Source: Griest et al. (2010).

2.7 Using the Calibration

We began our analysis of measuring $\frac{\Delta\alpha}{\alpha}$ with the hope that we could use the iodine exposures to characterize and correct the ThAr calibration so that the non-iodine exposures would have a pristine wavelength scale. This would enable us to fit for a change in the fine-structure constant with a clear understanding of any possible wavelength calibration distortions. However, the miscalibrations varied widely and unpredictably between exposures, making it difficult to extrapolate a wavelength correction to non-iodine exposures. It remains tempting to try and use the iodine cell exposures themselves, since we can correct their wavelength scale directly, but the thick forest of iodine lines attenuates the quasar spectra, thereby degrading our ability to fit the quasar absorption lines to the precision required. Hence, we are in a dilemma; we can fit the quasar line shapes very well, but not know the relative spacing to the desired level of accuracy, or, we can know the relative spacing with plenty of precision, but cannot fit the quasar line shapes well due to noise from the iodine lines.

2.8 VPFIT analysis

Researchers in the field use the program VPFIT, written by Carswell et al. (2008), as the standard fitting software. The program fits multiple Voigt profiles to absorption features in spectral data, and we use it to give our measurement of $\frac{\Delta\alpha}{\alpha}$.

The Voigt profile function describes the shape of the absorption feature and comes from a combination of several physical effects. The first effect comes from the natural line broadening of the transition due to quantum mechanics. The probability function that a frequency of light will cause an electron in an atom

to get kicked into an excited state has the shape of a general function called a Lorentzian. The Lorentzian is given in general by:

$$L(x,\gamma) = \frac{\gamma}{\pi(x^2+\gamma^2)}, \tag{2.5}$$

where γ is a parameter that governs the width of the function. The cross section (σ) of an atomic transition is given as a function of light frequency by:

$$\sigma(\omega) = \frac{2\pi^2 e^2}{mc} f_{ij} \frac{(\Gamma/2\pi\hbar)}{(\omega-\omega_{ij})^2 + (\Gamma/2\pi\hbar)^2}, \tag{2.6}$$

where Γ is the natural line width of the transition, f_{ij} the oscillator strength ratio of the transition, and ω_{ij} being the frequency of the transition. The shape of this function is a Lorentzian. The absorption of light by an atomic transition is directly related to the cross section around the natural frequency of the transition. This means that an absorption feature in a spectrum has the shape of a Lorentzian.

The second effect comes from the motion of the atom causing a Doppler shift to the background light in its frame of reference. We assume a Gaussian velocity distribution describes the motion of the atoms, which for the metal lines discussed here is dominated by the turbulent rather than thermal motions. The Gaussian is given in general by:

$$G(x,\sigma) = \frac{1}{\sigma\sqrt{2\pi}} e^{-x^2/(2\sigma^2)}, \tag{2.7}$$

with the velocity dispersion, σ, relating to the width of the function. The convolution of the two functions yields the Voigt profile function:

$$V(x;\sigma,\gamma) = \int_{-\infty}^{\infty} \left(\frac{1}{\sigma\sqrt{2\pi}} e^{-x'^2/(2\sigma^2)}\right) \left(\frac{\gamma}{\pi((x-x')^2+\gamma^2)}\right) \mathrm{d}x'. \tag{2.8}$$

Since we reviewed the physical reasons for fitting spectral features with a Voigt profile, we detail our fitting procedure below. To clarify terms that will be

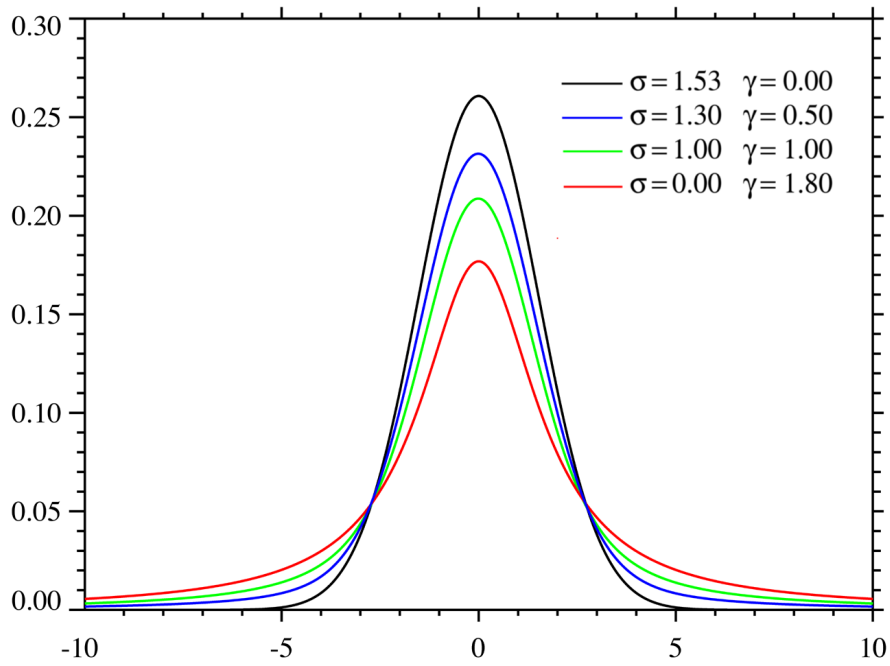

Figure 2.14 The black line is the profile for a Gaussian function. It has a relatively sharper peak at the center and a tail that rapidly approaches zero. The red line is the profile of a Lorentzian function. Contrasting the Lorentzian with the Gaussian, the Lorentzian is not as peaked in the center and the tails are much broader. The Voigt profile is the convolution of the two functions and so displays a combination of the features from both functions. Source: `http://en.wikipedia.org/wiki/File:Voigt_distributionPDF.png`

used, a "component" in the spectrum relates to a physical clump of gas. Within that clump of gas, there may be an element, like iron, which has several transitions, i.e. Fe II 1608 Å and 1611 Å. The absorption spectra will have an absorption feature due to both transitions (one line at 1608 Å, the other at 1611 Å). This means that a single component (or clump of gas) will have an absorption spectra that has several absorption lines. If this same clump of gas has other elements in it, like aluminum and nickel, even more transitions will appear for the same component.

We begin fitting components to our spectra with strong and unsaturated absorption features of a single element. Since the physical system is frequently composed of several gas clouds at different redshifts, i.e. mean velocities, multiple physical components usually need to be added. We add Voigt profiles to model the physical components of an absorption system. We determine the number of components by finding the number that minimizes the reduced χ^2 of the fit. Each transition can be described by three variables: the column density, the b-value, and the redshift. The column density is number of atoms (reported in terms of a logarithm, so a column density of 13.1 means $\log_{10}(N) = 13.1)$ cm^{-2}. The column density is an indicator of the strength of the absorption feature. The b-value equals $\sqrt{2}\sigma$ and is reported in km s^{-1}. The redshift value relates to the redshift of the transition from today's value. Naively, it may appear that these three parameters allow for a different height, width and redshift for each transition. However, multiple transitions within a single element are necessarily tied together, i.e., the iron atoms are at a single redshift, velocity dispersion, and column density. Thus, for a single element in a single component, there are three total parameters. Having multiple transitions for an element gives multiple constraints on the physical parameters affecting each element. The parameters are further constrained because we also

assume that elements that are at the same redshift and ionization state are in the same physical system. We therefore tie together the redshift values for the elements within each component. Thus, eventually we have all of the unsaturated transitions from different elements tied together in the fitting program. In our fitting process, we isolated Al III from the other transitions. Therefore, we do not tie redshift values of Al III to the other transitions, although we do tie the $\frac{\Delta\alpha}{\alpha}$ parameter across all transitions. Another difficulty arises in dealing with saturated transitions. A saturated transition occurs when effectively all of the background light is absorbed at the frequency of a specific transition (due to a high column density or a particularly strong oscillator strength ratio). Saturated transitions can cause problems with the fitting software, so they are the last to be included in the fits, and are done so with great care.

To fit for $\frac{\Delta\alpha}{\alpha}$, we coadded the non-iodine exposures that were reduced using the standard wavelength calibration software. Once a best fit to the physical components of the elements are obtained, we begin the fitting process for $\frac{\Delta\alpha}{\alpha}$. VPFIT has a setting which allows for an extra parameter representing a change in the fine-structure constant to be simultaneously fit with the other components. We fit a single parameter for a change in the fine-structure constant. We include our fit for $\frac{\Delta\alpha}{\alpha}$ with different elements and components in Table 2.3 and Table 2.4. We also include a plot of the various results that we can get depending on the transitions included in Figure 2.15. We present multiple fitting runs with different components included to demonstrate the conditions that change the measured value of $\frac{\Delta\alpha}{\alpha}$. Table 2.3 provides the details for the first five runs with each run having a different combination of unsaturated transitions fit. We report a final value (1σ statistical) of $\frac{\Delta\alpha}{\alpha}_{\text{unsaturated}} = (10.544 \pm 5.1094) \times 10^{-6}$ and a reduced

χ^2 of 1.11 for the fit that includes all unsaturated transitions. We then fit for $\frac{\Delta\alpha}{\alpha}$ using saturated transitions in the next five runs. We report a final value (1σ statistical) of $\frac{\Delta\alpha}{\alpha}_{\text{saturated}} = (-8.58 \pm 1.66) \times 10^{-6}$ and a reduced χ^2 of 1.65 for the fit of all saturated and unsaturated transitions. The unsaturated transitions suggest a positive value for $\frac{\Delta\alpha}{\alpha}$ while the saturated lines suggest a negative value for $\frac{\Delta\alpha}{\alpha}$. We suspect that the wavelength miscalibration errors introduce significant systematic errors to these measurements.

Table 2.3. Results from VPFIT

Run	$\frac{\Delta\alpha}{\alpha}\times10^{-6}$	$\sigma \times 10^{-6}$	$chi^2/d.o.f.$	Only Unsaturated Transitions
1	83.059	88.662	1.00	AlIII 1854/1862
2	15.014	19.305	0.93	NiII 1709/1741/1751
3	-3.0250	7.7420	1.03	FeII 1611 NiII 1709/1741/1751 SiII 1808
4	5.1163	5.2060	1.18	FeII 1611 NiII 1709/1741/1751 SiII 1808 ZnII 2026/2062 CrII 2056/2062/2066
5	10.544	5.1094	1.11	FeII 1611 NiII 1709/1741/1751 SiII 1808 CrII 2056/2062/2066 ZnII 2026/2062 AlIII 1854/1862

Table 2.4. Results from VPFIT

Run	$\frac{\Delta\alpha}{\alpha}\times10^{-6}$	$\sigma \times 10^{-6}$	$chi^2/d.o.f.$	Including Saturated Transitions
6	-5.6149	16.654	1.76	FeII 1608/1611/2344
7	-9.2446	3.2577	2.06	FeII 1608/1611/2344 SiII 1526/1808
8	-10.0	1.60	1.81	FeII 1608/1611/2344 NiII 1709/1741/1751 SiII 1526/1808
9	-8.74	1.72	1.78	FeII 1608/1611/2344 NiII 1709/1741/1751 SiII 1526/1808 CrII 2056/2062/2066 ZnII 2026/2062 AlII 1670
10	-8.58	1.66	1.65	AlIII 1854/1862 FeII 1608/1611/2344 CrII 2056/2062/2066 ZnII 2026/2062 NiII 1709/1741/1751 SiII 1526/1808 AlII 1670

2.9 Discussion

Our attempt to conclusively detect or rule out a change in the fine-structure constant at the level of 1×10^{-6} was unsuccessful. We found results that range from a positive detection to a negative detection to a null result depending on the transitions included. We developed a method of using the iodine cell on the Keck HIRES instrument to discover and quantify several new sources of systematic error. We found errors of up to 600 m s^{-1} within a single echelle order, and absolute shifts between exposures of up to 2000 m s^{-1}. With the theoretical prediction of absorption line shifts being online a couple hundred m s^{-1} for a fine-structure constant that differs by the amount claimed by Murphy et al. (2004), our errors become very relevant to the current $\frac{\Delta\alpha}{\alpha}$ controversy. We recommend caution when attempting to constrain $\frac{\Delta\alpha}{\alpha}$ from a single absorption system as it could easily be overwhelmed by systematic errors.

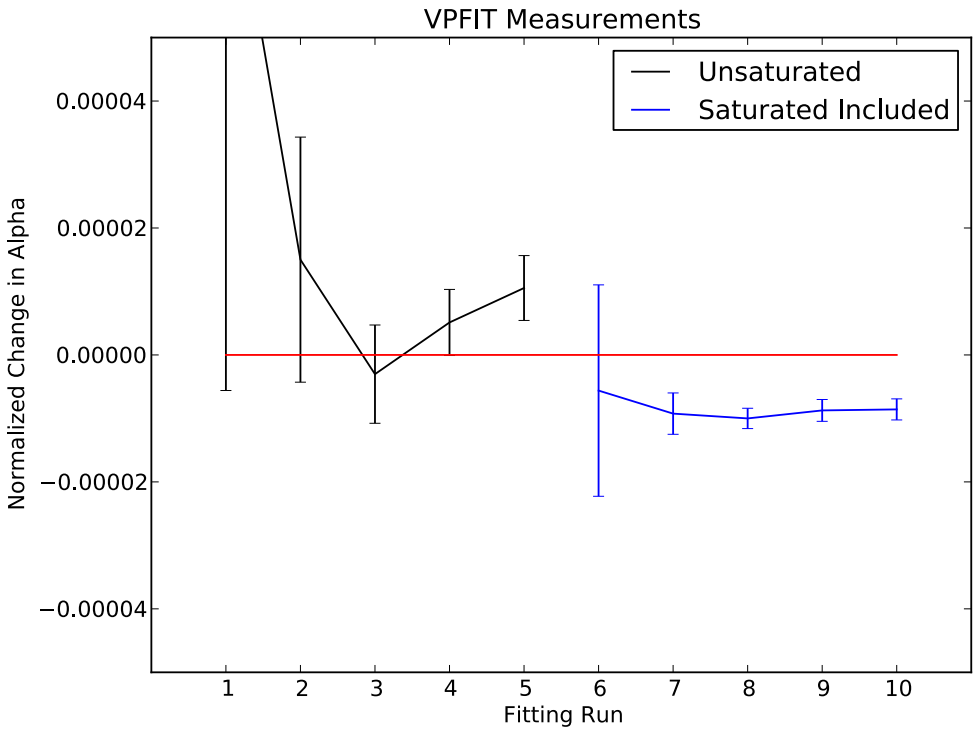

Figure 2.15 The black line (runs 1–5) corresponds to Table 2.3. The blue line (runs 6–10) corresponds to Table 2.4.

Bibliography

Agafonova, I. I., Molaro, P., Levshakov, S. A., & Hou, J. L. 2011, Astronomy and Astrophysics, 529, 28

Ashenfelter, T. P., Mathews, G. J., & Olive, K. A. 2004, The Astrophysical Journal, 615, 82

Bahcall, J. N. & Salpeter, E. E. 1965, Astrophysical Journal, 142, 1677

Bahcall, J. N., Sargent, W. L. W., & Schmidt, M. 1967, Astrophysical Journal, 149, L11

Bahcall, J. N. & Schmidt, M. 1967, Physical Review Letters, 19, 1294

Bahcall, J. N., Steinhardt, C. L., & Schlegel, D. 2004, The Astrophysical Journal, 600, 520, published in: Astrophys.J.600:520,2004 Added analysis of larger quasar sample from SDSS Data Release One. Accepted for publication ApJ

Beaver, E. A., Burbidge, E. M., McIlwain, C. E., Epps, H. W., & Strittmatter, P. A. 1972, The Astrophysical Journal, 178, 95

Bransden, B. H. & Joachain, C. J. 2003, Physics of Atoms and Molecules, 2nd edn. (Benjamin Cummings), book on Atomic Physics from UCSD library.

Butler, R. P., Marcy, G. W., Williams, E., McCarthy, C., Dosanjh, P., & Vogt, S. S. 1996, Publications of the Astronomical Society of the Pacific, 108, 500

Carswell, R. F., Webb, J. K., Cooke, A. J., & Irwin, M. J. 2008, VPFIT 9.5, `http://www.ast.cam.ac.uk/~rfc/vpfit.html`

Chand, H., Petitjean, P., Srianand, R., & Aracil, B. 2005, Astronomy and Astrophysics, 430, 47

Chand, H., Srianand, R., Petitjean, P., & Aracil, B. 2004, Astronomy and Astrophysics, 417, 853

Dirac, P. A. M. 1937, Nature, 139, 323

Dirac, P. A. M. 1938, in Proceedings of the Royal Society of London. Series A, 199–208

Dzuba, V. A., Flambaum, V. V., & Webb, J. K. 1999a, Physical Review A (Atomic, 59, 230

—. 1999b, Physical Review Letters, 82, 888

Edlén, B. 1966, Metrologia, 2, 71

Flambaum, V. V. 2008, The European Physical Journal Special Topics, 163, 159

Fujii, Y. & Iwamoto, A. 2005, Modern Physics Letters A, 20, 2417

García-Berro, E., Isern, J., & Kubyshin, Y. A. 2007, The Astronomy and Astrophysics Review, 14, 113

Gould, C. R., Sharapov, E. I., & Lamoreaux, S. K. 2006, Physical Review C, 74, 24607

Griest, K., Whitmore, J. B., Wolfe, A. M., Prochaska, J. X., Howk, J. C., & Marcy, G. W. 2010, The Astrophysical Journal, 708, 158

Ichikawa, K., Kanzaki, T., & Kawasaki, M. 2006, Physical Review D, 74, 23515

Ichikawa, K. & Kawasaki, M. 2004, Physical Review D, 69, 123506

Kaluza, T. 1921, Sitz Preuss Akad Wiss Phys Math

Kaufer, A., D'Odorico, S., Kaper, L., Ledoux, C., & James, G. 2007, Very Large Telescope Paranal Science Operations UV-Visual Echelle Spectrograph User manual, issue 82 edn.

Klein, O. 1926, Zeitschrift für Physik, 37, 895

Landau, S. J. & Scóccola, G. 2010, Astronomy and Astrophysics, 517, 62

Levshakov, S. A. 2004, Lecture Notes in Physics, 648, 151

Levshakov, S. A., Centurión, M., Molaro, P., D'Odorico, S., Reimers, D., Quast, R., & Pollmann, M. 2006, Astronomy and Astrophysics, 449, 879

Lorén-Aguilar, P., García-Berro, E., Isern, J., & Kubyshin, Y. A. 2003, Classical and Quantum Gravity, 20, 3885

Mohr, P. J., Taylor, B. N., & Newell, D. B. 2006, The 2006 CODATA Recommended Values of the Fundamental Physical Constants, `http://physics.nist.gov/constants`, this database was developed by J. Baker, M. Douma, and S. Kotochigova. National Institute of Standards and Technology, Gaithersburg, MD 20899. [Online; accessed 2011-03-15]

Molaro, P., Levshakov, S. A., Monai, S., Centurión, M., Bonifacio, P., D'Odorico, S., & Monaco, L. 2008a, Astronomy and Astrophysics, 481, 559

Molaro, P., Reimers, D., Agafonova, I. I., & Levshakov, S. A. 2008b, European Physical Journal Special Topics, 163, 173

Murphy, M. T., Flambaum, V. V., Webb, J. K., & al, e. 2004, Lecture Notes in Physics, 648, 131

Murphy, M. T., Tzanavaris, P., Webb, J. K., & Lovis, C. 2007, Monthly Notices of the Royal Astronomical Society, 378, 221

Murphy, M. T., Webb, J. K., & Flambaum, V. V. 2003, Monthly Notices of the Royal Astronomical Society, 345, 609

—. 2008a, Monthly Notices of the Royal Astronomical Society, 384, 1053

—. 2008b, Precision Spectroscopy in Astrophysics, 95

Murphy, M. T., Webb, J. K., Flambaum, V. V., Dzuba, V. A., Churchill, C. W., Prochaska, J. X., Barrow, J. D., & Wolfe, A. M. 2001a, Monthly Notices of the Royal Astronomical Society, 327, 1208

Murphy, M. T., Webb, J. K., Flambaum, V. V., Prochaska, J. X., & Wolfe, A. M. 2001b, Monthly Notices of the Royal Astronomical Society, 327, 1237

Naudet, R. 1974, Bull. Inf. Sci. Tech. (Paris)., no. 193, pp. 7-45

Olive, K. A., Pospelov, M., Qian, Y.-Z., Coc, A., Cassé, M., & Vangioni-Flam, E. 2002, Physical Review D, 66, 45022

Olive, K. A., Pospelov, M., Qian, Y.-Z., Manhès, G., Vangioni-Flam, E., Coc, A., & Cassé, M. 2004, Physical Review D, 69, 27701

Osterbrock, D. E., Waters, R. T., Barlow, T. A., Slanger, T. G., & Cosby, P. C. 2000, The Publications of the Astronomical Society of the Pacific, 112, 733

Peebles, P. J. & Dicke, R. H. 1962, Physical Review, 128, 2006

Peik, E., Lipphardt, B., Schnatz, H., Tamm, C., Weyers, S., & Wynands, R. 2008, THE ELEVENTH MARCEL GROSSMANN MEETING On Recent Developments in Theoretical and Experimental General Relativity, 941

Petrov, Y. V., Nazarov, A. I., Onegin, M. S., Petrov, V. Y., & Sakhnovsky, E. G. 2006, Physical Review C, 74, 64610

Reid, B. A., Percival, W. J., Eisenstein, D. J., Verde, L., Spergel, D. N., Skibba, R. A., Bahcall, N. A., Budavari, T., Frieman, J. A., Fukugita, M., Gott, J. R., Gunn, J. E., Ivezić, Z., Knapp, G. R., Kron, R. G., Lupton, R. H., McKay, T. A., Meiksin, A., Nichol, R. C., Pope, A. C., Schlegel, D. J., Schneider, D. P., Stoughton, C., Strauss, M. A., Szalay, A. S., Tegmark, M., Vogeley, M. S., Weinberg, D. H., York, D. G., & Zehavi, I. 2010, Monthly Notices of the Royal Astronomical Society, 404, 60

Reynaud, S., Salomon, C., & Wolf, P. 2009, Space Science Reviews, 148, 233, 145 pages, 10 figures, Review for Living Reviews in Relativity

Riess, A. G., Macri, L., Casertano, S., Sosey, M., Lampeitl, H., Ferguson, H. C., Filippenko, A. V., Jha, S. W., Li, W., Chornock, R., & Sarkar, D. 2009, The Astrophysical Journal, 699, 539

Rosenband, T., Hume, D. B., Schmidt, P. O., Chou, C. W., Brusch, A., Lorini, L., Oskay, W. H., Drullinger, R. E., Fortier, T. M., Stalnaker, J. E., Diddams, S. A., Swann, W. C., Newbury, N. R., Itano, W. M., Wineland, D. J., & Bergquist, J. C. 2008, Science, 319, 1808

Savedoff, M. P. 1956, Nature, 178, 688

Shlyakhter, A. I. 1976, Nature, 264, 340

Srianand, R., Chand, H., Petitjean, P., & Aracil, B. 2004, Physical Review Letters, 92, 121302

Srianand, R., Petitjean, P., Chand, H., Noterdaeme, P., & Gupta, N. 2009, Memorie della Società Astronomica Italiana, 80, 842

Suzuki, N., Tytler, D., Kirkman, D., O'Meara, J. M., & Lubin, D. 2003, The Publications of the Astronomical Society of the Pacific, 115, 1050

Uzan, J.-P. 2011, Living Reviews in Relativity, 14, 2

Vogt, S. S. 1994, HIRES User's Manual, `http://www2.keck.hawaii.edu/inst/hires/manual2.pdf`, [Online; accessed 2011-03-22]

Webb, J., Murphy, M., Flambaum, V., & Curran, S. 2003, Astrophysics and Space Science, 283, 565

Webb, J. K., Flambaum, V. V., Churchill, C. W., Drinkwater, M. J., & Barrow, J. D. 1999, Physical Review Letters, 82, 884

Webb, J. K., King, J. A., Murphy, M. T., Flambaum, V. V., Carswell, R. F., & Bainbridge, M. B. 2010, arXiv, 1008, 3907, 5 pages, 5 figures, submitted to Physical Review Letters

Webb, J. K., Murphy, M. T., Flambaum, V. V., Dzuba, V. A., Barrow, J. D., Churchill, C. W., Prochaska, J. X., & Wolfe, A. M. 2001, Physical Review Letters, 87, 91301

Whitmore, J. B., Murphy, M. T., & Griest, K. 2010, The Astrophysical Journal, 723, 89

Wilkinson, D. H. 1958, Philosophical Magazine, 3, 582

Wolfe, A. M., Brown, R. L., & Roberts, M. S. 1976, Physical Review Letters, 37, 179, a&AA ID. AAA018.022.121

Chapter 3

VLT-UVES

After discovering unexpected wavelength miscalibrations in the Keck HIRES spectrograph, several questions remained. First among them was whether the miscalibrations were unique to Keck, or whether other instruments were plagued with similar unknown systematic errors. The rival instrument being used in quasar absorption spectroscopy to measure the constancy of α is the VLT-UVES (Very Large Telescope - ultraviolet and visual echelle spectrograph). The other main question was whether the miscalibrations introduced a systematic error in the measurements of the fine-structure constant. We analyzed the VLT spectrograph accuracy by obtaining iodine exposures of the bright quasar HE0515-4414 (mentioned in the controversy in § 1.5.2). We found the same two characteristic wavelength miscalibrations that we found at Keck: a constant overall shift by exposure, and an intra-order shift that occurs within each echelle order. These miscalibrations are similar in nature to those found at Keck, but are significantly smaller. The overall shifts are of order 400 m s^{-1} and intra-order shifts of order 200 m s^{-1}. Below, we discuss several possible physical causes for these effects, and we use Monte Carlo simulations to characterize the potential these miscalibrations have to affect the measurement of a change in the fine-structure constant. We find that the effect of the miscalibrations can be well-modeled by random Gaussian wavelength shifts

whose width corresponds to the standard deviation of the miscalibrations across an exposure. The effect depends on the number of transitions and systems that are used in deriving a final fine-structure constant value. The principle method of determining the wavelength miscalibrations is to use the iodine cell, as described in § 2.4.

The outline of this chapter is as follows. We introduce the instrument in § 3.1. We detail the science exposures including data reduction in § 3.2. The results of our wavelength calibration analysis is presented in § 3.3. Possible software calibration effects are examined and ruled out in § 3.4. We explore in § 3.5 the wavelength miscalibrations' effect on the potential measurement of $\frac{\Delta\alpha}{\alpha}$.

3.1 UVES

The ultraviolet and visual echelle spectrograph (UVES) is the instrument used on the European Southern Observatory (ESO)'s Very Large Telescope (VLT) to detect quasar absorption lines for fine-structure constant work. We include a schematic of the VLT spectrograph in Figure 3.1. We trace out the light path through the spectrograph to introduce the various components of interest.

For a science exposure, the light from the telescope enters through the Telescope Shutter, which appears at the top of the schematic. The light then goes through the VLT iodine cell if it has been placed in the beam and then through the Derotator. The Mode Selector allows for selecting whether the light will go to the red arm of the spectrograph, blue arm, or be split to both the red and blue arms using a dichroic filter. The exposures we analyze were taken with the red arm of the spectrometer, and in the schematic, the red light continues straight and then bounces off a mirror into the red collimators. After striking the collimator, the light is dispersed by the echelle gratings and reflected back to the collimator. The light then bounces off mirrors and another transfer collimator before being dispersed by

the cross-disperser. The light finally strikes the CCD detectors (there are two chips per spectrograph arm). For a calibration exposure, the Telescope Shutter is closed, the calibration slide is inserted and light from the calibration lamps is reflected through the remainder of the spectrograph as previously described.

3.2 VLT Observations

In 2003, six exposures were acquired by Murphy, M. for us with the VLT telescope of the bright ($V \approx 14.9$mag) quasar HE0515-4414 that resides at a redshift of $z = 1.71$. Three of the exposures were taken with the VLT iodine cell in place. There are two chips in the red arm of the UVES spectrograph, an upper "u" chip and a lower "l" chip. The extracted spectra had a median signal-to-noise of 20 pixel^{-1} for the upper chip, and 11 pixel^{-1} for the lower chip. Across an order a single CCD pixel corresponds to about 1.5 km s^{-1} on the leading side and about 0.9 km s^{-1} on the trailing edge.

We analyzed three iodine exposures taken on two nights: two on 11 October 2003, and one on 13 October 2003. The same ThAr arc exposure was used on both exposures from the first night to calibrate the wavelength scale, and, unfortunately, the gratings were moved between the science and calibration exposures. A journal of observations is included in Table 3.1. An attempt was made to take the calibration and science exposures without moving any gratings during the second night, but due to VLT settings, the gratings were moved on the third night as well.

Since the UVES specifications were that the same grating positions should position the same light to about one tenth of a pixel, one might expect overall errors of about 140 m s^{-1} if the gratings were moved and then returned to the same position. Another potential source of wavelength error can be estimated from the effect of a misalignment of the object in the slit. The slit width that was used for

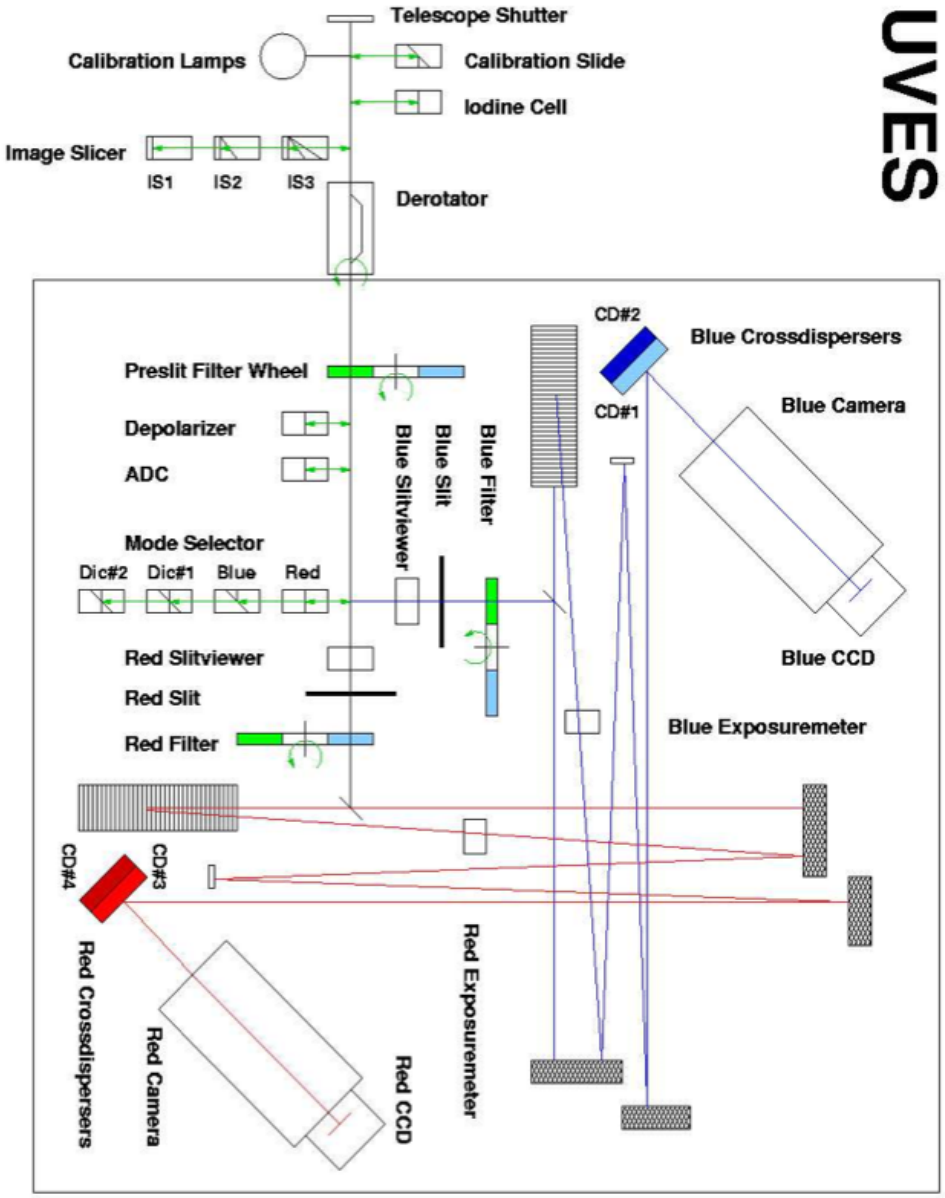

Figure 3.1 Source: (Kaufer et al., 2007).

Table 3.1. VLT-UVES Journal of Observations

Exposure and Date	Time (UT)	ThAr Time (UT)
1 2003-10-11	07:32	10:56
2 2003-10-11	08:13	10:56
3 2003-10-13	05:31	07:06

our observations was 0.7" with seeing between 0.65" and 0.85". At a resolution of about $R = 62,000$, the FWHM of the slit corresponds to about 4.8 km s^{-1} on the CCD. This means that a slit position error of 0.1" would cause a spurious constant wavelength offset of about 600 m s^{-1}. This error dominates any wavelength shifts introduced by moving the gratings.

The exposures were taken with the red arm of the spectrometer, which has two CCDs: an upper and lower chip. We did not bin on-chip, and with the size of the pixels corresponding to about 1.3 km s^{-1} in velocity space, the FWHM resolution falls across 3.7 pixels. We extracted the quasar data using the standard UVES Common Pipeline Language (CPL) software package. The CPL utilizes the ThAr line list that was selected by an objective line selection algorithm developed and described by Murphy et al. (2007). The bias and flat fields were generated by the median filter of five bias and flat field exposures, respectively. The basic physical model of the interior of the spectrograph was refined by taking short-and-narrow slit exposures of the quartz and ThAr lamps. This procedure allows for the flux distribution across each echelle order to be predicted. We used the quasar flux to determine its own spatial profile. The object weights used in the following extraction were determined by this spatial profile.

3.3 Analysis

We implemented a similar iodine method as described in detail in § 2.5, but we use the FTS scan of the iodine cell used on the VLT provided by ESO.[1] The iodine cell on UVES is kept at 70°C by the use of heaters. An overall fit between each small section of the FTS iodine spectrum and the quasar exposure was performed by fitting three variables simultaneously: a wavelength shift, the Gaussian profile width, and an overall normalization factor. We adopt the following notation to discuss the results of our analysis:

$$\lambda_{\rm I}(\lambda) = \lambda_{\rm ThAr}(\lambda) + v_{\rm shift}(\lambda), \tag{3.1}$$

where $\lambda_{\rm ThAr}$ is the wavelength scale given by the standard wavelength calibration solution, $\lambda_{\rm I}$ is the fiducial iodine wavelength scale (presumed correct), and $v_{\rm shift}$ is the amount that the ThAr calibration needs to be shifted in order to align with the iodine scale.

We use a binning size of 350 km s^{-1} or about 6Å at 5500Å. The resulting fits are plotted after converting the wavelength shift to a velocity scale via $\Delta v = c\frac{\Delta\lambda}{\lambda}$ in Figure 3.2.

We did not co-add the iodine exposures, so we have independent tests for each order in each of the three iodine exposures. We give a brief overview of the fitting process. The exposures are continuum fit and strong quasar absorption features are masked. In each order we cut out pixels where the S/N < 8 pixel^{-1} (which occurs near the edges of the orders). A first fit to the entire order is performed with a total of three parameters: a wavelength shift, a Gaussian profile width, and an overall normalization factor. We then fix the Gaussian width and

[1] Available: `http://www.eso.org/sci/facilities/paranal/instruments/uves/tools`

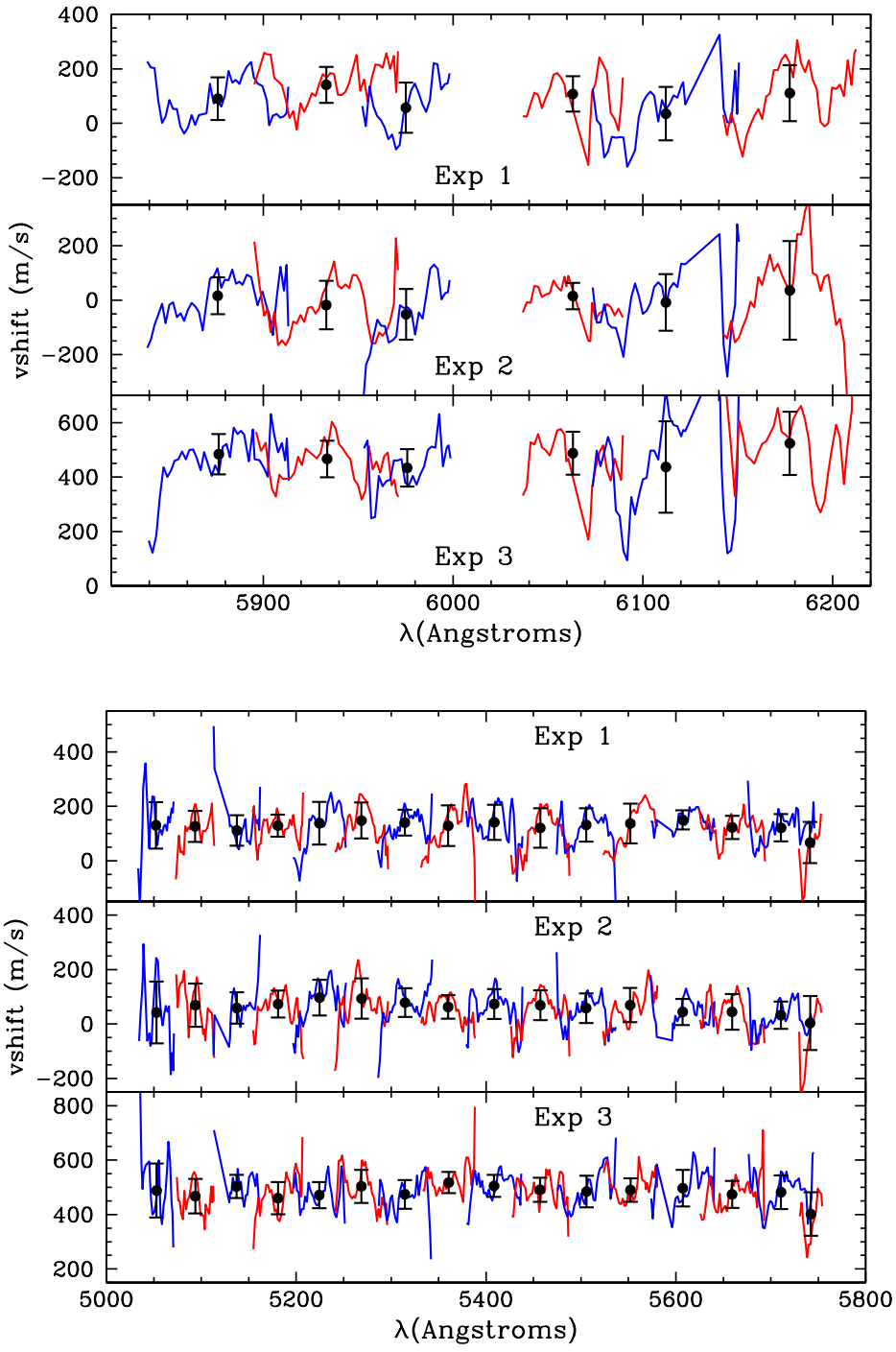

Figure 3.2 Calibration shift in m s^{-1} to align with the iodine cell. We alternate the color of adjacent orders between red and blue to aid visual distinguishing. The large points are the average and standard deviation of the average for each order. Source: (Whitmore et al., 2010).

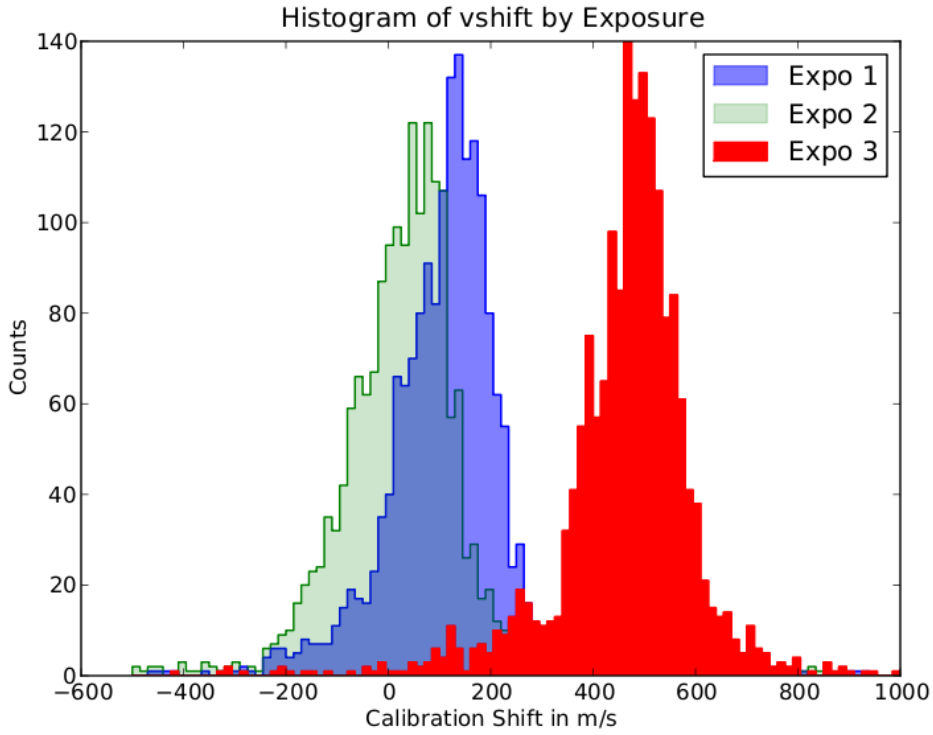

Figure 3.3 Histograms of the wavelength calibration shifts found in the three iodine exposures taken with VLT HIRES. Exposure 1 is in the middle and shaded blue, Exposure 2 is on the left and shaded green, and Exposure 3 is on the right and shaded red. Source: (Whitmore et al., 2010).

overall normalization factor, and refit each bin with only the wavelength shift as a free parameter. We plot a histogram of the shift values in our bins for each exposure in the Figure 3.3.

The average velocity shift is not important for fine-structure constant work, but the width of the distribution corresponds with the spread of different wavelength shifts within each order – which could contribute to a spurious $\frac{\Delta\alpha}{\alpha}$ measurement. The wavelength shifts of nearby pixels are correlated, but the quasar absorption

Table 3.2. Means[a] and Standard Deviations[a] of Calibration Shifts

Exposure	Chip	Unweighted	Weighted and Clipped[b]
1	l	118 ± 76	133 ± 58
2	l	45 ± 86	63 ± 69
3	l	487 ± 75	485 ±60
1	u	116 ± 138	107 ± 87
2	u	0 ± 137	-5 ± 87
3	u	477 ± 174	499 ± 115

[a]All numbers are in m s^{-1}

[b]The mean is calculated using the error bars as weights and then recalculated after throwing out points more than 3σ from the mean

lines occur across the entire wavelength scale and are sampled over a range of redshift values. We reproduce the mean and standard deviation for each exposure in Table 3.2. The average shifts are about what is expected from nominal slit positioning errors. In preliminary work with star iodine exposures, we have found that guiding errors of $\pm 0.2''$ that were deliberately undertaken to probe this effect, cause constant shifts of the expected magnitude $\approx$ 1500m s^{-1}.

3.4 Degree Polynomial Calibration Effects

Since the wavelength calibration appears to have errors that are somewhat similar in shape between different orders, and the wavelength scale is a calculated result produced by pipeline software, we investigate the possibility of using higher ordered polynomial fits to the ThAr exposures. For each echelle order, a polynomial is fit to the known ThAr arc lines and their location on the CCD. This polynomial

solution is then used to interpolate the wavelength scale for every pixel in that echelle order. The standard method employs a fourth order polynomial during the extraction process. For the purposes of testing whether using a higher ordered polynomial might mitigate the observed errors, we re-extracted the exposures using both a fifth and sixth order polynomial. We directly compared the wavelength scale solutions in several ways. We plot the residuals of the fourth order solution to the wavelength scale subtracted from the fifth and sixth order solutions in Figure 3.4. We also plot the residual difference between the fifth and sixth order solutions in the same Figure. The disagreement is within about 10–20 m s^{-1} for most of the lower chip, while near the edges of the upper chip the solutions begin to diverge substantially.

Having different wavelength calibrations also gives us a unique test on our iodine cell method. We fit the different ordered solutions with our iodine cell method and plot the comparison in Figure 3.5. One can see that the inevitable conclusion remains that the majority of the intra-order miscalibrations remain largely unaffected by using a higher degree polynomial. This is unsurprising given the small difference between the two solutions, and suggests that better fitting to the ThAr scale will not improve the main miscalibrations that we detect.

3.5 Effect on Fine-Structure Constant Measurements

It was mentioned in § 2.9, that the wavelength miscalibrations were larger than the wavelength shifts that would be introduced by the fine-structure constant differing by the amount of the claimed detection (Murphy et al., 2003). However,

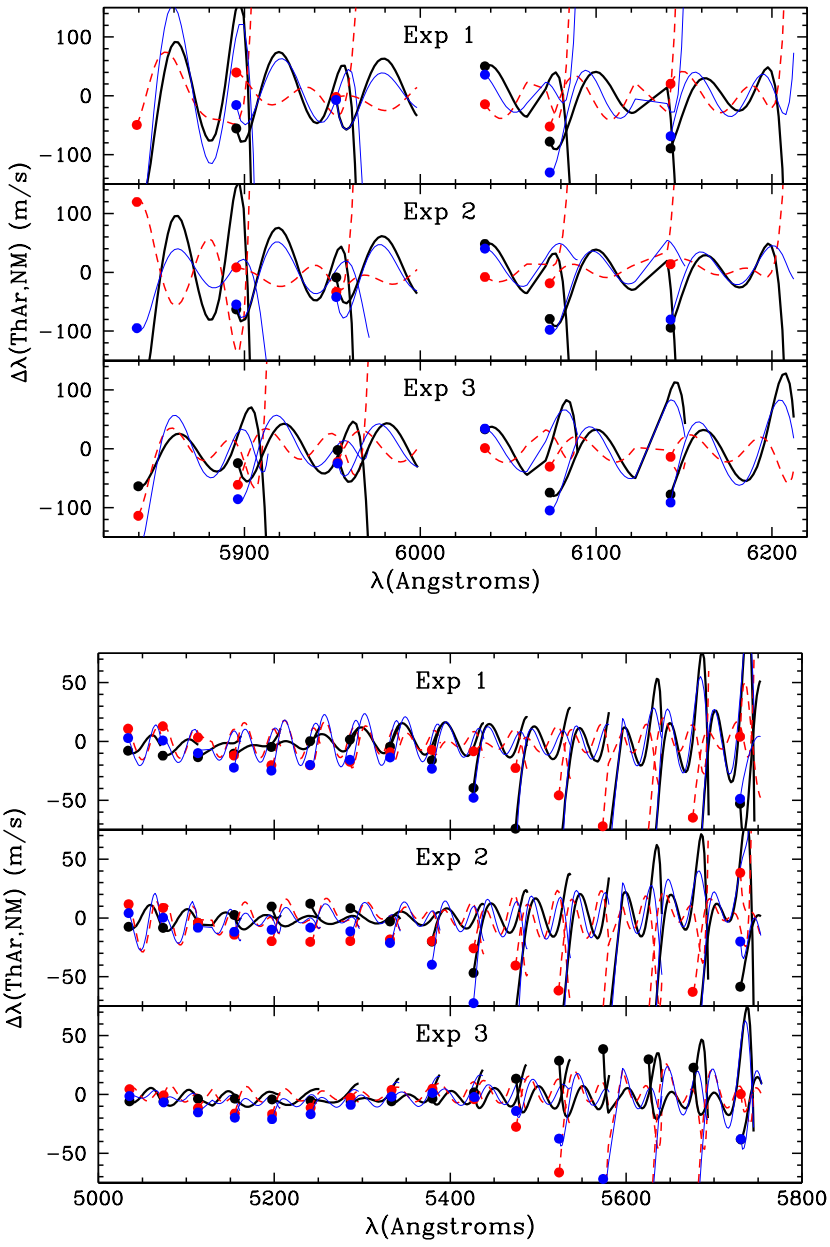

Figure 3.4 Differences in the wavelength scale between the fourth and fifth order polynomial extraction (black), the fourth and sixth order extraction (blue), and the fifth and sixth order extraction (dashed red). Large dots show the beginning of each echelle order. Source: (Whitmore et al., 2010).

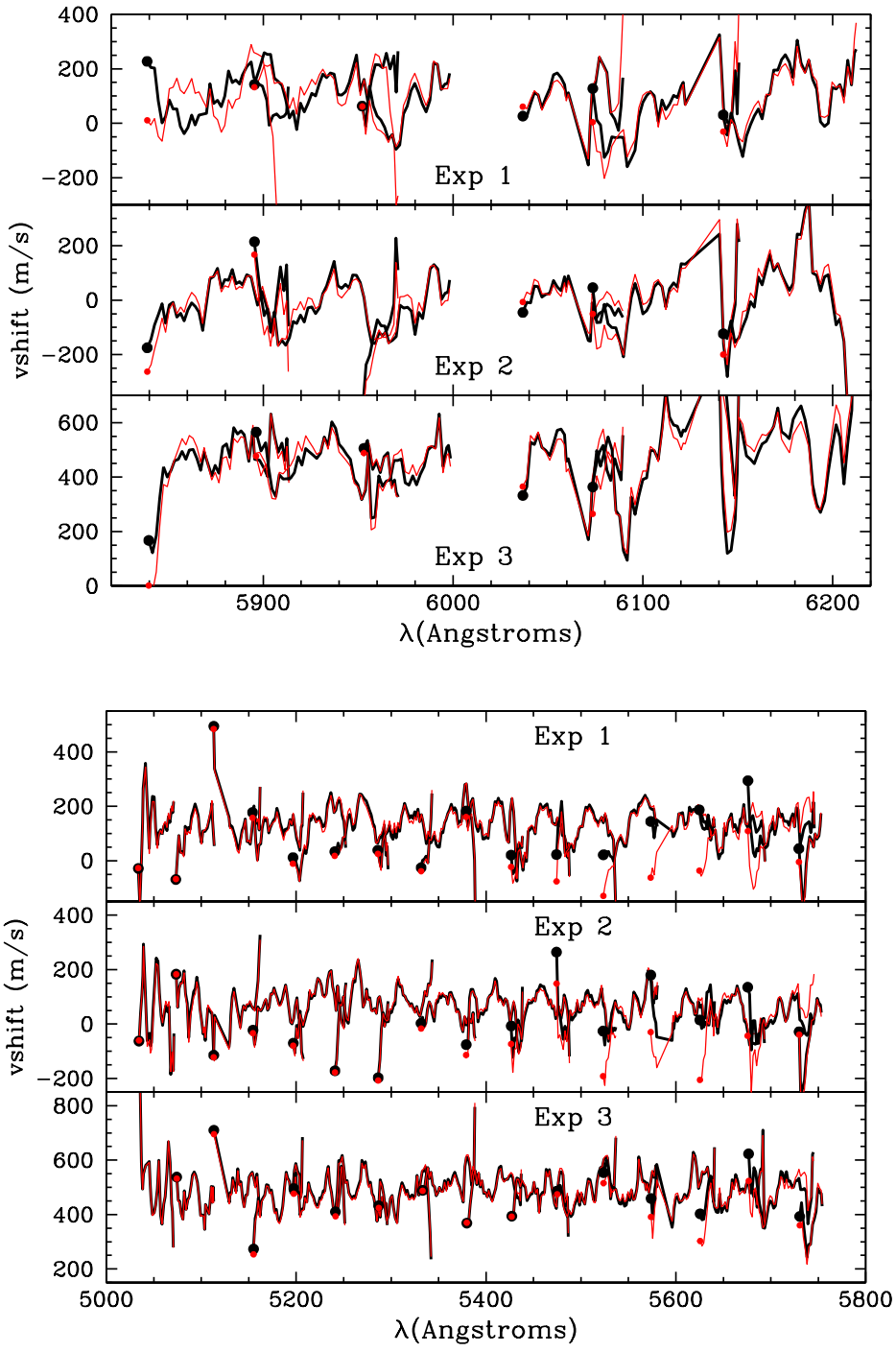

Figure 3.5 The velocity shift needed to correct the ThAr UVES calibration for the fourth degree (black) and sixth degree (red) polynomial fits. Upper panel is the upper CCD chip, the lower panel is the lower CCD chip. The higher order does not improve the calibration. Source: (Whitmore et al., 2010).

the claimed detection was a statistical average over many individual measurements, and the effect of the miscalibrations might average away with a large enough sample. We examine the statistical effect that the miscalibrations would have on a large number of observations.

In this section we investigate the effect that intra-order miscalibrations have on the determination of $\frac{\Delta\alpha}{\alpha}$. If this systematic error generates both negative and positive shifts with equal likelihood, then the miscalibrations only adds random noise, allowing $\frac{\Delta\alpha}{\alpha}$ to be accurately determined by averaging measurements. However, the shifts may contribute so much noise that an unreasonably large number of measurements may be required to converge on a statistically significant result, or the effect may be a systematic shift which does not average away. If negative and positive shifts are not equally likely, the miscalibrations may not average away, resulting in a spurious detection of $\frac{\Delta\alpha}{\alpha}$.

We investigate the effect of these intra-order wavelength miscalibrations by running Monte Carlo simulations. We avoid the difficult aspect of a real measurement which requires precise determination of absorption components and line shape by focusing on the effect of the wavelength miscalibration alone have on a fine-structure constant measurement. Since the published detections were weighted averages of a large number of absorption systems, we decided to artificially create Monte Carlo experiments that each had some number of absorption systems ($N_{\rm sys}$). The method is described below for a single system. We begin by setting $\frac{\Delta\alpha}{\alpha} = 0$ and place a Monte Carlo absorption system at a random redshift in the range probed by Murphy et al. (2003), $z = 0.2$ to 3.7. For each transition that falls within our iodine cell wavelength coverage, that transition is then "miscalibrated" by a wavelength shift using either our measured calibration error or a model of the

Table 3.3. Monte Carlo results[a] for mean and standard deviation of $\frac{\Delta\alpha}{\alpha}$

Exposure	$N_{\rm min}$	$\frac{\Delta\alpha}{\alpha}$mean/$10^{-6}$	$\frac{\sigma}{10^{-6}}$ ($N_{\rm sys}$=1)	$\frac{\sigma}{10^{-6}}$ ($N_{\rm sys}$=143)
1	2	1.74	41.6	3.57
1	4	0.53	5.21	0.443
1	6	-0.041	3.28	0.267
2	2	-1.68	44.7	3.74
2	4	0.330	6.41	0.540
2	6	0.297	3.36	0.279
3	2	1.02	58.9	4.83
3	4	0.706	6.67	0.548
3	6	0.245	3.43	0.280
Gaussian	2	-0.502	115	-
Gaussian	4	-0.080	11.2	-
Gaussian	6	-0.012	4.23	-
Sine	2	-1.78	104	-
Sine	4	-3.13	12.6	-
Sine	6	-0.308	4.64	-

[a]Only transitions within the iodine cell coverage are included from 200,000 realizations of $N_{\rm sys} = 1$.

calibration error. We then fit this artificially miscalibrated spectra for $\frac{\Delta\alpha}{\alpha}$. Since the only wavelength shifts come from our artificial miscalibration, any nonzero $\frac{\Delta\alpha}{\alpha}$ would be a spurious detection. The number of transitions that fall onto the iodine coverage is denoted as $N_{\rm tran}$ for each system that is considered. This process is repeated until the desired number of absorption systems (or $N_{\rm sys}$) is attained for the experiment. We then find the value of $\frac{\Delta\alpha}{\alpha}$ for that Monte Carlo experiment. We ran 200,000 Monte Carlo experiments and find the mean of $\frac{\Delta\alpha}{\alpha}$, the standard deviation of the mean, and the distribution of $\frac{\Delta\alpha}{\alpha}$ in our Monte Carlo experiments. We report the results in Table 3.3.

We list the cases where $N_{\rm sys} = 1$ and $N_{\rm sys} = 143$ and note that as expected, the scaling is essentially $\frac{1}{\sqrt{N_{\rm sys}}}$. Thus we report the results for $N_{\rm sys} = 1$ and encourage researchers to scale by $\frac{1}{\sqrt{N_{\rm sys}}}$ for any number of systems that they desire. Besides the measured wavelength miscalibration distribution, we investigated two other models for systematic wavelength miscalibration: a sine wave and random Gaussian noise. The sigma of the Gaussian was 91 m s^{-1}, and the amplitude of the sine wave was 131 m s^{-1}. The wavelength for the sine function was about one echelle order, but we found that the wavelength did not have a noticeable effect on the results. The mean and standard deviation of each wavelength miscalibration (Gaussian, sine, or empirical) appear to substantially agree with each other. This suggests that the effect on the overall measurement of $\frac{\Delta\alpha}{\alpha}$ is determined by the variance in the scatter in the wavelength miscalibration. In other words, we can model the wavelength miscalibration as Gaussian noise, see Table 3.3.

The $N_{\rm tran}$ is the exact number of transitions that were used in fitting an absorption system. If more than $N_{\rm tran}$ transitions were within the wavelength range for a given redshift, then exactly $N_{\rm tran}$ of those were randomly chosen are used for the $\frac{\Delta\alpha}{\alpha}$ fit. One interesting observation can be made by analyzing the dependence of σ on $N_{\rm tran}$. The standard deviation falls off faster than the expected $1/\sqrt{N_{\rm tran}}$, especially at the lowest $N_{\rm tran}$. This observation suggests using extreme caution when attempting to measure $\frac{\Delta\alpha}{\alpha}$ using systems with only a few transitions. Thus, the Many Multiplet method may have lower systematic errors than the Alkali Doublet method, a method that focuses on only a few transitions. We present our data in Table 3.4.

We did attempt to allow for varying numbers of transitions by applying a lower cutoff on the number of transitions allowed. We call the floor number of

Table 3.4. Standard deviation[a] of $\frac{\Delta\alpha}{\alpha}$ from wavelength calibration errors as a function of the number of transitions.

$N_{\rm tran}$	Percentage of realizations	Exposure 1: $\sigma/10^{-6}$	Gaussian: $\sigma/10^{-6}$
2	20.7%	228	91.4
3	29.7%	30.3	44.0
4	18.7%	8.61	11.2
5	11.7%	5.90	5.00
6	10.7%	3.34	4.17
7	6.3%	3.10	3.73
8	1.3%	3.36	3.60
9	1.0%	2.59	3.18

[a]For transitions that occur within the iodine cell coverage region of the spectrum, and for 200,000 realizations of $N_{\rm sys} = 1$

transitions $N_{\rm min}$, which is simply the minimum number of transitions required to accept a particular z-value. In other words, we rejected any particular z-value that did not shift at least $N_{\rm min}$ transitions into the wavelength range covered by the iodine cell. Thus, the number of transitions in our Monte Carlo is somewhat lower than typically found in the Many Multiplet method. In order to make a more realistic measurement, we decided to extend the region that had wavelength corrections artificially by simply repeating the wavelength calibration results across the entire wavelength region that Murphy et al. (2003) probed, (≈3500Å–10500Å). We also extended the Gaussian and sine offsets as well, and we ran the above process on the new wavelength scales. We report the results in Table 3.5 and in Figure 3.6. We find several interesting results. The most important is the fact that there does not appear to be a systematic bias toward a spurious nonzero measurement of $\frac{\Delta\alpha}{\alpha}$. The second is that the effect of the systematic miscalibrations

can be modeled as random Gaussian noise. The random Gaussian noise and the wavelength miscalibrations both yield results that are consistent with each other over a large wavelength range and for different numbers of N_{min}.

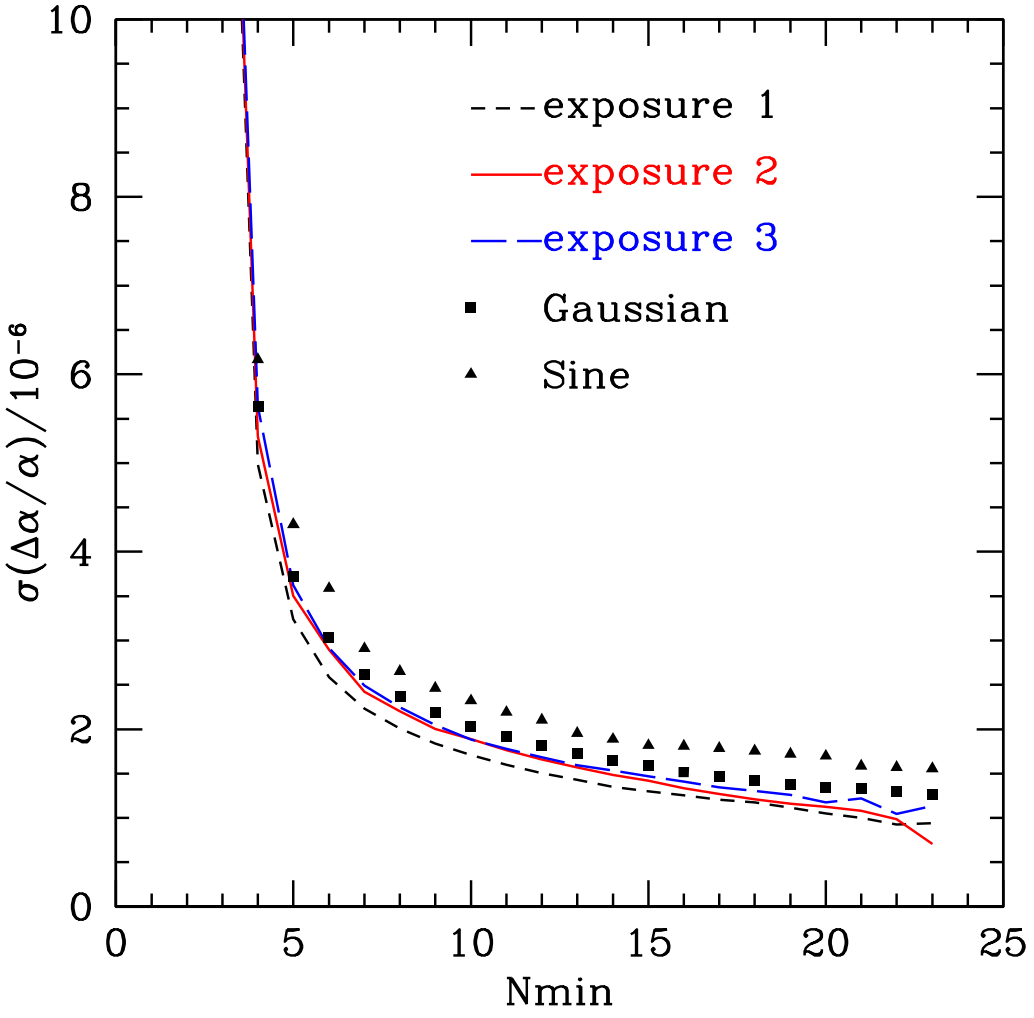

Figure 3.6 The scaling of $\sigma\left(\frac{\Delta\alpha}{\alpha}\right)$ with $N_{\rm min}$, the minimum number of transitions allowed in a system. This plots the results from $N_{\rm sys} = 1$, for the entire wavelength range (3000Å–10500Å), and with the fit calibration errors repeated to cover the range. Source: (Whitmore et al., 2010).

Table 3.5. Monte Carlo results[a] for mean and standard deviation of $\frac{\Delta\alpha}{\alpha}$

$N_{\rm min}$	Exposure 1: mean/10^{-6}	Exposure 1: $\sigma/10^{-6}$	Gaussian: mean/10^{-6}	Gaussian: $\sigma/10^{-6}$
2	-0.018	81.2	0.185	91.6
4	-0.101	4.99	-0.036	5.64
6	-0.064	2.59	-0.028	3.04
8	-0.051	2.00	-0.006	2.38
10	-0.042	1.71	-0.005	2.03
15	-0.029	1.30	0.004	1.59
20	0.153	1.05	0.007	1.35

[a]All of the 23 transitions falling between 3000Å and 10500Å are included (see text), for 200,000 realizations of $N_{\rm sys} = 1$.

Table 3.6. Coefficients for Model

C_{Nt}	$N_{\rm tran}$
21	2
5.1	3
1.7	4
1.3	5
1.1	6, 7
≈ 1	≥ 8

Finally, in order to help other investigators, we attempted to summarize our many Monte Carlo results in a simple fitting formula. We find that a wavelength calibration error of $\sigma(v)$ introduces an error into a fine-structure constant measurement by:

$$\sigma\left(\frac{\Delta\alpha}{\alpha}\right) = 7.5 \times 10^{-8} C_{Nt} \frac{\sigma(v)}{(N_{\rm sys} N_{\rm tran})^{1/2}}, \tag{3.2}$$

where $\sigma(v)$ is in m s^{-1}, and the values of C_{Nt} for different $N_{\rm tran}$ values can be found in Table 3.6. This formula gives investigators a direct way to estimate the required number of systems and transitions to observe to bring down the systematic error due to wavelength miscalibrations to the desired level.

3.6 Conclusions

We analyzed the wavelength calibration of the VLT-UVES spectrograph by recalibrating three iodine exposures. We find two kinds of errors. The first is a constant shift of up to 500–600 m s^{-1} that probably arises due to slit positioning errors. This error will not have a large impact on fine-structure constant work unless transitions are fit across different exposures. The second shift is an intra-order

shift that distorts the wavelength scale by up to several hundred m s^{-1} within a single echelle order of a single exposure. We investigated the causes of these intra-order shifts, and ruled out the order of the polynomial used in fitting the ThAr wavelength solution. The different wavelength solutions gave us an independent check on the reliability of our iodine cell method, and we were able to correct the different wavelength scale to better than 5 m s^{-1}. Since we did not discover the physical cause of these intra-order miscalibrations, we used the calibration shifts that we found to quantify the effect these errors would have on fine-structure constant work. We find that the effect of the errors are well modeled by a random Gaussian wavelength miscalibrations of $\sigma \approx$ 80–120 m s^{-1}. Larger than expected errors were found in systems that use a small number of transitions.

Bibliography

Agafonova, I. I., Molaro, P., Levshakov, S. A., & Hou, J. L. 2011, Astronomy and Astrophysics, 529, 28

Ashenfelter, T. P., Mathews, G. J., & Olive, K. A. 2004, The Astrophysical Journal, 615, 82

Bahcall, J. N. & Salpeter, E. E. 1965, Astrophysical Journal, 142, 1677

Bahcall, J. N., Sargent, W. L. W., & Schmidt, M. 1967, Astrophysical Journal, 149, L11

Bahcall, J. N. & Schmidt, M. 1967, Physical Review Letters, 19, 1294

Bahcall, J. N., Steinhardt, C. L., & Schlegel, D. 2004, The Astrophysical Journal, 600, 520, published in: Astrophys.J.600:520,2004 Added analysis of larger quasar sample from SDSS Data Release One. Accepted for publication ApJ

Beaver, E. A., Burbidge, E. M., McIlwain, C. E., Epps, H. W., & Strittmatter, P. A. 1972, The Astrophysical Journal, 178, 95

Bransden, B. H. & Joachain, C. J. 2003, Physics of Atoms and Molecules, 2nd edn. (Benjamin Cummings), book on Atomic Physics from UCSD library.

Butler, R. P., Marcy, G. W., Williams, E., McCarthy, C., Dosanjh, P., & Vogt, S. S. 1996, Publications of the Astronomical Society of the Pacific, 108, 500

Carswell, R. F., Webb, J. K., Cooke, A. J., & Irwin, M. J. 2008, VPFIT 9.5, `http://www.ast.cam.ac.uk/~rfc/vpfit.html`

Chand, H., Petitjean, P., Srianand, R., & Aracil, B. 2005, Astronomy and Astrophysics, 430, 47

Chand, H., Srianand, R., Petitjean, P., & Aracil, B. 2004, Astronomy and Astrophysics, 417, 853

Dirac, P. A. M. 1937, Nature, 139, 323

Dirac, P. A. M. 1938, in Proceedings of the Royal Society of London. Series A, 199–208

Dzuba, V. A., Flambaum, V. V., & Webb, J. K. 1999a, Physical Review A (Atomic, 59, 230

—. 1999b, Physical Review Letters, 82, 888

Edlén, B. 1966, Metrologia, 2, 71

Flambaum, V. V. 2008, The European Physical Journal Special Topics, 163, 159

Fujii, Y. & Iwamoto, A. 2005, Modern Physics Letters A, 20, 2417

García-Berro, E., Isern, J., & Kubyshin, Y. A. 2007, The Astronomy and Astrophysics Review, 14, 113

Gould, C. R., Sharapov, E. I., & Lamoreaux, S. K. 2006, Physical Review C, 74, 24607

Griest, K., Whitmore, J. B., Wolfe, A. M., Prochaska, J. X., Howk, J. C., & Marcy, G. W. 2010, The Astrophysical Journal, 708, 158

Ichikawa, K., Kanzaki, T., & Kawasaki, M. 2006, Physical Review D, 74, 23515

Ichikawa, K. & Kawasaki, M. 2004, Physical Review D, 69, 123506

Kaluza, T. 1921, Sitz Preuss Akad Wiss Phys Math

Kaufer, A., D'Odorico, S., Kaper, L., Ledoux, C., & James, G. 2007, Very Large Telescope Paranal Science Operations UV-Visual Echelle Spectrograph User manual, issue 82 edn.

Klein, O. 1926, Zeitschrift für Physik, 37, 895

Landau, S. J. & Scóccola, G. 2010, Astronomy and Astrophysics, 517, 62

Levshakov, S. A. 2004, Lecture Notes in Physics, 648, 151

Levshakov, S. A., Centurión, M., Molaro, P., D'Odorico, S., Reimers, D., Quast, R., & Pollmann, M. 2006, Astronomy and Astrophysics, 449, 879

Lorén-Aguilar, P., García-Berro, E., Isern, J., & Kubyshin, Y. A. 2003, Classical and Quantum Gravity, 20, 3885

Mohr, P. J., Taylor, B. N., & Newell, D. B. 2006, The 2006 CODATA Recommended Values of the Fundamental Physical Constants, `http://physics.nist.gov/constants`, this database was developed by J. Baker, M. Douma, and S. Kotochigova. National Institute of Standards and Technology, Gaithersburg, MD 20899. [Online; accessed 2011-03-15]

Molaro, P., Levshakov, S. A., Monai, S., Centurión, M., Bonifacio, P., D'Odorico, S., & Monaco, L. 2008a, Astronomy and Astrophysics, 481, 559

Molaro, P., Reimers, D., Agafonova, I. I., & Levshakov, S. A. 2008b, European Physical Journal Special Topics, 163, 173

Murphy, M. T., Flambaum, V. V., Webb, J. K., & al, e. 2004, Lecture Notes in Physics, 648, 131

Murphy, M. T., Tzanavaris, P., Webb, J. K., & Lovis, C. 2007, Monthly Notices of the Royal Astronomical Society, 378, 221

Murphy, M. T., Webb, J. K., & Flambaum, V. V. 2003, Monthly Notices of the Royal Astronomical Society, 345, 609

—. 2008a, Monthly Notices of the Royal Astronomical Society, 384, 1053

—. 2008b, Precision Spectroscopy in Astrophysics, 95

Murphy, M. T., Webb, J. K., Flambaum, V. V., Dzuba, V. A., Churchill, C. W., Prochaska, J. X., Barrow, J. D., & Wolfe, A. M. 2001a, Monthly Notices of the Royal Astronomical Society, 327, 1208

Murphy, M. T., Webb, J. K., Flambaum, V. V., Prochaska, J. X., & Wolfe, A. M. 2001b, Monthly Notices of the Royal Astronomical Society, 327, 1237

Naudet, R. 1974, Bull. Inf. Sci. Tech. (Paris)., no. 193, pp. 7-45

Olive, K. A., Pospelov, M., Qian, Y.-Z., Coc, A., Cassé, M., & Vangioni-Flam, E. 2002, Physical Review D, 66, 45022

Olive, K. A., Pospelov, M., Qian, Y.-Z., Manhès, G., Vangioni-Flam, E., Coc, A., & Cassé, M. 2004, Physical Review D, 69, 27701

Osterbrock, D. E., Waters, R. T., Barlow, T. A., Slanger, T. G., & Cosby, P. C. 2000, The Publications of the Astronomical Society of the Pacific, 112, 733

Peebles, P. J. & Dicke, R. H. 1962, Physical Review, 128, 2006

Peik, E., Lipphardt, B., Schnatz, H., Tamm, C., Weyers, S., & Wynands, R. 2008, THE ELEVENTH MARCEL GROSSMANN MEETING On Recent Developments in Theoretical and Experimental General Relativity, 941

Petrov, Y. V., Nazarov, A. I., Onegin, M. S., Petrov, V. Y., & Sakhnovsky, E. G. 2006, Physical Review C, 74, 64610

Reid, B. A., Percival, W. J., Eisenstein, D. J., Verde, L., Spergel, D. N., Skibba, R. A., Bahcall, N. A., Budavari, T., Frieman, J. A., Fukugita, M., Gott, J. R., Gunn, J. E., Ivezić, Z., Knapp, G. R., Kron, R. G., Lupton, R. H., McKay, T. A., Meiksin, A., Nichol, R. C., Pope, A. C., Schlegel, D. J., Schneider, D. P., Stoughton, C., Strauss, M. A., Szalay, A. S., Tegmark, M., Vogeley, M. S., Weinberg, D. H., York, D. G., & Zehavi, I. 2010, Monthly Notices of the Royal Astronomical Society, 404, 60

Reynaud, S., Salomon, C., & Wolf, P. 2009, Space Science Reviews, 148, 233, 145 pages, 10 figures, Review for Living Reviews in Relativity

Riess, A. G., Macri, L., Casertano, S., Sosey, M., Lampeitl, H., Ferguson, H. C., Filippenko, A. V., Jha, S. W., Li, W., Chornock, R., & Sarkar, D. 2009, The Astrophysical Journal, 699, 539

Rosenband, T., Hume, D. B., Schmidt, P. O., Chou, C. W., Brusch, A., Lorini, L., Oskay, W. H., Drullinger, R. E., Fortier, T. M., Stalnaker, J. E., Diddams, S. A., Swann, W. C., Newbury, N. R., Itano, W. M., Wineland, D. J., & Bergquist, J. C. 2008, Science, 319, 1808

Savedoff, M. P. 1956, Nature, 178, 688

Shlyakhter, A. I. 1976, Nature, 264, 340

Srianand, R., Chand, H., Petitjean, P., & Aracil, B. 2004, Physical Review Letters, 92, 121302

Srianand, R., Petitjean, P., Chand, H., Noterdaeme, P., & Gupta, N. 2009, Memorie della Società Astronomica Italiana, 80, 842

Suzuki, N., Tytler, D., Kirkman, D., O'Meara, J. M., & Lubin, D. 2003, The Publications of the Astronomical Society of the Pacific, 115, 1050

Uzan, J.-P. 2011, Living Reviews in Relativity, 14, 2

Vogt, S. S. 1994, HIRES User's Manual, `http://www2.keck.hawaii.edu/inst/hires/manual2.pdf`, [Online; accessed 2011-03-22]

Webb, J., Murphy, M., Flambaum, V., & Curran, S. 2003, Astrophysics and Space Science, 283, 565

Webb, J. K., Flambaum, V. V., Churchill, C. W., Drinkwater, M. J., & Barrow, J. D. 1999, Physical Review Letters, 82, 884

Webb, J. K., King, J. A., Murphy, M. T., Flambaum, V. V., Carswell, R. F., & Bainbridge, M. B. 2010, arXiv, 1008, 3907, 5 pages, 5 figures, submitted to Physical Review Letters

Webb, J. K., Murphy, M. T., Flambaum, V. V., Dzuba, V. A., Barrow, J. D., Churchill, C. W., Prochaska, J. X., & Wolfe, A. M. 2001, Physical Review Letters, 87, 91301

Whitmore, J. B., Murphy, M. T., & Griest, K. 2010, The Astrophysical Journal, 723, 89

Wilkinson, D. H. 1958, Philosophical Magazine, 3, 582

Wolfe, A. M., Brown, R. L., & Roberts, M. S. 1976, Physical Review Letters, 37, 179, a&AA ID. AAA018.022.121